Technical feasibility of a Dutch radioactive waste repository in Boom Clay
Geomechanical validation

Li, Yajun; Vardon, Phil; Hicks, Michael; Hart, Jaap; Fokker, Peter A.

Publication date
2018

Document Version
Final published version

Citation (APA)
Li, Y., Vardon, P., Hicks, M., Hart, J., & Fokker, P. A. (2018). *Technical feasibility of a Dutch radioactive waste repository in Boom Clay: Geomechanical validation*. Delft University of Technology.

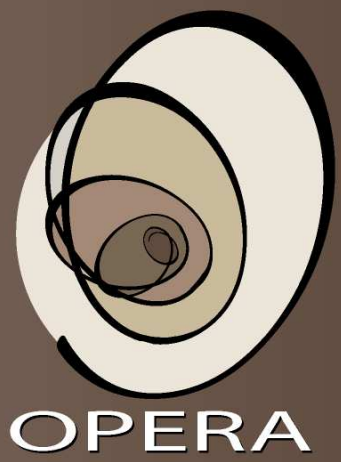

Technical feasibility of a Dutch radioactive waste repository in Boom Clay: Geomechanical validation

OPERA-PU-TUD321d

Radioactive substances and ionizing radiation are used in medicine, industry, agriculture, research, education and electricity production. This generates radioactive waste. In the Netherlands, this waste is collected, treated and stored by COVRA (Centrale Organisatie Voor Radioactief Afval). After interim storage for a period of at least 100 years radioactive waste is intended for disposal. There is a world-wide scientific and technical consensus that geological disposal represents the safest long-term option for radioactive waste.
Geological disposal is emplacement of radioactive waste in deep underground formations. The goal of geological disposal is long-term isolation of radioactive waste from our living environment in order to avoid exposure of future generations to ionising radiation from the waste. OPERA (OnderzoeksProgramma Eindberging Radioactief Afval) is the Dutch research programme on geological disposal of radioactive waste.
Within OPERA, researchers of different organisations in different areas of expertise will cooperate on the initial, conditional Safety Cases for the host rocks Boom Clay and Zechstein rock salt. As the radioactive waste disposal process in the Netherlands is at an early, conceptual phase and the previous research programme has ended more than a decade ago, in OPERA a first preliminary or initial safety case will be developed to structure the research necessary for the eventual development of a repository in the Netherlands. The safety case is conditional since only the long-term safety of a generic repository will be assessed. OPERA is financed by the Dutch Ministry of Economic Affairs and the public limited liability company Electriciteits-Produktiemaatschappij Zuid-Nederland (EPZ) and coordinated by COVRA. Further details on OPERA and its outcomes can be accessed at `www.covra.nl`.

OPERA-PU-TUD321d
Title: Technical feasibility of a Dutch radioactive waste repository in Boom Clay: Geomechanical validation
Authors: Yajun Li, Philip J. Vardon, Michael A. Hicks, Jaap Hart and Peter A. Fokker
Date of publication: July 2018
Keywords: Boom Clay, feasibility, radioactive waste disposal, reliability, geomechanics, COx, Opalinus Clay.

TU Delft Delft University of Technology

Technical feasibility of a Dutch radioactive waste repository in Boom Clay: Geomechanical validation

July 2018

Yajun Li[1], Philip J. Vardon[1], Michael A. Hicks[1]
Jaap Hart[2] and Peter A. Fokker[3]

[1] Delft University of Technology (TUD), Geo-Engineering Section, Delft
[2] Nuclear Research and consultancy Group (NRG), Petten
[3] Nederlandse Organisatie voor Toegepast Natuurwetenschappelijk Onderzoek (TNO), Utrecht

Contents

Summary . . . 1
Samenvatting . . . 2
Notation . . . 4
1 Introduction . . . 6
1.1 Background . . . 6
1.2 Objectives . . . 7
1.3 Outline of the report . . . 7
2 Case studies used . . . 8
2.1 Introduction . . . 8
2.2 French geological disposal programme . . . 8
2.2.1 Geological environment . . . 8
2.2.2 The underground research laboratory . . . 8
2.2.3 Mechanical properties . . . 8
2.3 Swiss geological disposal programme . . . 15
2.3.1 Geological environment . . . 15
2.3.2 Mechanical properties . . . 15
3 Numerical analysis . . . 17
3.1 Methodology . . . 17
3.2 Probabilistic methods . . . 17
3.3 Investigation of tunnels in COx . . . 21
3.3.1 Modelled experiment: The GCS drift . . . 21
3.3.2 Probabilistic interpretation of the test results . . . 22
3.3.3 Analytical model investigation . . . 29
3.3.4 Numerical model investigation . . . 37
3.3.5 Concluding remarks . . . 42
3.4 Investigation of tunnels in Opalinus Clay . . . 44
3.4.1 Modelled experiment: ED-B tunnel . . . 44
3.4.2 Numerical model investigation . . . 46
3.4.3 Concluding remarks . . . 49
4 New Boom Clay simulations . . . 50
4.1 Material properties . . . 50
4.2 Model . . . 52
4.3 Results . . . 52
5 Discussion . . . 54
5.1 Introduction . . . 54
5.2 Model development . . . 54
5.2.1 Analytical modelling . . . 54
5.2.2 Numerical modelling approaches . . . 55
5.2.3 Probabilistic modelling . . . 56
5.3 Code validation . . . 56

5.4 Model application 57
5.4.1 Tunnel construction 57
5.4.2 Plugs and seals 58
5.4.3 Tunnel crossings 58
5.4.4 Effect of heating 58
5.5 Newly collected data from Boom Clay experiments 59
5.6 Future 59
6 Summary and conclusions 61
References 62

Summary

The *Onderzoeks Programma Eindberging Radioactief Afval* (OPERA) is the third national research programme for the geological disposal of radioactive waste in the Netherlands, operating during the period 2011 to 2016. This document reports part of Work Package 3.2.1, where a number of aspects related to the technical feasibility were investigated.

In previous work by the same research group, presented in Arnold et al. (2015), a series of geomechanical models were presented, investigating the stability and reliability of a proposed repository situated in the Boom Clay layer. With limited experimental data available a series of reliability analyses were carried out, with the conclusion that is was likely that the proposed repository would be feasible. This work applies the same models and treatment of data to other geological disposal programmes, where field data are available, to build confidence in the performance of the models, and an updated deterministic analysis for the proposed repository in the Boom Clay layer based on newly collected experimental evidence.

Two case studies have been used: these are experiments carried out as part of the French and the Swiss geological disposal programmes. The models are able to simulate results in line with those observed and other numerical modelling investigations carried out in relation to those experiments. The key characteristics of the material and system behaviours can be included. In the models and data treatment undertaken in this work, a probability of certain behaviour and an exceedance probability of behaviour can be determined. This can be used within performance and safety assessments.

Significant amounts of data are required to be able to undertake this sort of analysis, which were available in the French case study but not in the Swiss. In the French case study, both analytical and numerical models were used with good results. An assessment of parameter importance was carried out. Higher levels of anisotropy were observed in the Swiss case, meaning that simulation via the developed analytical model was not possible, but good results were found using the numerical model. The behaviour of the models in the aforementioned geological environments was compared to that of Boom Clay.

As a result of this investigation, there is more confidence in the ability of the models to simulate the behaviour of repository galleries, in particular the plastic deformation around the tunnels. This requires, as always, a good understanding of the geotechnical behaviour of the material and of the assumptions and limitations of the developed numerical and material models.

A new deterministic analysis was undertaken based on newly collected Boom Clay data, where the samples were mechanically conditioned to the stress levels expected at 500 m depth. The interpretation of these tests gave a friction angle higher than previously expected, and the simulations consequently predicted a significantly smaller plastic zone and moderately lower stresses on the liner. Further tests would be needed to confirm these results.

Samenvatting

Het *Onderzoeks Programma Eindberging Radioactief Afval* (OPERA) is het derde nationale onderzoeksprogramma voor geologische eindberging van radioactief afval in Nederland, uitgevoerd tussen 2011 en 2016. Dit document beschrijft een deel van Work Package 3.2.1, waarin een aantal aan de technische haalbaarheid gerelateerde aspecten onderzocht zijn.

In eerder werk door dezelfde onderzoeksgroep, gepresenteerd in Arnold et al. (2015), is een reeks geomechanische modellen gepresenteerd. Deze modellen zijn gebruikt voor de analyse van de stabiliteit en betrouwbaarheid van een eindbergingsconcept in de Boomse Klei. Met een beperkte hoeveelheid beschikbare data is een reeks betrouwbaarheidsanalysen gedaan, waaruit de haalbaarheid van de voorgestelde eindberging waarschijnlijk is gebleken. Dit rapport past dezelfde modellen en dataverwerking toe op andere geologische eindbergingsprogrammas waarvan velddata beschikbaar is. Doel van dit rapport is zekerheid op te bouwen in de beschreven modellen en een herziene deterministische analyse van de eindberging in de Boomse kleilaag te presenteren, gebaseerd op nieuw verworven experimenteel bewijs.

Twee casestudies zijn gebruikt, beide als experiment uitgevoerd als onderdeel van respectievelijk de Franse en de Zwitserse eindbergingsprogrammas. De modellen zijn in staat resultaten te genereren in overeenkomst met de waarnemingen en analyses op basis van numeriek modelleren, uitgevoerd met betrekking op bovengenoemde experimenten. De belangrijkste kenmerken van het materiaal- en systeemgedrag kunnen gemodelleerd worden. De benadering van de data en de modellen in dit werk zijn zo opgezet dat een waarschijnlijkheid en een overschrijdingskans voor het optreden van specifiek gedrag bepaald kunnen worden. Deze resultaten kunnen gebruikt worden in de prestatie- en veiligheidsbeoordelingen.

Een significante hoeveelheid data is vereist voor het uitvoeren van dergelijke analyses. Deze data bleek beschikbaar in de Franse studie en niet in de Zwitserse studie. Zowel de analytische als de numerieke methoden zijn met succes toegepast op de data van de Franse studie en een gevoeligheidsanalyse is uitgevoerd op de parameters. Hoge mate van anisotropie is waargenomen in de Zwitserse studie, waardoor de ontwikkelde analytische modellen niet toepasbaar bleken. De numerieke modellen hebben echter tot goede resultaten geleid. Het gedrag van de modellen in de voorgenoemde geologische settings is vervolgens vergeleken met de Boomse Klei.

Een resultaat van dit onderzoek is de vergrootte zekerheid in het vermogen van de modellen tot het simuleren van de eindberging, met name de plastische vervorming rond de tunnels. Dit vereist, zoals altijd, een goed begrip van het geotechnisch materiaalgedrag en de aannames en beperkingen van de ontwikkelde numerieke methodes en materiaalmodellen.

Een nieuwe deterministische analyse is uitgevoerd op basis van nieuwe data van de Boomse Klei, waar de grondmonsters mechanisch belast zijn op het te verwachten spanningsniveau op 500 m diepte. De interpretatie van deze testen hebben geleid tot een grotere hoek van inwendige wrijving dan eerder verwacht werd, met als gevolg een significant kleinere plastische zone en een bescheiden verlaging van de spanningen op de tunnelwand. Voor bevestiging van deze resultaten zouden verdere materiaaltesten nodig zijn.

:

Notation

This list contains definitions of acronyms and symbols including dimensions. All symbols are also defined in the text. The dimensions are defined in typical SI units.

Symbol	Definition	Unit
Acronyms		
ANDRA	Agence nationale pour la gestion des déchets radioactifs / French national radioactive waste management agency	
COx	Callovo-Oxfordian	
FORM	First Order Reliability Method	
HADES	High-Activity Disposal Experimental Site underground research facility	
HLW	High Level Waste	
HS	Hardening soil model	
HZ	Hardening zone	
LILW	Low and Intermediate Level Waste	
MC	Monte Carlo	
NRG	Nuclear Research and consultancy Group (NL)	
OCR	Over-consolidation ratio	
OPA	Opalinus Clay	
OPERA	Onderzoeks Programma Eindberging Radioactief Afval	
PCE	Polynomial chaos expansion	
PZ	Plastic zone	
SORM	Second Order Reliability Method	
TNO	Nederlandse Organisatie voor Toegepast Natuurwetenschappelijk Onderzoek (NL)	
TUD	Delft University of Technology (NL)	
UCS	Uniaxial compressive strength	
WP	Work Package	
Greek letters		
α	Polynomial degree	
$\boldsymbol{\alpha}$	Vector of polynomial degrees	
β	Reliability index	[-]
γ	Unit weight	[N m^{-3}]
γ_i^2	FORM importance factor	[-]
μ	Mean	[-]
ν	Poisson's ratio	[-]
ν_{ur}	Unloading-reloading Poisson's ratio	[-]
ϕ'	Effective friction angle	[°]
Φ_{α^k}	Univariate polynomial	
$\Phi_{\boldsymbol{\alpha}_k}$	Multivariate polynomial	
ρ	Density	[g cm^{-3}]
ρ	Pearson correlation coefficient	
$\bar{\sigma}_{\theta\theta}$	Total tangential (hoop) stress at EP interface	[Pa]
$\bar{\sigma}_{rr}$	Total radial stress at EP interface	[Pa]
$\hat{\sigma}_{\theta\theta}$	Total tangential (hoop) stress at RP interface	[Pa]
$\hat{\sigma}_{rr}$	Total radial stress at RP interface	[Pa]
σ	Standard deviation	[Pa]

σ_0	Total in-situ (far-field) stress	[Pa]
σ_1	Major principle stress	[Pa]
σ_3	Minor principle stress	[Pa]
σ_H	Major horizontal stress	[Pa]
σ_h	Minor horizontal stress	[Pa]
σ_v	Vertical stress	[Pa]
$\sigma_{\theta\theta}$	Total tangential (hoop) stress	[Pa]
σ_{rr}	Total radial stress	[Pa]
σ_{zz}	Total axial stress	[Pa]
θ	Angle of y-axis rotation	[°]
ψ	Dilation angle	[°]

Latin letters

a	Coefficients of the response surface	
c'	Effective cohesion	[Pa]
c_0	Peak (initial) cohesion	[Pa]
c_r	Residual (initial) cohesion	[Pa]
E	Young's modulus	[Pa]
e	Void ratio	[-]
E_t	Tangent modulus	[Pa]
E_{50}	Secant modulus	[Pa]
E_{oed}	Oedometer modulus	[Pa]
E_{ur}	Unloading/reloading modulus	Pa]
$\hat{g}$	Approximate performance function	
g	Performance function	
k	Permeability	[m^2]
K_0	At rest coefficient of lateral earth pressure	[-]
K_0^{NC}	Coefficient of earth pressure for at rest NC conditions	[-]
K_w	Saturated hydraulic conductivity	[$m\,s^{-1}$]
m	HS model exponent	[-]
n	Porosity	[-]
N_f	Number of failed realisations	
N_r	Number of realisations	
n_X	Number of random variables	[-]
P	Number of terms in the PCE	
P	Probability	
p^{ref}	Reference stress	Pa]
r_c	Cavity radius	[m]
R_f	Failure ratio	[-]
r_w	Radius beyond which the pore water pressure is not influenced by the cavity	[m]
r_p	Plastic (yield) radius	[m]
r_{rp}	Residual plastic radius	[m]
s	Triaxial mean stress	[MPa]
t	Triaixal shear stress	[MPa]
$\bar{u}_w$	Pore-water pressure at EP interface	[Pa]
u	Random variable in standard normal space	[-]
$u_{w,0}$	In-situ (far-field) pore water pressure	[Pa]
$u_{w,c}$	Pore-water pressure at cavity	[Pa]
w	Water content	[-]
$\mathbf{x}$	Vector of random variables	
x	Physical random variable	[various]
x^*	Design point in physical space	[various]
$\hat{y}$	Approximate response random variable	[various]
y	Response random variable	[various]

1 Introduction

This report is part of an investigation into the principle feasibility of a deep geological repository for radioactive waste in the Netherlands. This work is undertaken as part of the *Onderzoeks Programma Eindberging Radioactief Afval* (OPERA) research programme in Work Package (WP) 3.2.1. This report follows from WP 3.1 where a number of additional aspects relating to the principle feasibility were identified for further investigation. The results of WP 3.2.1 are presented in the following reports:

- Yuan, J., Vardon, P.J., Hicks, M.A., Hart, J., Fokker, P.A. (2017) Technical feasibility of a Dutch radioactive waste repository in Boom Clay: Plugs and seals. OPERA-PU-TUD321a.
- Yuan, J., Vardon, P.J., Hicks, M.A., Hart, J., Fokker, P.A. (2017) Technical feasibility of a Dutch radioactive waste repository in Boom Clay: Tunnel crossings. OPERA-PU-TUD321b.
- Vardon, P.J., Buragohain, P., Hicks, M.A., Hart, J., Fokker, P.A., Graham, C.C. (2017) Technical feasibility of a Dutch radioactive waste repository in Boom Clay: Thermo-hydro-mechanical behaviour. OPERA-PU-TUD321c.
- Li, Y., Vardon, P.J., Hicks, M.A., Hart, J., Fokker, P.A. (2018) Technical feasibility of a Dutch radioactive waste repository in Boom Clay: Geomechanical validation. OPERA-PU-TUD321d.

The main objective of this report is to investigate and build confidence in the geomechanical modelling undertaken in Arnold et al. (2015). Without experimental evidence to compare the numerical results to, limited confidence can be drawn to predictive analyses. Therefore a series of modelling exercises have been undertaken to relevant experimental work, i.e. similar depths, constructions and host rocks, to investigate the modelling capabilities. The majority of the research was undertaken by*Delft University of Technology* (TUD), *Nuclear Research and consultancy Group* (NRG) and *Nederlandse Organisatie voor Toegepast Natuurwetenschappelijk Onderzoek* (TNO) during the period from 5-2015 till 6-2016, with the additional analysis with newly collected data on the Boom Clay properties undertaken in early 2018.

1.1 Background

Storage and disposal of radioactive waste in deep geological formations is proposed as the most likely option for the Netherlands and worldwide. In this concept of the geological disposal system, Boom Clay is considered as a potential host rock in the Netherlands. The repository concept in the Netherlands (Verhoef et al., 2014) consists of a series of galleries excavated in Boom Clay including a concrete tunnel lining.

In Arnold et al. (2015) the behaviour of a single tunnel, including the plastic behaviour of the Boom Clay and the required spacing between adjacent tunnels was investigated. The results suggested that the tunnel spacing, for mechanical stability, could be reduced. An analytical model and a numerical model (using the finite element method) were undertaken, and included an investigation into the model and parameter sensitivity.

As concluded in Arnold et al. (2015), there are only a limited amount of data available on Boom Clay from relevant depths, and, moreover, there are even less data available on comparable constructions in comparable material at comparable depths. Therefore, a further numerical investigation was proposed, to examine comparable constructions, i.e. those of other geological disposal programmes, in reasonably comparable rock formations, at reasonably comparable depths, where a substantial amount of data are available. Due to the aforementioned lack of comparable sites in Boom Clay, the following geological disposal programmes were considered:

(i) The French disposal programme - which is excavated in Callo-Oxfordian (COx) Clay at approximately 490 m depth.

(ii) The Swiss disposal programme - in particular the Mont Terri URL excavations in Opalinus Clay, at approximately 300 m depth.

In addition, a limited amount of new geomechanical data was collected as part of the OPERA programme. This experimental programme (Harrington et al., 2017) focused on reproducing the mechanical conditions expected at the proposed repository and collected geomechanical data, alongside data on the permeability, gas migration and effects of temperature. A limited re-evaluation of the simulations executed in Arnold et al. (2015) was undertaken based on this new data.

1.2 Objectives

The main objective of this report is to investigate the geomechanical modelling approach used in Arnold et al. (2015) against experimental data. The sub-objectives are:

(i) To investigate the simplified analytical model, including probabilistic analyses, against experimental data.

(ii) To investigate the numerical model, including probabilistic analyses, against experimental data.

(iii) To compare the results from COx, Opalinus Clay to those previously reported for Boom Clay.

(iv) To re-evaluate the simulation undertaken in Arnold et al. (2015) based on new experimental data.

1.3 Outline of the report

Chapter 2 introduces the two case studies used, i.e. experiments from the French and Swiss geological disposal programmes. Background information with regards to their respective geological environments, the proposed conceptual repositories and the mechanical properties of the COx and Opalinus Clay are introduced separately in Sections 2.2 and 2.3. Chapter 3 presents the numerical analysis. The methodology of the numerical investigation is presented in section 3.1; followed by the investigations for both cases. The French case (Section 3.3) was investigated in greater detail with both the analytical model and numerical model, due to the amount of data available to enable an useful probabilistic investigation. The Swiss case (Section 3.4) was investigated using the best estimate model parameters found in literature. Chapter 4 presents new simulations of the proposed repository in Boom Clay, with a discussion presented in Chapter 5 and conclusions presented in Chapter 6.

2 Case studies used

2.1 Introduction

The case studies utilised for the numerical modelling investigation are outlined in the sections below.

2.2 French geological disposal programme

For the disposal of high-level long-lived radioactive waste, ANDRA have selected geological disposal in the Callovo-Oxfordian (COx) Clay as the disposal method to investigate in detail. An underground research laboratory, the Meuse/Haute-Marne site, has been constructed to allow detailed investigation of the geological environment and to assess the long-term behaviour. The site is located in eastern France, on the boundary between the Meuse and Haute-Marne districts (Figure 2.1, ANDRA, 2005b).

2.2.1 Geological environment

The Meuse/Haute-Marne site is in the eastern region of the Paris Basin (Figure 2.2, ANDRA, 2005a). The Paris Basin is composed of alternating Jurassic sedimentary layers, which are primarily argillaceous and limestone layers. Within the sedimentary sequence, the Callovo-Oxfordian layer has been selected for the repository feasibility study (Figure 2.3, ANDRA, 2005a). It is surrounded by geological formations with low permeability and therefore slow water flow (approximated by ANDRA to be one kilometre per hundred thousand years based on the Darcy water velocity). The formation is thought to be structurally stable, located away from large faults and with stresses oriented similarly for the past 20 million years (ANDRA, 2005b).

The depth of the Callovo-Oxfordian roof varies from 420 m at the underground research laboratory to over 600 m along the dip direction, and the thickness of the layer varies from 130 m at the laboratory to 160 m towards the north.

2.2.2 The underground research laboratory

The Meuse/Haute-Marne underground laboratory was initially selected to be constructed in 1998 and the first shaft reached the COx clay in 2004. From 2005 an experimental programme was undertaken in the laboratory. The drift networks are shown in Figure 2.4. For both the shafts and a number of the tunnels geomechanical monitoring during and after the excavation was carried out within a detailed and comprehensive experimental programme.

2.2.3 Mechanical properties

The COx clay is characterised as a stiff clay rock; an argillite. It is not, however, strong enough to be self supporting at 500 m depth (ANDRA, 2005a). Typical behaviour of the COx clay in triaxial conditions is shown in Figure 2.5. It is characterised by a fairly stiff, almost linear stiffness at the beginning, showing limited hardening, prior to the peak strength (labelled rupture), followed by considerable softening until a residual strength (labelled phase residuelle).

Figure 2.1: Geographic location of the Meuse/Haute-Marne site (ANDRA, 2005b).

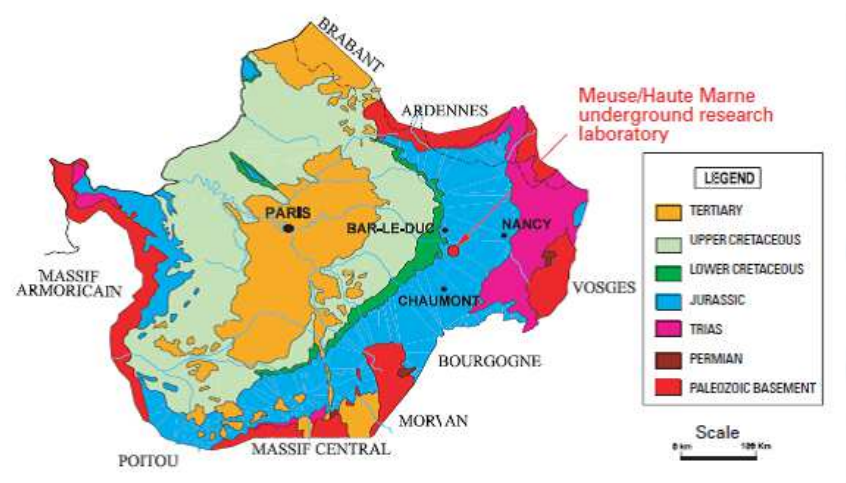

Figure 2.2: Geological location of the Meuse/Haute-Marne site within the Paris Basin (ANDRA, 2005a).

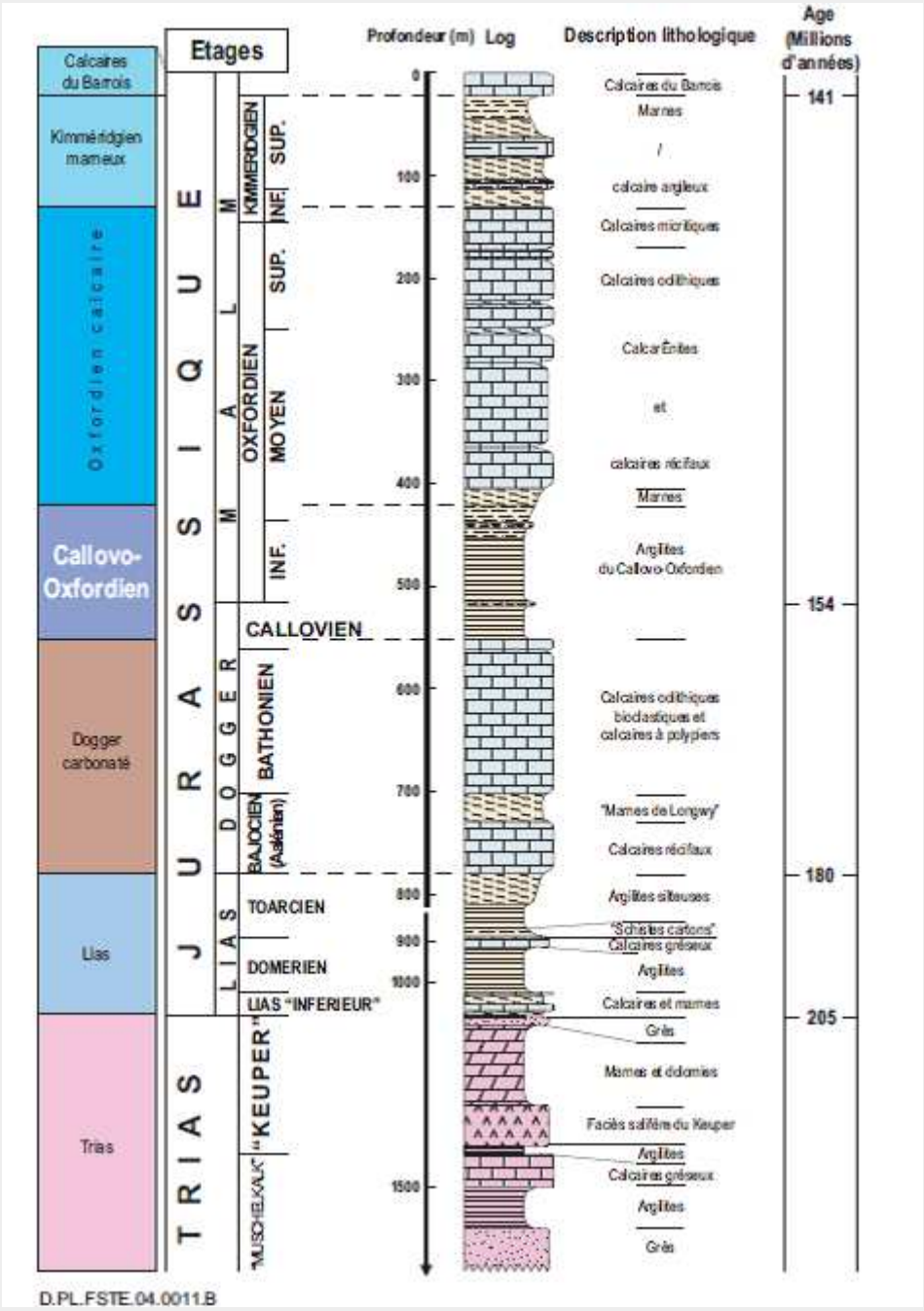

Figure 2.3: Geological cross-section at the Meuse/Haute-Marne site ANDRA, 2005a.

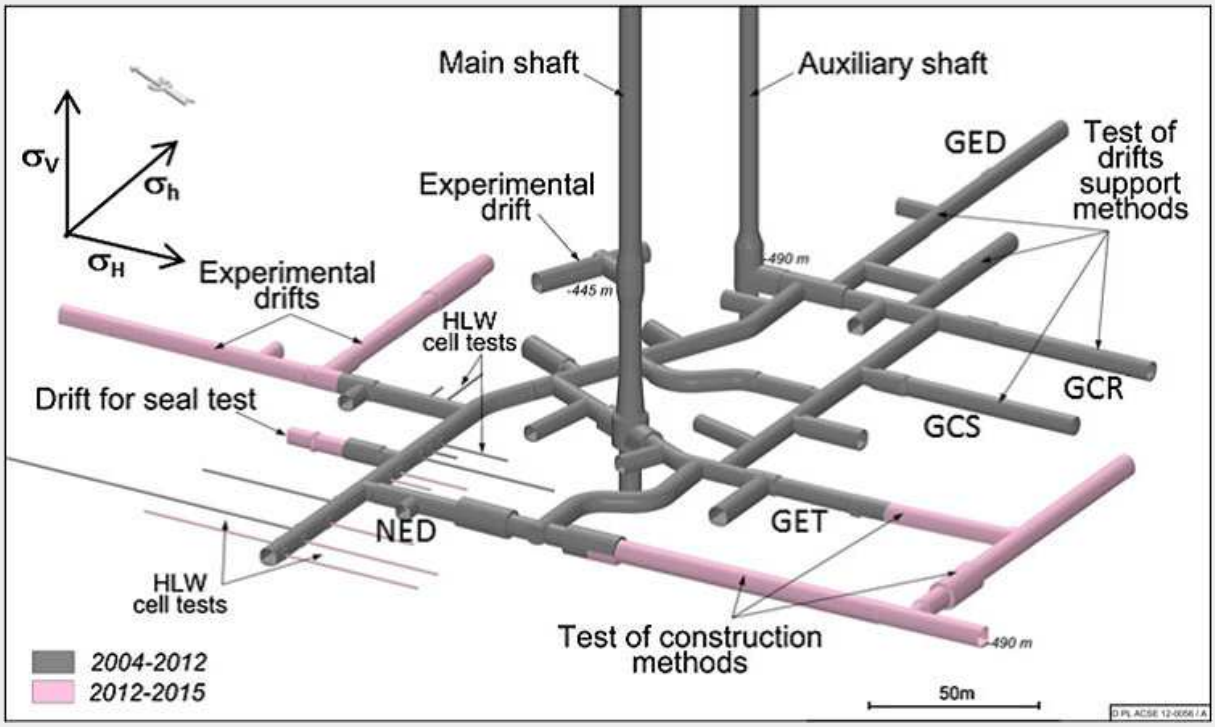

Figure 2.4: Meuse/Haute-Marne URL drifts network (grey: already excavated, pink: to be excavated) (Armand et al., 2014).

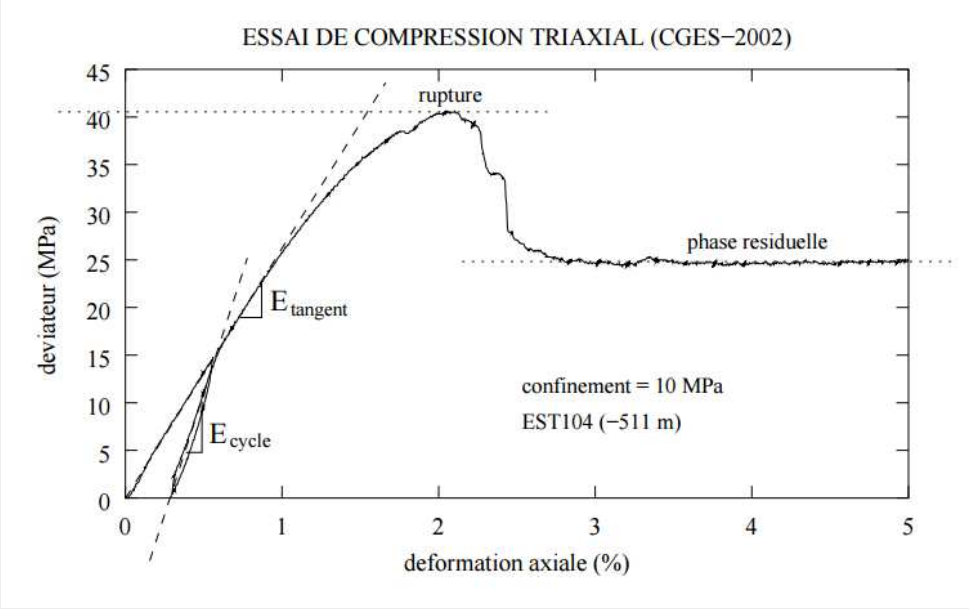

Figure 2.5: Deviator stress (deviateur) against axial deformation (deformation axiale) (Miehe, 2004).

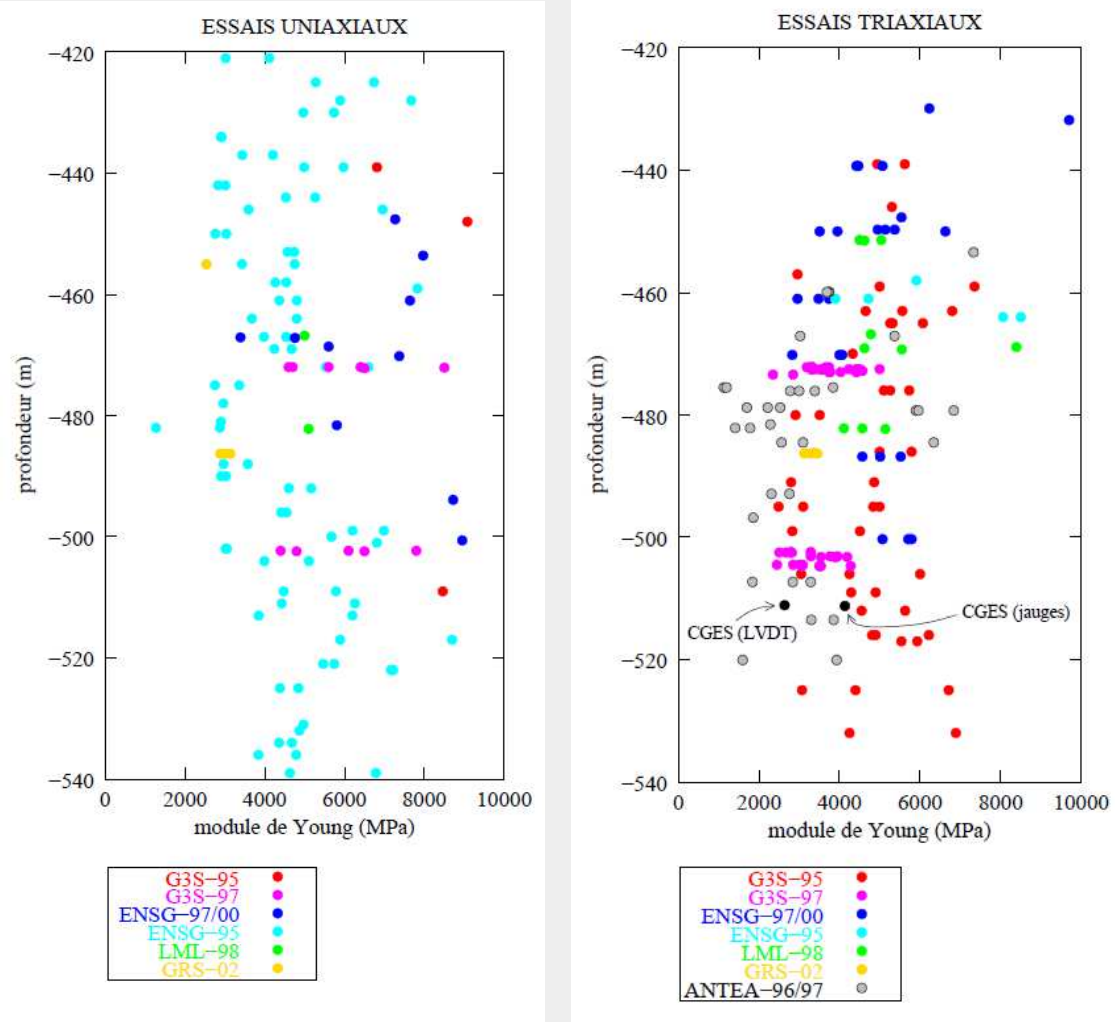

(a) Uniaxial tests

(b) Triaxial tests

Figure 2.6: Young's modulus (module de Young) versus the depth (profondeur) data obtained by different laboratories running (a) uniaxial tests and (b) triaxial tests (Miehe, 2004).

In the period 1995 to 2000, around 300 uniaxial and triaxial tests were conducted (Freissmuth, 2002; Miehe, 2004) by four different institutions (G3S, ANTEA, ENSG and LML).

Miehe (2004) analysed the results obtained from the tests with specific reference to their variation. The Young's modulus, the Poisson ratio and the failure (peak) strength were determined in relation to an elastic-plastic model taking post rupture softening into account. Figure 2.6 illustrates the variation of the Young's modulus with depth obtained by a variety of different laboratories running uniaxial and triaxial tests. The spread for both charts is in the range of about 400% between the minimum and the maximum values obtained. The values determined do not allow a reliable interpretation of a depth based Young's modulus, as the variation is too strong.

Miehe (2004) also found a strong variation of the shear strength results between the different labs. He concluded that this dispersion might be due to differing storage and testing procedures in the labs that fostered physico-chemical solid liquid reactions (Figure 2.7). For example, the shear strengths obtained by ANTEA were much lower than the results of the other laboratories. ANTEA resaturated the samples by using water, whereas the other laboratories used untreated samples

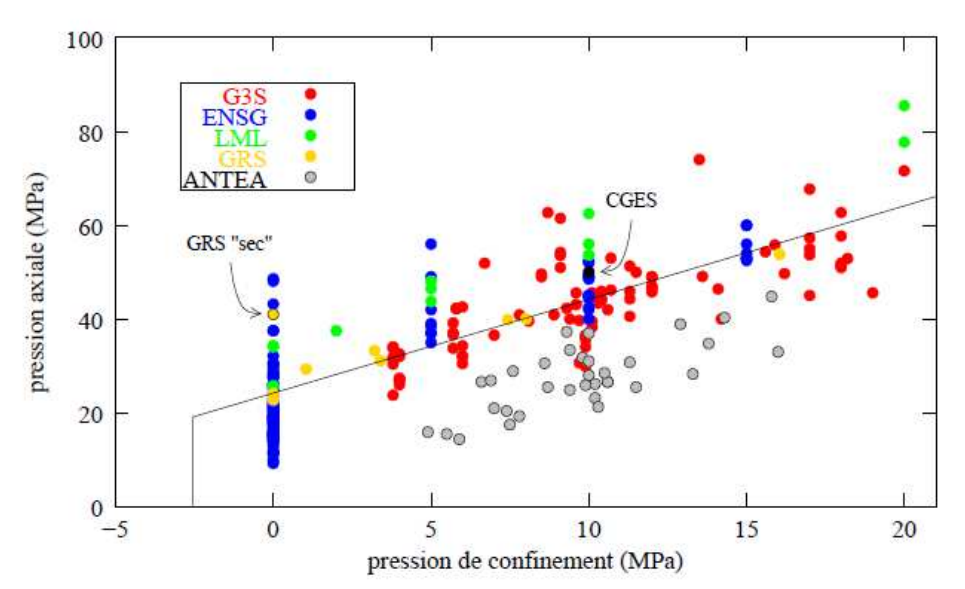

Figure 2.7: Shear strength in terms of axial stress (pression axiale) against the confining pressure (pression de confinement) obtained by triaxial tests (Miehe, 2004).

without resaturation. The results of LML show, in general, higher values than those of the other institutions. A possible explanation is the usage of slower load rates, relaxation-load cycles and drained conditions during the tests, which may have led to a higher mechanical resistance. However, all values are relatively consistent with the interpretation of an average Mohr-Coulomb criteria as shown in the figure. It can be seen, however, that even within the data from the same laboratory, a considerable spread is found.

A compilation of hydro-mechanical property values found for COx clay from literature is presented in Table 2.1.

Table 2.1: COx clay property values governing the hydro-mechanical behaviour.

Definition	Symb.	Unit	Range ⟨min;max⟩		μ	σ	Depth		Test[1]	Location	Note	Source
Density	ρ	g cm^{-3}		-	2.39			-490		Meuse/Haute-Marne		Armand et al. (2014)
			2.38	2.44	2.41±0.03		-434	-506	7	MHM		Zhang and Rothfuchs (2004)
					2.42	0.05	-420	-460		MHM	Upper zone	Hoteit et al. (2000)
					2.42	0.05	-460	-515		MHM	Median zone	Hoteit et al. (2000)
					2.46	0.05	-515	-550		MHM	Lower zone	Hoteit et al. (2000)
Porosity	n	–	14%	21%	18±1%			-490		MHM		Armand et al. (2014)
					15%							Wileveau and Bernier (2008)
			15%	19.2%	16.8±2.0%		-434	-506	7	MHM		Zhang and Rothfuchs (2004)
Young's modulus	E	MPa			4000±1470			-490		MHM		Armand et al. (2014)
					4000					MHM		Wileveau and Bernier (2008)
					5500–7500		-434	-506		MHM		Zhang and Rothfuchs (2004)
					5837	2455	-420	-460		MHM	Upper zone	Hoteit et al. (2000)
					4723	1218	-460	-515		MHM	Median zone	Hoteit et al. (2000)
					6118	1550	-515	-550		MHM	Lower zone	Hoteit et al. (2000)
Poisson's ratio	ν	–			0.29±0.05			-490		MHM		Armand et al. (2014)
					0.3			-490		MHM		Wileveau and Bernier (2008)
Uniaxial compressive strength	UCS	MPa			21±6.8			-490		MHM		Armand et al. (2014)
					24.5		-434	-506		MHM		Zhang and Rothfuchs (2004)
					27	9.5	-420	-460		MHM	Upper zone	Hoteit et al. (2000)
					19	3.2	-460	-515		MHM	Median zone	Hoteit et al. (2000)
					21	3.6	-515	-550		MHM	Lower zone	Hoteit et al. (2000)
Permeability	k	m^2			5 ×10^{-20}			-490		MHM		Armand et al. (2014)
			5 × 10^{-19}	8 × 10^{-19}			-434	-506	7	MHM		Zhang and Rothfuchs (2004)
Saturated hydraulic conductivity	K_w	m s^{-1}			1 × 10^{-13}			-490		MHM		Wileveau and Bernier (2008)
			5 × 10^{-14}	5 × 10^{-13}				-495				Tsang et al. (2012)
Water content	w	-	5%	8%	7.2±1.4%			-490		MHM		Armand et al. (2014)
			6.35%	8.93%	7.66±1.27%		-434	-506	7	MHM		Zhang and Rothfuchs (2004)
					6.1	1.5%	-420	-460		MHM	Upper zone	Hoteit et al. (2000)
					7.1	1.0%	-460	-515		MHM	Median zone	Hoteit et al. (2000)
					5.9	0.7%	-515	-550		MHM	Lower zone	Hoteit et al. (2000)
Friction angle	ϕ'	°			25							Wileveau and Bernier (2008)
					19		-434	-506		MHM		Zhang and Rothfuchs (2004)
Cohesion	c'	MPa			7							Wileveau and Bernier (2008)
					9		-434	-506		MHM		Zhang and Rothfuchs (2004)

[1] Test number

2.3 Swiss geological disposal programme

For the disposal of high-level radioactive waste, NAGRA have selected geological disposal in Opalinus Clay (OPA) as the disposal method to investigate. An underground research laboratory, the Mont Terri site, has been constructed to allow detailed investigation of the geological environment and to assess the long-term behaviour. The site is located near the town of St. Ursanne in the Jura Mountains of north-western Switzerland (Figure 2.8, Corkum and Martin, 2007b).

2.3.1 Geological environment

Mont Terri is an asymmetrical anticline folded during the late Miocene to Pliocene period as shown in the geological section in Fig. 2.9(a). The stratigraphy consists of competent limestones and incompetent marly/shaly formations. At the location of the underground laboratory the overburden varies between 230 and 320 m (Bossart et al., 2002) and where the stratigraphy generally dips about 45° to the southeast (Corkum and Martin, 2007a). The OPA is immediately overlain by a limestone layer and underlain by marly units. Where it intersects the laboratory, the OPA is about 250m thick along the length of the tunnel. There are three main parts of the OPA with differing properties: a sandy part, a carbonate-rich sandy part and a shaly part, the latter being of most interest for repository construction. The ED-B tunnel (to be investigated in Section 3.4.1) is located entirely within the shaly part. One major fault zone runs through the laboratory south of the ED-B tunnel (see Fig. 2.9(b)) and a number of discrete minor faults and joint sets have been observed throughout the tunnel system.

2.3.2 Mechanical properties

The mechanical property ranges and best estimates of OPA are listed in Table 2.2. It is noted that the mechanical properties are highly anisotropic.

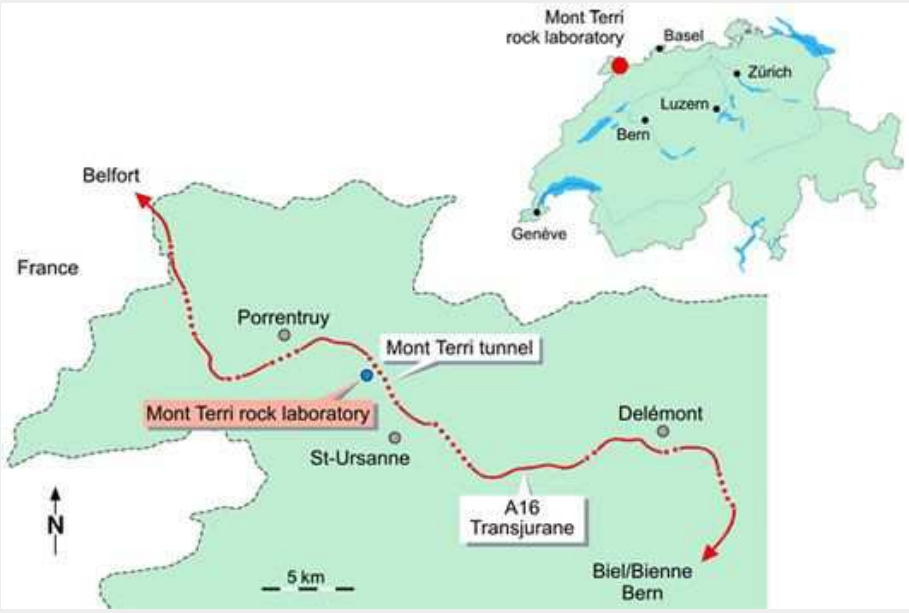

Figure 2.8: Geographic location of the Mont Terri rock laboratory site (Corkum and Martin, 2007b).

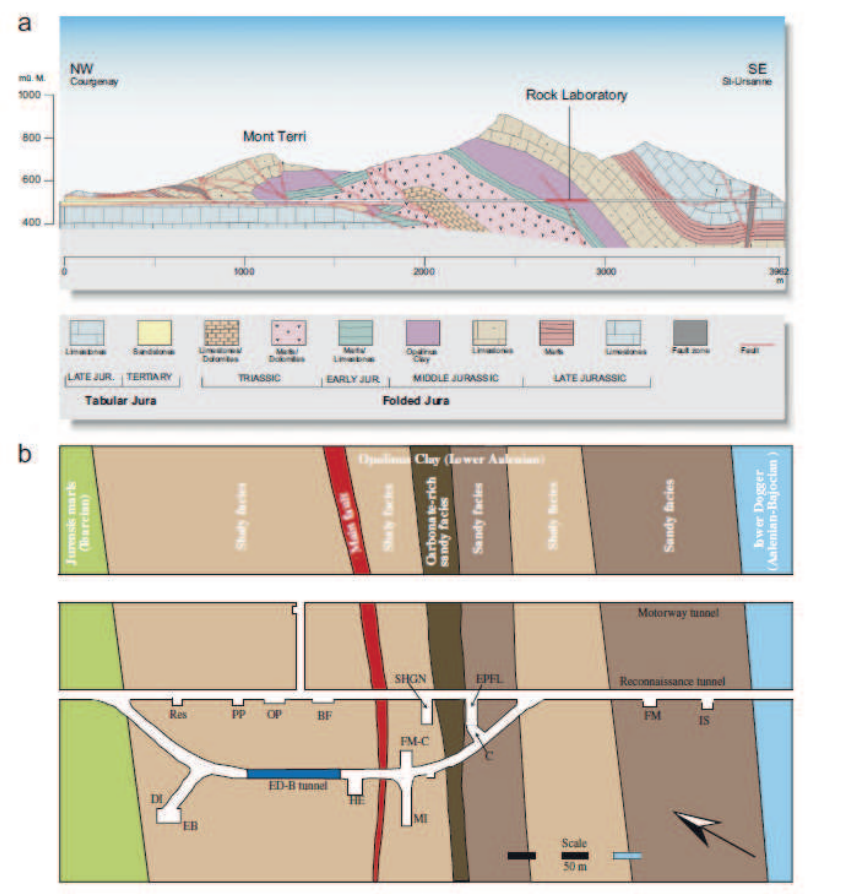

Figure 2.9: (a) Geological section along A16 Transjurane motorway, and (b) Geological map of the early part of the Mont Terri rock laboratory (Corkum and Martin, 2007a).

Table 2.2: Summary of OPA hydro-mechanical property values (Bossart and Thury, 2008).

Parameter	Unit	Range	Best estimate
Density, bulk saturated	g/cm^3	2.40 – 2.53	2.45
Water content, saturated wt	%	5.0 – 8.9	6.6
Porosity, total physical	vol%	14.0 – 24.7	18.3
Hydraulic conductivity	m/s	2×10^{-14} – 1×10^{-12}	2×10^{-13}
Young's modulus normal to bedding	MPa	2100 – 3500	2800
Young's modulus parallel to bedding	MPa	6300 – 8100	7200
Poisson's ratio normal to bedding	-	0.28 - 0.38	0.33
Poisson's ratio parallel to bedding	-	0.16 - 0.32	0.24
Uniaxial compressive strength normal to bedding	MPa	23.1 – 28.1	25.6
Uniaxial compressive strength parallel to bedding	MPa	4.0 – 17.0	10.5
Uniaxial tensile strength normal to bedding	MPa	-	1
Uniaxial tensile strength parallel to bedding	MPa	-	2
Cohesion	MPa	2.2 – 5	3.6
Internal friction angle	°	23 – 25	24

3 Numerical analysis

3.1 Methodology

Two numerical methods have been used in this investigation: an analytical model and a numerical model. The analytical model, developed and presented in Arnold et al. (2015), has the advantage of being extremely quick and therefore a thorough parametric analysis, i.e. a Monte Carlo analysis, can be undertaken. Numerical models, in this case PLAXIS (Plaxis, 2014), have the advantage of being able to simulate more complex stress states and material behaviour, but analyses are more computationally intensive.

As seen in Section 2.2.3, there is a considerable spread in calculated property values. Therefore, to understand the feasibility and performance of the tunnels, probabilistic calculations can be carried out to determine the probability of certain behaviour, e.g. unsatisfactory performance. Following the probabilistic assessment of Boom Clay behaviour in Arnold et al. (2015), this work aims to gain more confidence in the approach by utilising more comprehensive data available from other programmes.

Therefore in this work the following steps have been undertaken:

(i) Characterisation of the host rock properties, including variability where possible;

(ii) A numerical investigation using the analytical model and comparison against experimental observations, comprising:
   - Determinstic analyses, to understand the mechanical behaviour shown; and
   - Probabilistic (Monte Carlo) analyses, to understand the variability of the behaviour predicted.

(iii) A numerical investigation using the numerical finite element model and comparison against experimental observations, comprising:
   - Determinstic analyses, to understand the mechanical behaviour shown; and
   - Probabilistic (FORM) analyses, to understand the variability of the behaviour predicted.

A general description of the variation in stresses and material behaviour around a supported tunnel cavity is presented in Figure 3.1. Starting from in-situ stress conditions, the host rock will undergo elastic deformations until yielding occurs, with irreversible plastic deformations taking place in the closer vicinity of the tunnel. This plastic zone is made up of two parts, a residual plastic zone and a hardening or softening plastic zone. For more information on the models the reader is referred to Arnold et al. (2015).

3.2 Probabilistic methods

In Arnold et al. (2015) the probabilistic response was calculated by use of a Monte Carlo (MC) analysis, and the First or Second Order Reliability Method (FORM or SORM) was used to estimate the limit state surface which was then used to calculate the importance of the various parameters in the analysis. The limit state surface is a surface, in this case defined in standard normal space, which separates the failure domain from the non-failure domain. In this work, the same methodology

has been used, but in addition a response surface approach has also been used, which allows a further reduction in computation. More details of the limit state and response surfaces can be found in the OpenTURNS (2016) documentation.

FORM/SORM

In FORM and SORM the limit state surface is estimated using a polynomial function of first and second order, respectively. A design point is defined, where the FORM or SORM polynomial is centred, and this point is defined as the closest point (in standard normal space) to the mean response. The probabilities of failure can then be estimated by quantifying the relative size of the failure and non-failure domains. This method allows a significantly reduced amount of analyses to be undertaken than a complete Monte Carlo analysis (see Arnold et al. (2015) for more details and a comparison of the accuracy).

Once the limit state surface has been estimated, the relative importance of the input parameters can be determined, by using so-called importance factors. As an example, a summary of FORM importance factors is given below. These importance factors offer a way to quantify the importance of the input components with respect to the threshold exceedance by their influence on the quantity of interest. They are defined as

$$\gamma_i^2 = \frac{s_i^2}{\|s\|^2} \tag{3.1}$$

where

$$s_i = \frac{\partial \beta}{\partial x_i}(x^*) = \sum_{j=1}^{n} \frac{\partial \beta}{\partial u_j} \frac{\partial u_j}{\partial x_i}(x^*) \tag{3.2}$$

where β is the reliability index, u is the reduced random variable (in standard normal space), x is the physical random variable and x^* is the design point in the physical space. Note that $\sum_{i=1}^{n} \gamma_i^2 = 1$.

They are often interpreted also as indicators of the impact of modeling the input components as random variables rather than deterministic values. They can be seen as a specific sensitivity analysis technique dedicated to the quantity of interest around a particular threshold.

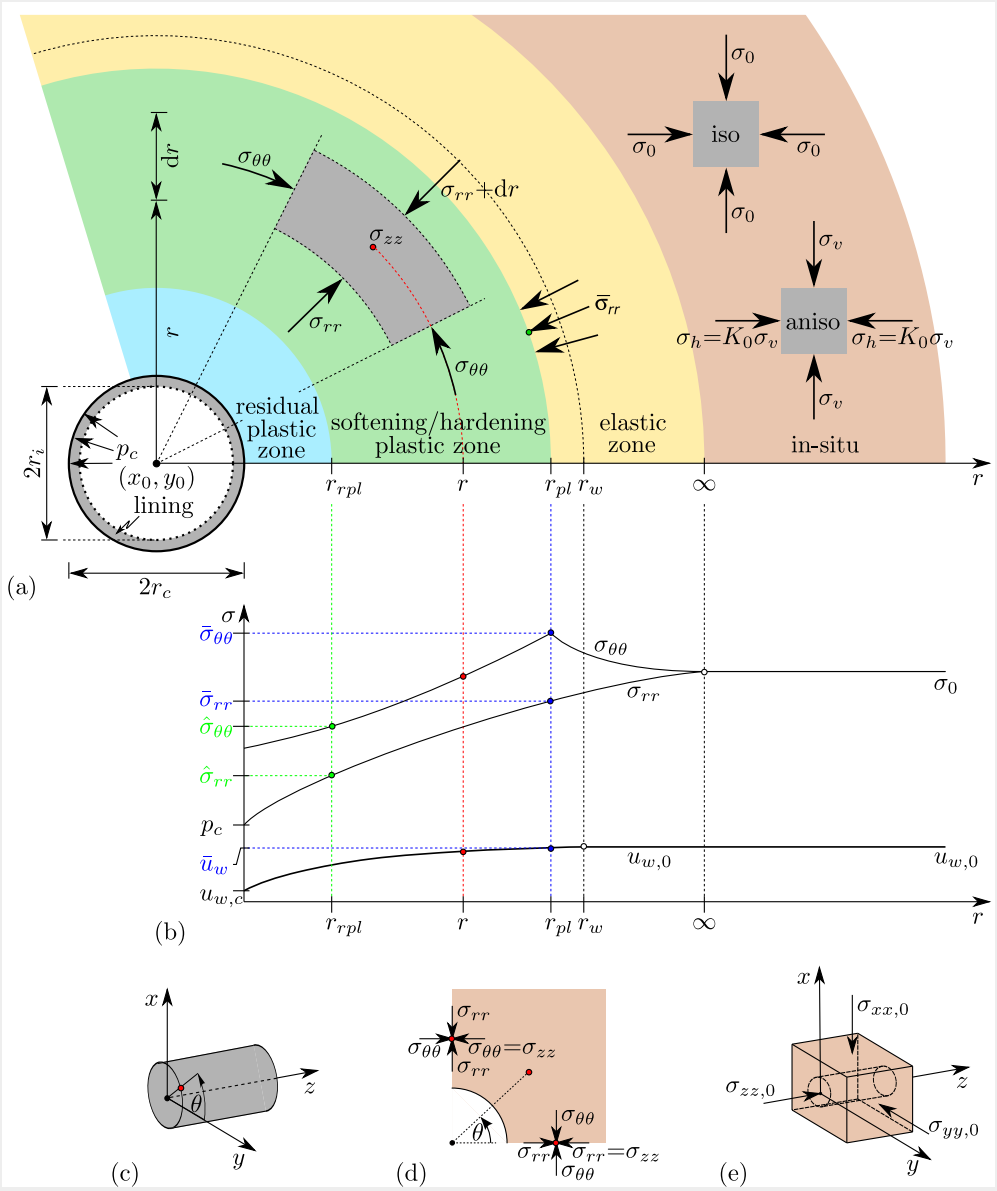

Figure 3.1: (a) Schematic description of stresses around a cavity opening (Arnold et al., 2015), where r_c is the excavated cavity radius, r_i is the target inner tunnel radius, p_c is the cavity pressure (i.e. acting on the liner), r is the radial polar coordinate of a point in the surrounding subsoil, r_p is the plastic (yield) radius, r_{rp} is the residual plastic radius in which the material reached the residual state, r_w is the radius beyond which the pore water pressure is not influenced by the cavity, σ_{rr} is the total radial stress, $\sigma_{\theta\theta}$ is the total tangential stress, σ_{zz} is the total axial stress, $\bar{\sigma}_{rr}$ is the total radial stress at the initial yield interface, $\sigma_{h,0}$ and $\sigma_{v,0}$ are the total horizontal and vertical in-situ stresses, and K_0 is the earth pressure coefficient. (b) Associated stress in the subsoil where $\bar{\sigma}_{\theta\theta}$ is the total tangential stress at the yield interface, $\hat{\sigma}_{rr}$ and $\hat{\sigma}_{\theta\theta}$ are the total radial and tangential stress at the residual plastic interface, u_w is the pore water pressure, $u_{w,0}$ is the in-situ pore water pressure, $\bar{u}_w$ is the pore water pressure at yield and $u_{w,c}$ is the pore water pressure on the cavity. (c) Tunnel coordinates with θ being the angle of y-axis rotation. (d) Total stresses around cavity. (e) Boundary conditions with σ_0 being the total far-field stress in Cartesian directions.

Deterministic response surface method

The response surface method (RSM) is a technique proposed by Box and Wilson (1951) and it allows a further reduction in computation time. The basic idea of the response surface method is to approximate an unknown performance/response function, in terms of the input variables, by a simple nth order polynomial (Wong, 1985; Xu and Low, 2006). It is therefore a surrogate or meta model that mimics the behaviour of some simulation model.

When approximating the true performance function using a polynomial function, experiments or numerical analyses based on some simulation model are performed at various sampling points x_i, to determine the unknown coefficients in the approximate polynomial function. Usually, it is thought to be sufficient to take a second-order polynomial approximation function. Note that, although a higher order polynomial can improve the accuracy of the approximation, albeit with more computational effort, the system of equations for solving the coefficients can become ill-conditioned and higher order polynomial functions can exhibit erratic behaviour in the parts of the domain not covered by experiments or numerical analyses (Xu and Low, 2006).

For example, the following second-order polynomial function (Bucher and Bourgund, 1990), with interaction terms (i.e. $x_i x_j$, $i \neq j$), can be used:

$$\hat{g}(\mathbf{x}) = a_0 + \sum_{i=1}^{n_X} a_i x_i + \sum_{i=1}^{n_X} \sum_{j=1}^{n_X} a_{i,j} x_i x_j \tag{3.3}$$

where $\mathbf{x}$ is the random variable vector with components x_i ($i = 1, 2, \ldots, n_X$ and n_X is the number of random variables), $\hat{g}(\mathbf{x})$ is the approximate performance function and a_0, a_i and $a_{i,j}$ are the coefficients that need to be determined by experiments. First, the values at sampling points for each variable are selected; then the values of the function can be determined by carrying out a number of finite element analyses. The function at any point in the parameter space can then be estimated by fitting a second order polynomial to the sampling function values via least squares. The number of unknown coefficients is $P = 1 + n_X + n_X + C_{n_X}^2 = 1 + 2n_X + \frac{n_X!}{(n_X-2)!2!} = 1 + 2n_X + \frac{n_X(n_X-1)}{2}$, where C is the combination operator.

After the polynomial response surface is approximated, one can proceed with either Monte Carlo simulation by directly using the approximated function $\hat{g}$, or FORM analysis by constraining x_i on the explicitly approximated limit state surface $\hat{g}$. The advantage of using the response surface method is that an explicit performance function, which builds up the relationship between the input variables and the geotechnical system response, can be approximated. This function can later be used repeatedly in a structural response analysis avoiding the computationally expensive process of carrying out a detailed analysis by, for example, the nonlinear finite element method. However, this also means that the accuracy of the method relies on how close the true performance function is approximated.

Stochastic response surface method

A specific type of response surface, which allows more flexibility in functional form and propagates the random response from the input to the output is the stochastic response surface. It requires the representation of the random response in a suitable functional space, such as the Hilbert space (OpenTURNS, 2016). Specifically, this concerns an expansion of the model response onto an orthogonal basis, e.g. via polynomial chaos expansion (PCE).

The PCE of a response random variable $y(\mathbf{x})$ is:

$$y(\mathbf{x}) = \sum_{k=0}^{\infty} a_k \Phi_{\boldsymbol{\alpha}_k}(\mathbf{x}) \tag{3.4}$$

Table 3.1: Example of multivariate polynomials used in PCE, corresponding to $(p = 2, n = 3,\ P = 10)$ $(\Phi_0(x_i) = 1, i = 1, 2, 3)$ $(k = 0, 1, \ldots, 9)$.

Coefficients a_k	Order p_k	Multi-index vector $\boldsymbol{\alpha}_k$	Multivariate polynomial $\Phi_{\boldsymbol{\alpha}_k}(\mathbf{x}) = \prod_{i=1}^{3} \Phi_{\alpha_i^k}(x_i)$
a_0	$p_0 = 0$	$\boldsymbol{\alpha}_0 = [\alpha_1^0, \alpha_2^0, \alpha_3^0] = [0, 0, 0]$	$\Phi_{\boldsymbol{\alpha}_0}(\mathbf{x}) = \Phi_{\alpha_1^0}(x_1) \times \Phi_{\alpha_2^0}(x_2) \times \Phi_{\alpha_3^0}(x_3) = 1$
a_1	$p_1 = 1$	$\boldsymbol{\alpha}_1 = [\alpha_1^1, \alpha_2^1, \alpha_3^1] = [1, 0, 0]$	$\Phi_{\boldsymbol{\alpha}_1}(\mathbf{x}) = \Phi_{\alpha_1^1}(x_1) = \Phi_1(x_1)$
a_2	$p_2 = 1$	$\boldsymbol{\alpha}_2 = [\alpha_1^2, \alpha_2^2, \alpha_3^2] = [0, 1, 0]$	$\Phi_{\boldsymbol{\alpha}_2}(\mathbf{x}) = \Phi_{\alpha_2^2}(x_2) = \Phi_1(x_2)$
a_3	$p_3 = 1$	$\boldsymbol{\alpha}_3 = [\alpha_1^3, \alpha_2^3, \alpha_3^3] = [0, 0, 1]$	$\Phi_{\boldsymbol{\alpha}_3}(\mathbf{x}) = \Phi_{\alpha_3^3}(x_3) = \Phi_1(x_3)$
a_4	$p_4 = 2$	$\boldsymbol{\alpha}_4 = [\alpha_1^4, \alpha_2^4, \alpha_3^4] = [2, 0, 0]$	$\Phi_{\boldsymbol{\alpha}_4}(\mathbf{x}) = \Phi_{\alpha_1^4}(x_1) = \Phi_2(x_1)$
a_5	$p_5 = 2$	$\boldsymbol{\alpha}_5 = [\alpha_1^5, \alpha_2^5, \alpha_3^5] = [0, 2, 0]$	$\Phi_{\boldsymbol{\alpha}_5}(\mathbf{x}) = \Phi_{\alpha_2^5}(x_2) = \Phi_2(x_2)$
a_6	$p_6 = 2$	$\boldsymbol{\alpha}_6 = [\alpha_1^6, \alpha_2^6, \alpha_3^6] = [0, 0, 2]$	$\Phi_{\boldsymbol{\alpha}_6}(\mathbf{x}) = \Phi_{\alpha_3^6}(x_3) = \Phi_2(x_3)$
a_7	$p_7 = 2$	$\boldsymbol{\alpha}_7 = [\alpha_1^7, \alpha_2^7, \alpha_3^7] = [1, 1, 0]$	$\Phi_{\boldsymbol{\alpha}_7}(\mathbf{x}) = \Phi_{\alpha_1^7}(x_1) \times \Phi_{\alpha_2^7}(x_2) = \Phi_1(x_1) \times \Phi_1(x_2)$
a_8	$p_8 = 2$	$\boldsymbol{\alpha}_8 = [\alpha_1^8, \alpha_2^8, \alpha_3^8] = [1, 0, 1]$	$\Phi_{\boldsymbol{\alpha}_8}(\mathbf{x}) = \Phi_{\alpha_1^8}(x_1) \times \Phi_{\alpha_3^8}(x_3) = \Phi_1(x_1) \times \Phi_1(x_3)$
a_9	$p_9 = 2$	$\boldsymbol{\alpha}_9 = [\alpha_1^9, \alpha_2^9, \alpha_3^9] = [0, 1, 1]$	$\Phi_{\boldsymbol{\alpha}_9}(\mathbf{x}) = \Phi_{\alpha_2^9}(x_2) \times \Phi_{\alpha_3^9}(x_3) = \Phi_1(x_2) \times \Phi_1(x_3)$

where $\Phi_{\boldsymbol{\alpha}_k}(\mathbf{x}) = \Phi_{\boldsymbol{\alpha}_k}(x_1, x_2, \ldots, x_n)$ is the k-th multivariate polynomial in the series, corresponding to the k-th vector of indices $(\boldsymbol{\alpha}_k = [\alpha_1^k, \alpha_2^k, \ldots, \alpha_n^k], \alpha_i^k \in \mathbb{N}, i = 1, 2, \ldots, n)$. For the k-th vector of indices $\boldsymbol{\alpha}_k$, the k-th multivariate polynomial is

$$\Phi_{\boldsymbol{\alpha}_k}(\mathbf{x}) = \prod_{i=1}^{n} \Phi_{\alpha_i^k}(x_i) \tag{3.5}$$

where $\Phi_{\alpha_i^k}(x_i)$ is the univariate polynomial of degree α_i^k.

Let p_k be the sum of the indices in the multi-index vector $\boldsymbol{\alpha}_k$, that is $p_k = \sum_{i=1}^{n} \alpha_i^k$. In practical applications, the series of Eq. 3.4 is truncated to a degree of p, i.e. $p_k \leq p$. As an illustration, Table 3.1 lists all the multivariate polynomials corresponding to $(p = 2, n = 3)$, ordered such that $p_k \leq p_{k+1}$.

The total number of terms (P) in the truncated expansion is

$$P = \frac{(p+n)!}{n!p!} \tag{3.6}$$

The truncated series takes the form:

$$\hat{y}(\mathbf{x}) = \sum_{k=0}^{P-1} a_k \Phi_{\boldsymbol{\alpha}_k}(\mathbf{x}) = \Phi(\mathbf{x})\mathbf{a} \tag{3.7}$$

where $\mathbf{a} = [a_0, a_1, \ldots, a_{P-1}]^T$ and $\Phi(\mathbf{x}) = [\Phi_{\boldsymbol{\alpha}_0}(\mathbf{x}), \Phi_{\boldsymbol{\alpha}_1}(\mathbf{x}), \ldots, \Phi_{\boldsymbol{\alpha}_{P-1}}(\mathbf{x})]$ are the vectors of the PCE coefficients and of the multivariate polynomials evaluated at $\mathbf{x}$.

3.3 Investigation of tunnels in COx

3.3.1 Modelled experiment: The GCS drift

The GCS drift (see Figure 2.4) has been selected as the case study. It has a circular section with a radius of 2.6 m. It was excavated with a road header and shotcrete was applied shortly after excavation. An over excavation (overcut) of 15 mm is used in the simulation (Armand et al., 2013).

The support (fiber shotcrete) is 21 cm thick (Guayacán-Carrillo et al., 2016). The drift is parallel to the major horizontal stress σ_H and the initial in-situ stress state is quasi-isotropic ($\sigma_H = 16.12$ MPa, $\sigma_h = \sigma_v = 12.4$ MPa) (MartÃηn et al., 2011) (see Fig. 2.4 for the their notation, this corresponds to $\sigma_h = 12.4$ MPa and $\sigma_v = 16.12$ MPa seen in Fig. 3.2). A pore water pressure of $u_{w,0} = 4.5$ MPa is used at a depth of 490 m.

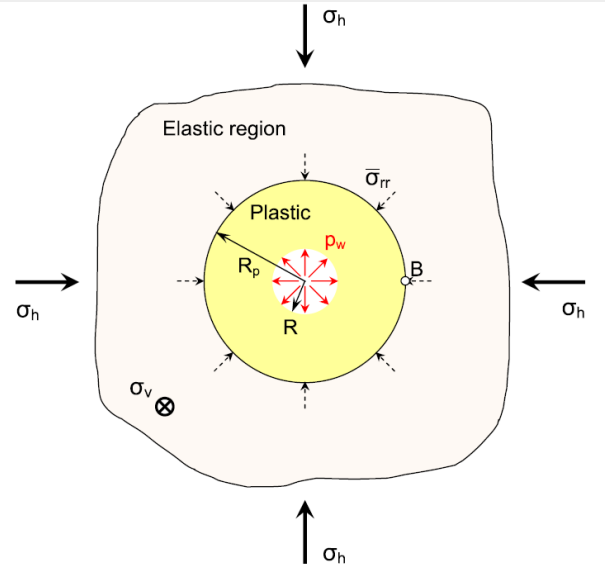

Figure 3.2: Circular deep tunnel with axisymmetric loading.

3.3.2 Probabilistic interpretation of the test results

The data from different laboratories showed considerable variability. This will be interpreted probabilistically in this section to obtain the point statistics that will be used in the Monte Carlo simulation in the next section. Fig. 3.3 shows the peak and residual strength of the COx clay at MHM URL from ANDRA and GRS (Zhang and Rothfuchs, 2004). Based on the values σ_1 and σ_3 (the major and minor principle stresses), the Mohr circles at failure for pairs of tests are plotted. Then a straight line that is tangential to the two circles is defined (i.e. the failure envelope defining c and ϕ, see Fig. 3.4). In this way, multiple envelope lines can be defined, resulting in a range of values for c_0 and ϕ using the peak strength and c_r and ϕ for the residual state. The distributions of ϕ, c_0 and c_r are shown in Figures 3.6 and 3.7, with a fitted normal distribution, reported in Table 3.2 in terms of the means (μ), standard deviations (σ) and the coefficients of variation (cov). A normal distribution is seen to fit to the data reasonably well. Note that the distance between the circle centres is set to be larger than 10 MPa to ensure reliable failure envelopes.

The elastic modulus and Poisson's ratio versus depth data for COx claystones from different laboratories (G3S, ENSG, LML, GRS, ANTEA) are shown in Figure 3.8. These data have also been processed probabilistically to define the point statistics for E and ν (Figure 3.9). It is seen that the depth dependency is relatively small compared to the magnitude of the two parameters. Therefore, data detrending has not been carried out before deriving the point statistics. A summary of the point statistics describing the properties of COx claystones at MHM URL is shown in Table 3.2. Note that the mean of the tangential modulus is assumed to be approximately half that of the elastic modulus and the COV is assumed to be the same, as little data are available about the tangential modulus.

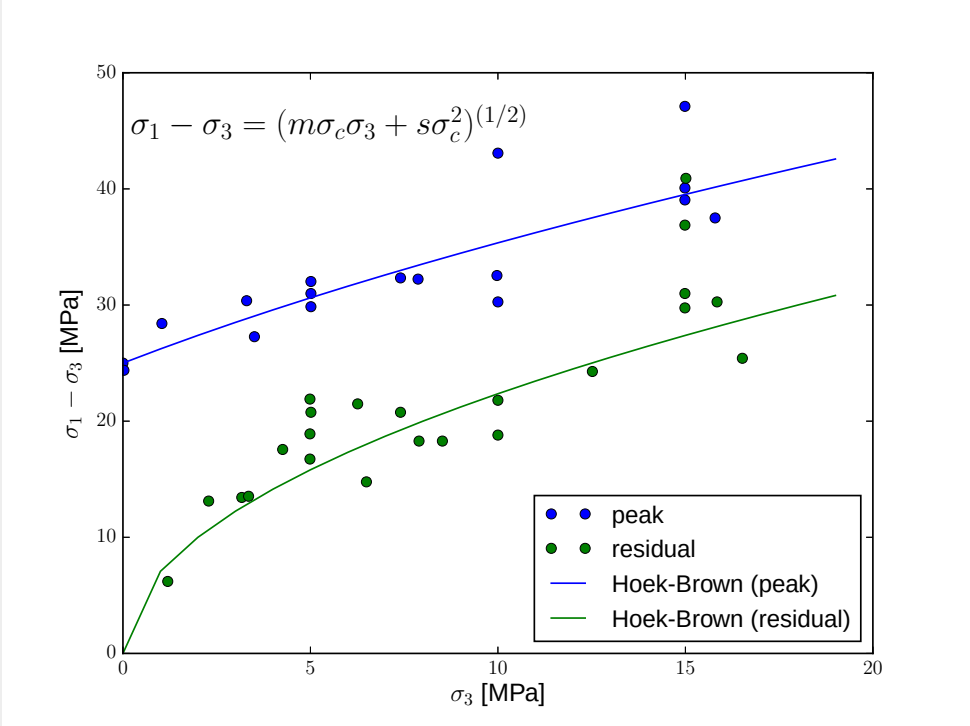

Figure 3.3: Peak and residual strength of the Callovo-Oxfordian argillite at MHM-URL (after Zhang and Rothfuchs, 2004).

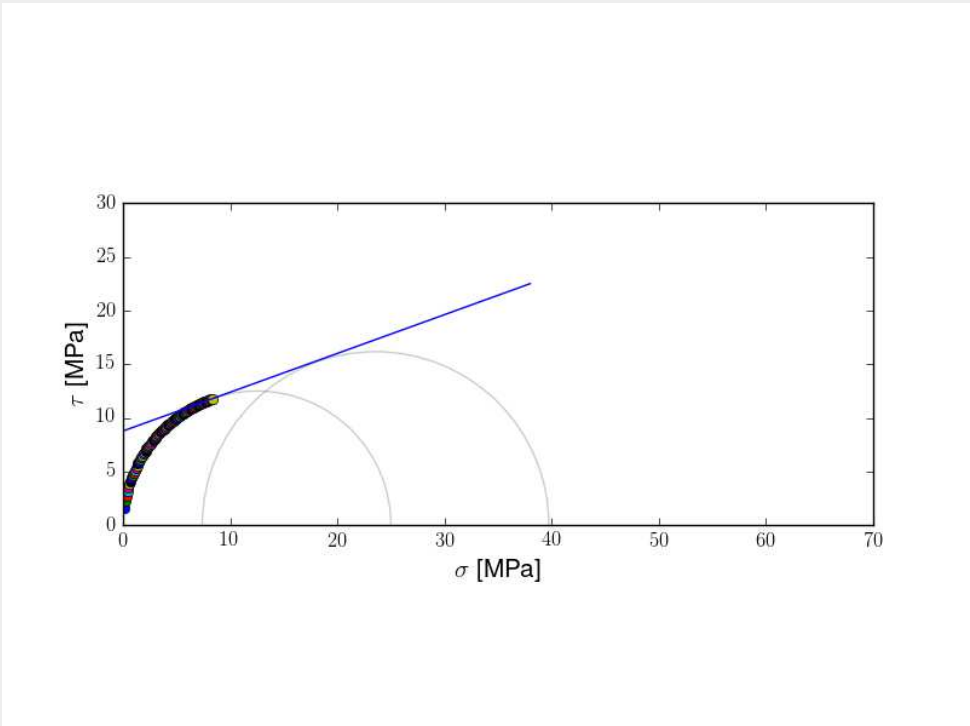

Figure 3.4: Example illustration of the searching algorithm for the failure envelope for a pair of Mohr circles defined by centre $((\sigma_1 + \sigma_3)/2,\ 0)$ and radius $r = (\sigma_1 - \sigma_3)/2$. The points on the left circle represent the searching path.

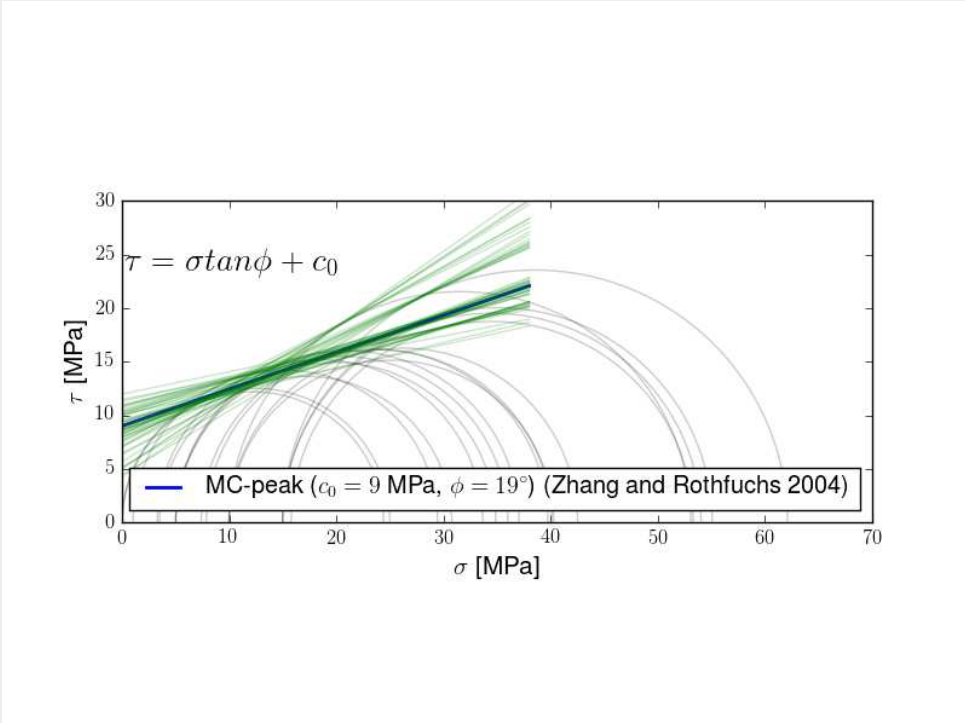

Figure 3.5: Mohr circles (grey) and failure envelopes (green) reinterpreted from Fig. 3.3 for the initial failure, after Zhang and Rothfuchs (2004).

Table 3.2: Point statistics describing the properties of COx claystones at MHM URL.

Variable X	Symbol	Unit	μ_X	$Cov(X) = \sigma_X/\mu_X$	Distribution type
Initial cohesion	c_0	MPa	8.6	0.21	Normal
Residual cohesion	c_r	MPa	3.3	0.43	Normal
Friction angle	ϕ	°	20.7	0.29	Normal
Young's modulus	E	MPa	4257	0.34	Normal
Tangent modulus	E_t	MPa	2100	0.34	Normal
Poisson's ratio	ν	-	0.29	0.28	Normal

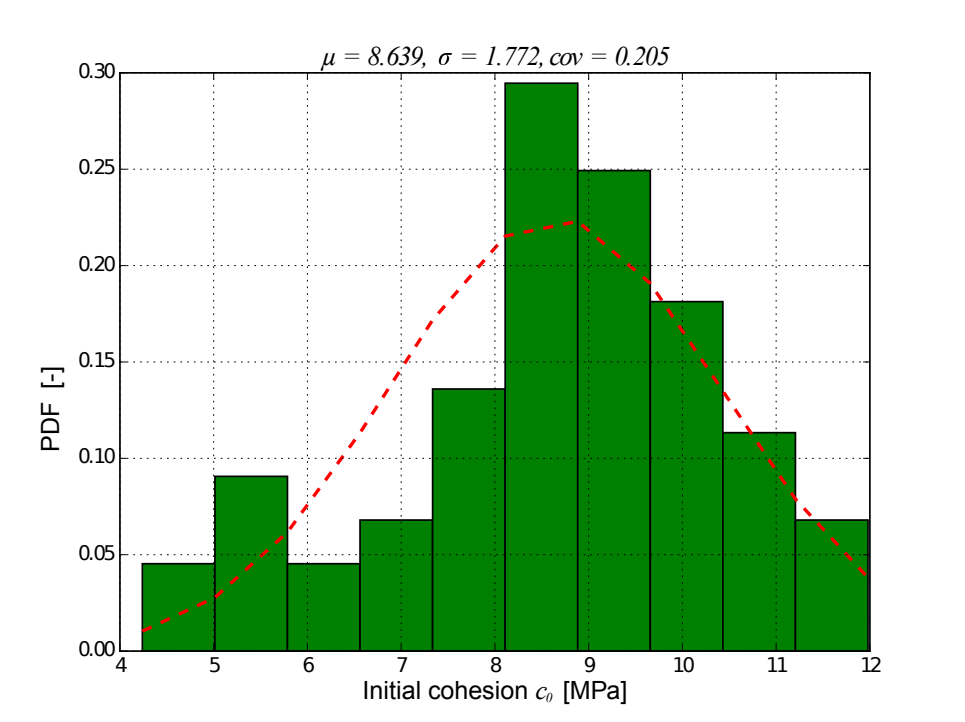

(a) Initial cohesion

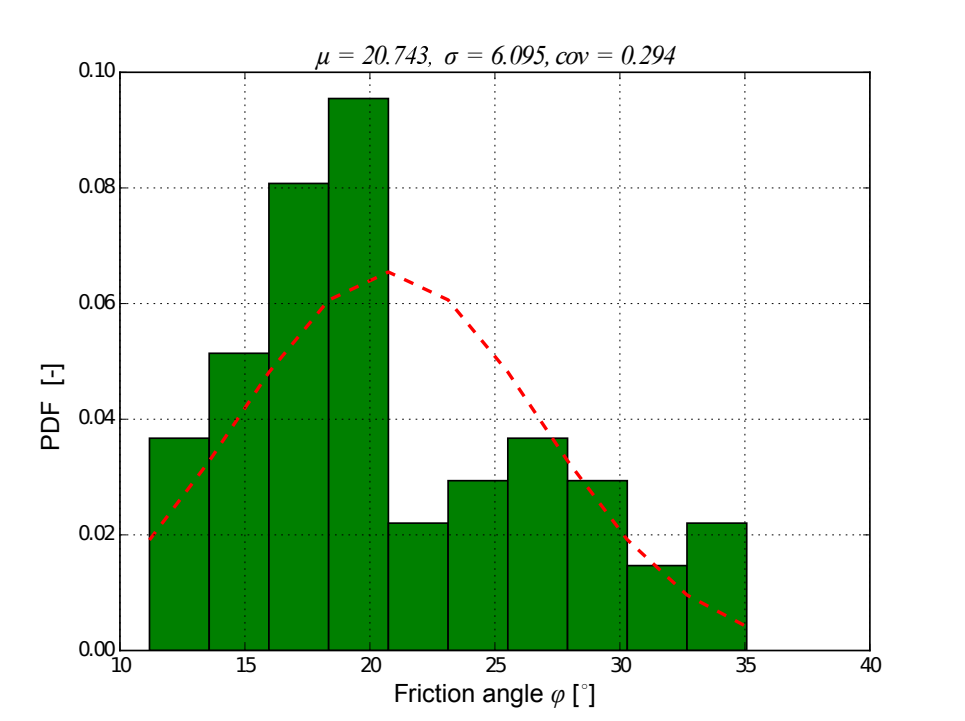

(b) Friction angle

Figure 3.6: Normalised histograms and fitted probability density functions (pdf) for variables c_0, ϕ.

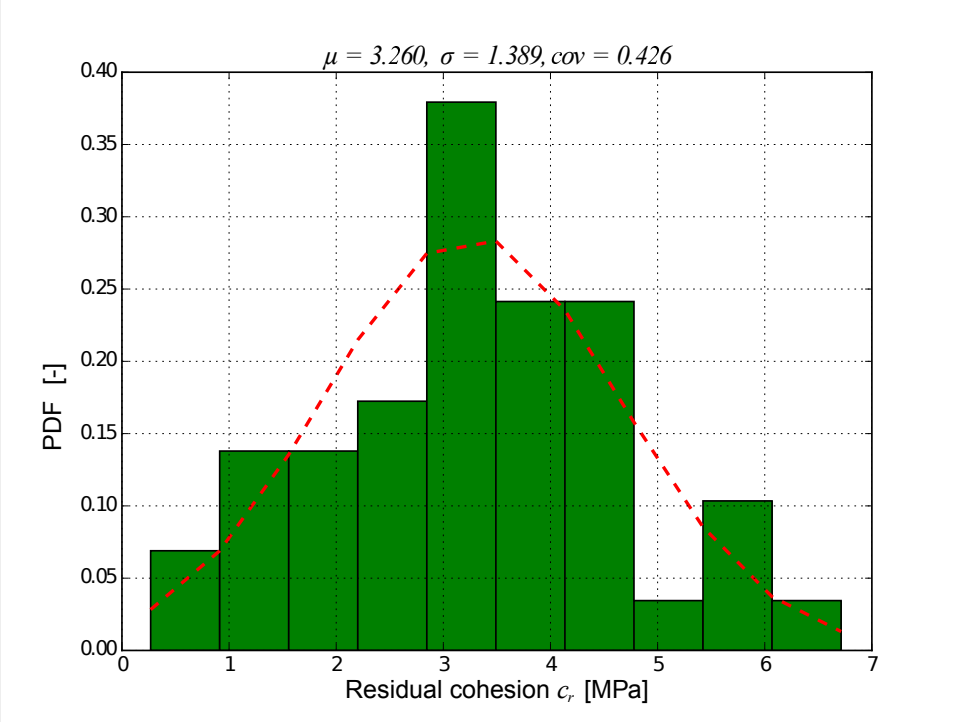

Figure 3.7: Normalised histograms and fitted probability density functions (pdf) for variable c_r.

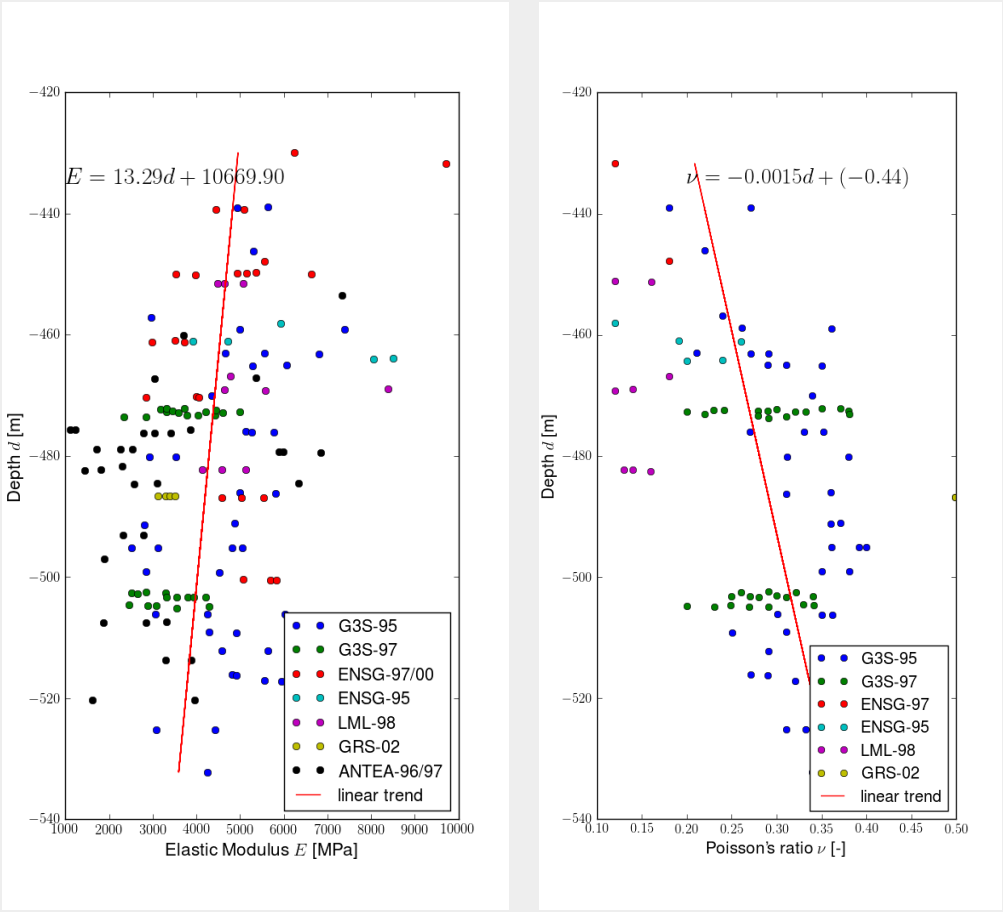

(a) Elastic modulus

(b) Poisson's ratio

Figure 3.8: Elastic modulus and Poisson's ratio versus depth for COx claystones from different laboratories (digitised from Miehe 2004, linear trend line added).

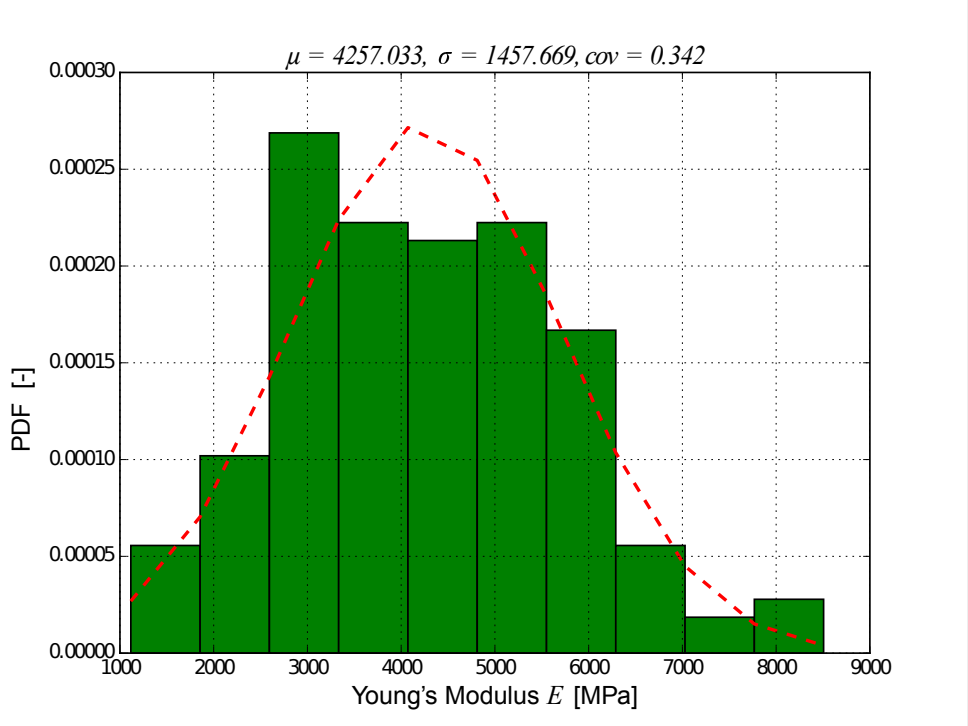

(a) Elastic modulus

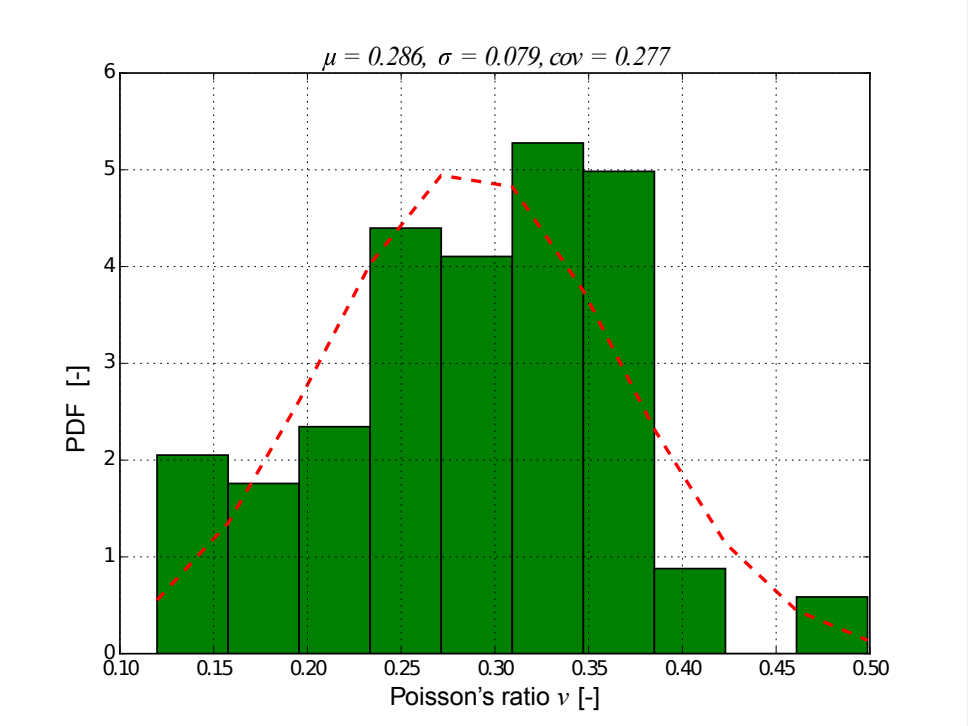

(b) Poisson's ratio

Figure 3.9: Normalised histograms and fitted probability density functions (pdf) for variables E, ν.

3.3.3 Analytical model investigation

Deterministic analysis

By comparing the reported values in literature (presented in Table 2.1) and those calculated here (presented in Table 3.2), it can be seen that the mean value of initial cohesion $\mu_{c_0} = 8.6$ MPa is within the range of 7 MPa (Wileveau and Bernier, 2008) and 9 MPa (Armand et al., 2014), and the mean value of friction angle $\mu_\phi = 20.7°$ is within the range of 19° (Armand et al., 2014) and 25° (Wileveau and Bernier, 2008). The deterministic results based on the mean property values are shown in Fig. 3.10 and the radial displacements are compared to the measurements (Armand et al., 2013).

Two analytical solutions were undertaken based on two values of E, one based on the mean value from Table 3.2, $\mu_E \approx 4300$ MPa; the other based on the lower bound recommendations by Armand et al. (2014), where $E \approx \mu_E - \sigma_E = 4000 - 1470 = 2500$ MPa. It is seen that the results bracket the measurements well.

The displacements further away from the tunnel match the stiffer analysis (using the mean Young's modulus) better and closer to the tunnel the less stiff analysis (using the lower bound value) match better, suggesting that some level of hardening or plasticity is seen. The model used here does not include hardening and focuses on the softening behaviour. The hardening behaviour will be investigated in Section 3.3.4 using the numerical model.

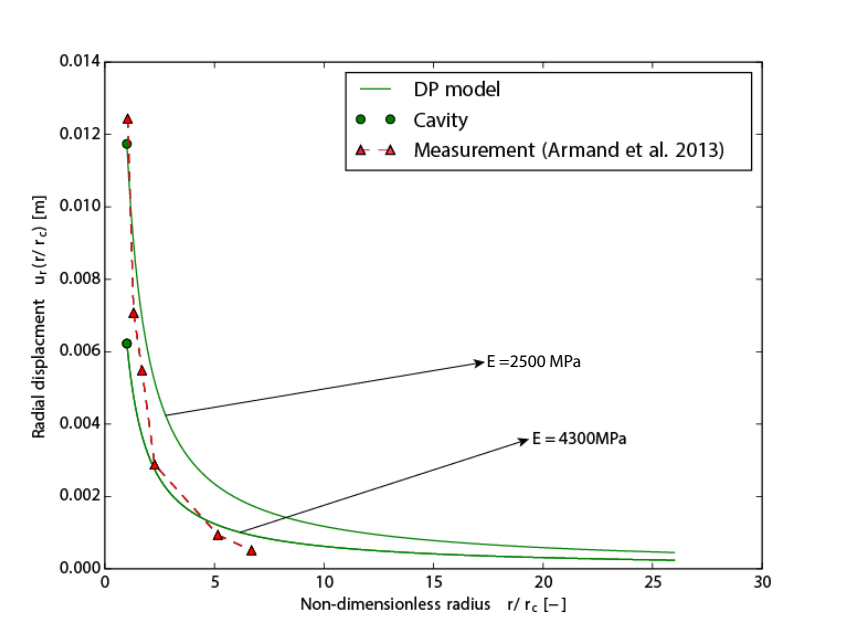

Figure 3.10: Deterministic radial displacement for GCS drift based on two values of E and the mean property values (μ_X) shown in Table 3.2.

Figs. 3.11, 3.13 and 3.15 show the total stress distributions around the excavated cavity for GCS drift (impermeable concrete liner), based on the three cases: (1) the mean property values (μ_X) shown in Table 3.2; (2) c_0 and ϕ values of $\mu_X - 2\sigma_X$ and other property values of μ_X, and (3) c_0 of $\mu_X - 2\sigma_X$, ϕ of $\mu_X - 3\sigma_X$ and other property values μ_X . Figs. 3.12, 3.14 and 3.16 show the stress path at the cavity surface for GCS drift, based on the same cases. It is seen that the cavity exhibits elastic behaviour for the first case, elasto-plastic behaviour (i.e. a softening plastic zone around the close vicinity of the cavity appears) for the second case when the effective strength parameters (c_0 and ϕ) take lower values, and residual plastic behaviour (i.e. a residual plastic zone appears inside the softening plastic zone) for the third case when the friction angle reduces further. The (softening)

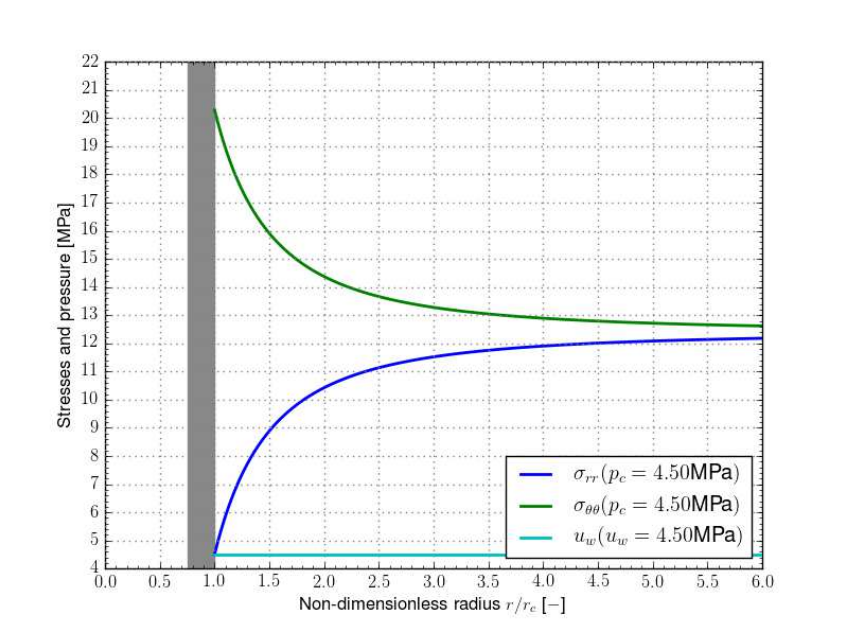

Figure 3.11: Deterministic total stress distributions around the excavated cavity for GCS drift (impermeable concrete liner), based on the mean property values (μ_X) shown in Table 3.2.

plastic and residual plastic radius (r_p and r_{rp}) are also shown in the figures, and they indicate the potential range of plastic zones (i.e. the possible extent of excavation disturbed/damaged zone).

Comparing the central numerical simulation (i.e. Figure 3.11) with Chapter 5 of Miehe (2004), the results match well both qualitatively and quantitatively. The reduction in c and ϕ (i.e. Figures 3.13–3.16) shows the possibility that the claystone in the vicinity of the opening goes to softening plastic (and residual plastic) conditions upon excavation of the tunnel. This will be demonstrated in the following Monte Carlo simulation, where various combinations of material parameters are possible and thereby the possibility of the material going to softening plastic (see Figure 3.17) and the probability of exceeding some value of softening plastic zone (and residual zone) will be investigated and presented. Note that, the predicted elastic response for the central analytical analysis does not mean there is no plasticity occurring (it only means no softening plasticity) due to the model formulation, as the investigation shown in Fig. 3.10 indicates some level of hardening.

Probabilistic analysis (Monte Carlo)

The statistics in Table 3.2 are used in the MC simulation in this section, assuming truncated normal distributions where required due to physical limitations (e.g. ν is in the range of 0.0 to 0.5) and a softening material behaviour before reaching the residual state (i.e. $c_0 \geq c_r$).

The results based on $N_r = 25000$ realisations are shown in Fig. 3.17 and 3.18 for the uncorrelated case (i.e. $\rho_{X_i,X_j}(i \neq j) = 0.0$). The exceedance probability is computed as

$$P[g(\mathbf{x}) \geq 0] = P[r_p \geq r_{p,lim}] = N_f/N_r \tag{3.8}$$

where P[-] is the probability of an event, $g(\mathbf{x}) = r_p - r_{p,lim}$ is the performance function of variables $\mathbf{x} = (x_1, x_2, \ldots, x_6) = (c_0, c_r, \phi, E, E_t, \nu)$, N_f indicates the number of realisations for which the plastic radius r_p is larger than, or equal to, a certain threshold value of the plastic radius $r_{p,lim}$ and N_r is the total number of MC realisations.

It is seen in Fig. 3.17 that the plastic radius can develop as far as $r_p \approx 4$ m (i.e. $r_p - r = 0.54r$)

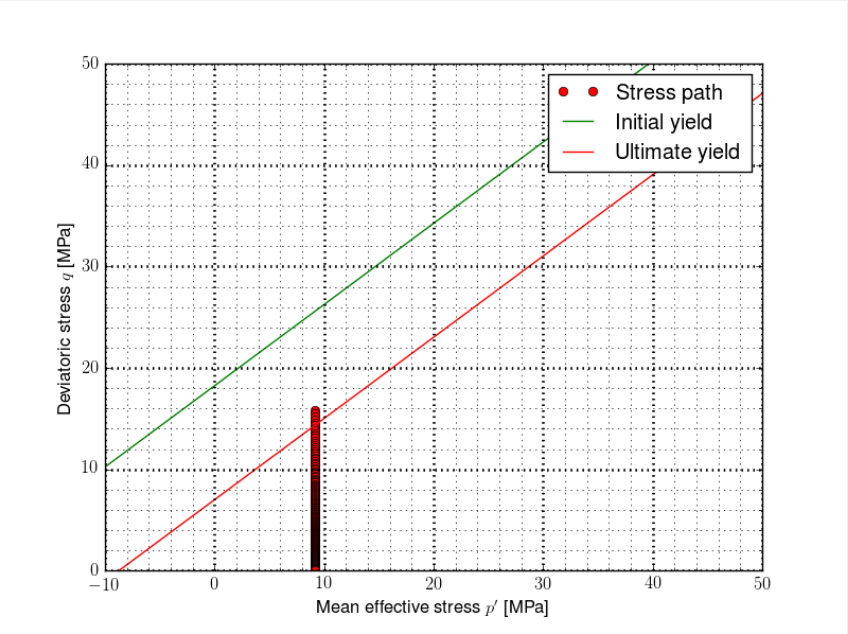

Figure 3.12: Deterministic stress path at cavity surface for GCS drift, based on the mean property values (μ_X) shown in Table 3.2.

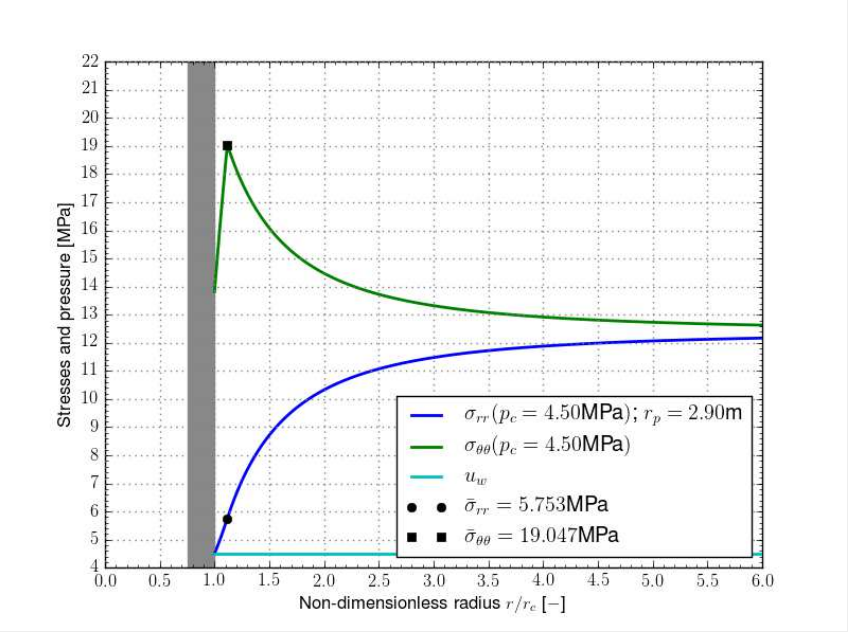

Figure 3.13: Deterministic total stress distributions around the excavated cavity for GCS drift (impermeable concrete liner), based on c_0 and ϕ values of $\mu_X - 2\sigma_X$ and the other propertiy values of μ_X; $\bar{\sigma}$ denotes the stresses at the elastic-plastic interface, r_p is the plastic radius.

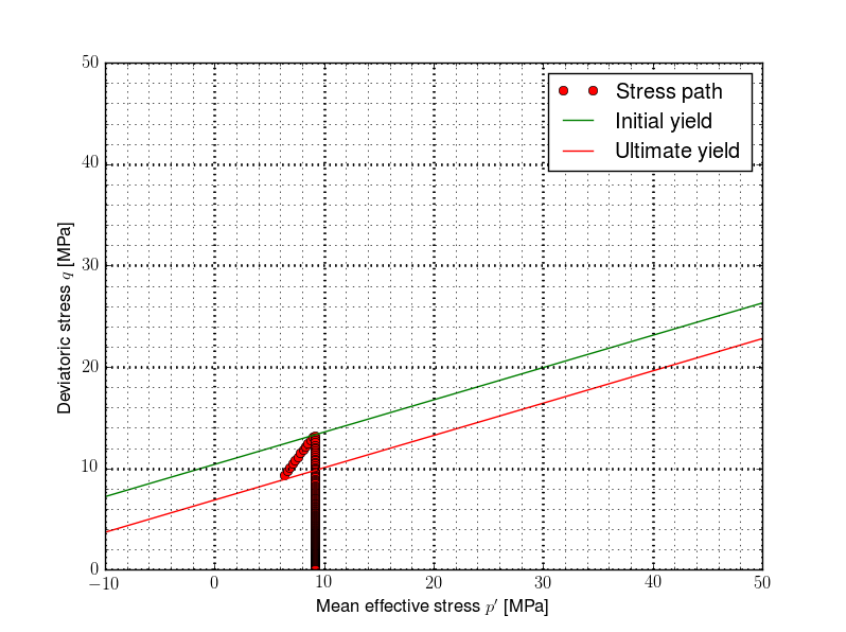

Figure 3.14: Deterministic stress path at cavity surface for GCS drift, based on c_0 and ϕ values of $\mu_X - 2\sigma_X$ and the other propertiy values of μ_X.

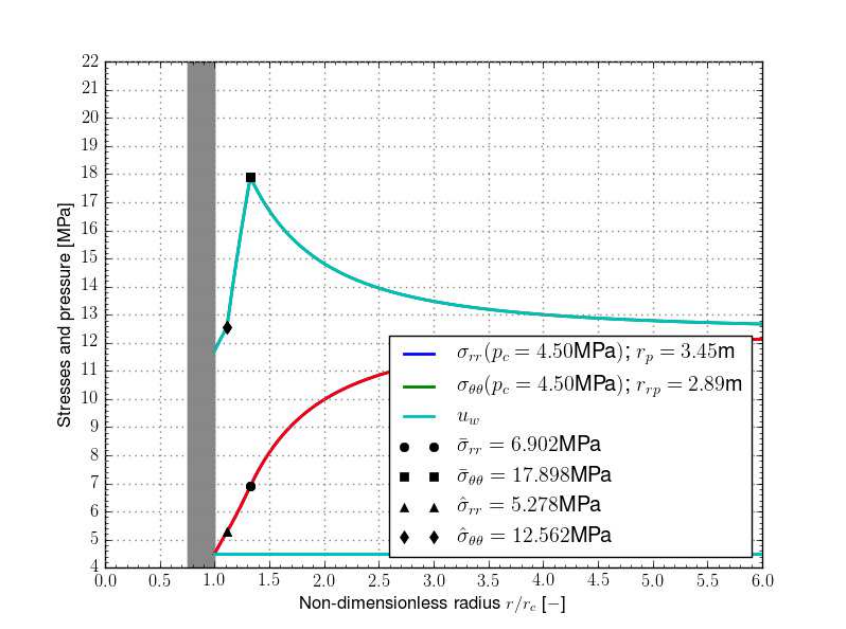

Figure 3.15: Deterministic total stress distributions around the excavated cavity for GCS drift (impermeable concrete liner), based on c_0 of $\mu_X - 2\sigma_X$, ϕ of $\mu_X - 3\sigma_X$ and the other propertiy values of μ_X; $\bar{\sigma}$ ($\hat{\sigma}$) denotes the stresses at the elastic-plastic (plastic-residual) interface, r_p is the plastic radius and r_{rp} is the residual plastic radius.

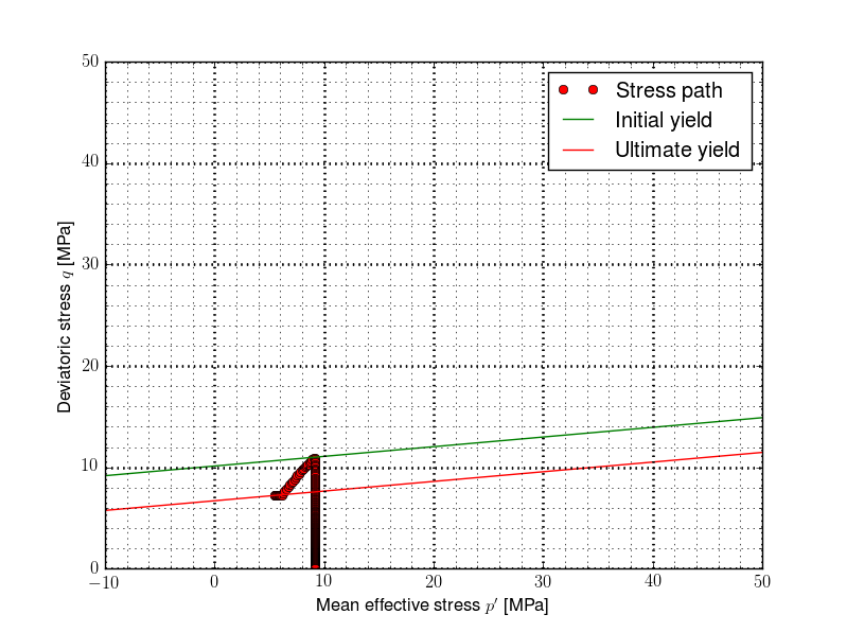

Figure 3.16: Deterministic stress path at cavity surface for GCS drift, based on c_0 of $\mu_X - 2\sigma_X$, ϕ of $\mu_X - 3\sigma_X$ and the others (mean μ_X) shown in Table 3.2.

with a cavity radius of $r = 2.6$ m. This result can be compared to Seyedi et al. (2015) who showed that the extent of the EDZ (i.e. $r_p - r$) can be in the range of 0–r for the various models shown in Fig. 3.19. It is noted that the anisotropic behaviour cannot be observed due to the isotropic assumptions in the model. Given some design exceedance criterion for the extent of the plastic zone (e.g. $r_{p,lim} = 2.8$ m, beyond which it is considered as unsatisfactory performance), the exceedance probability (or probability of unsatisfactory performance) can be assessed ($P_f = 0.316\%$ as shown in Fig. 3.18).

It may be argued that some less likely parameter combinations are included in the simulation for the uncorrelated case, when one considers the possible cross correlations between the variables. For example, soil cohesion and friction angle may exhibit a negative correlation, i.e. $\rho_{c,\phi}$ may be negative (Arnold, 2011; Lumb, 1970; Vardon et al., 2016), so that a combination of small values of c and ϕ may be less likely than a combination of small c and large ϕ. Therefore, uncertainties may be reduced by taking account of the possible cross correlations among different variables (Arnold et al., 2014, 2015). Rackwitz (2000) and Uzielli et al. (2006) recommend, in general (not refering to any specific soil type), $\rho_{c,\phi} \approx -0.5$ and $-0.25 \leq \rho_{c,\phi} \leq -0.5$, respectively. Compared to soil, there is even less correlation information on rock in literature. Given the above, reasonable estimates have been made for the correlated case. The correlation matrix is shown in Table 3.3. The correlated case has also been investigated, although, the probability of having a plastic radius larger than the limit specified (i.e. $r_{p,lim} = 2.8$ m) is significantly reduced to $4.07 \times 10^{-3}\%$, due to the negative correlation between c_0 and ϕ and c_r and ϕ. Compared to the uncorrelated case, the chances of the rock having a small c and ϕ are smaller for the correlated case as a result of the imposed negative correlation. The plastic zone expands generally as the rock becomes weaker (i.e. small values of c and ϕ). Therefore, the probability of the plastic zone exceeding a certain limit reduces due to the lower likelihood of the rock having both strength parameters which are weak.

Response Surface Method + FORM importance

An explicit representation (i.e. a meta model) of the random response of the model under consideration has been here obtained by PCE. FORM has be applied to the meta model to investigate the

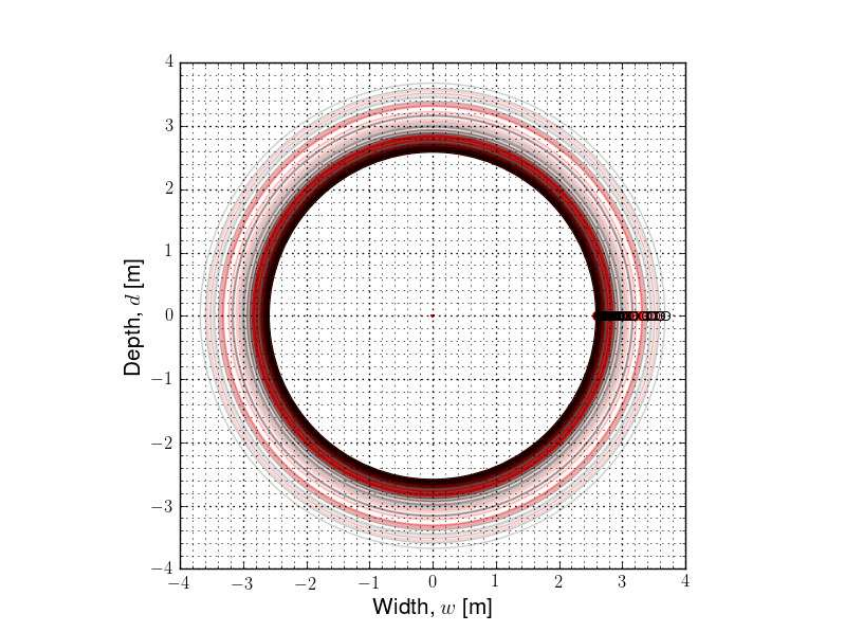

Figure 3.17: Plastic radius around the tunnel opening (plastic softening zone in grey and plastic residual zone in red).

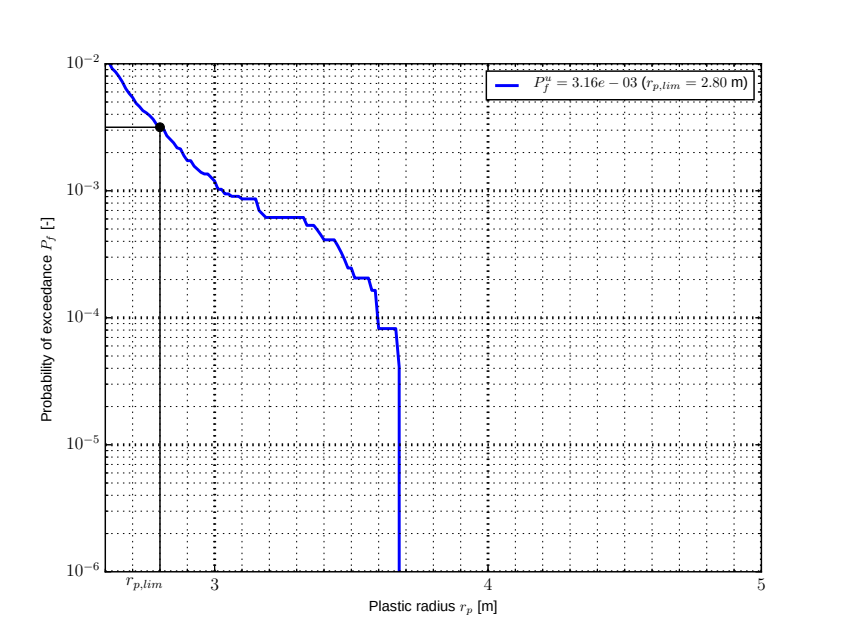

Figure 3.18: Probability of exceedance (P_f^u) of a plastic zone limit ($r_{p,lim}$).

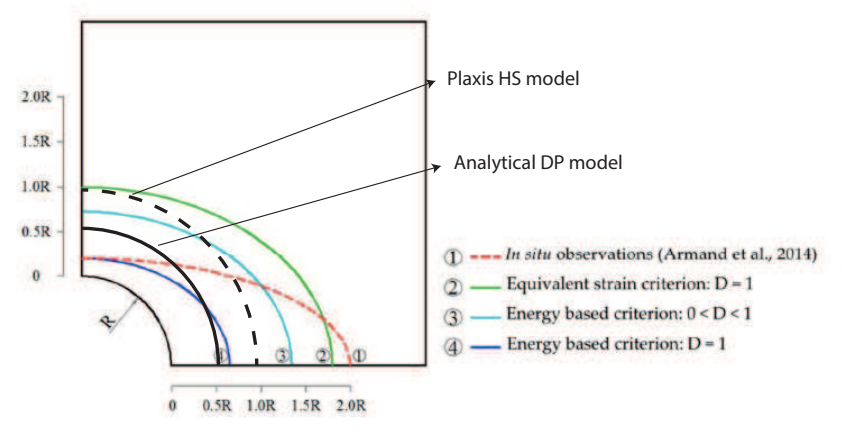

Figure 3.19: The extent of the damaged zone evaluated using the proposed analytical model and compared to results presented in Seyedi et al. (2015).

Table 3.3: Cross-correlation matrix C with components ρ_{X_i,X_j}.

	c_0	c_r	ϕ	E	E_t	ν
c_0	1.0	0.75	-0.5	0.5	0.25	0.5
c_r	ρ_{c_r,c_0}	1.0	-0.5	0.5	0.25	0.5
ϕ	ρ_{ϕ,c_0}	ρ_{ϕ,c_r}	1.0	0.25	0.25	-0.5
E	ρ_{E,c_0}	ρ_{E,c_r}	$\rho_{E,\phi}$	1.0	0.5	-0.25
E_t	ρ_{E_t,c_0}	ρ_{E_t,c_r}	$\rho_{E_t,\phi}$	$\rho_{E_t,E}$	1.0	-0.25
ν	ρ_{ν,c_0}	ρ_{ν,c_r}	$\rho_{\nu,\phi}$	$\rho_{\nu,E}$	ρ_{ν,E_t}	1.0

importance factors (γ_i^2).

Fig. 3.20 shows the importance factors (i.e. γ_i^2, $i = 1, 2, \ldots, 6$) in terms of pie charts as a result of FORM analysis using the meta model obtained by PCE. It is seen that the friction angle is the most important factor for the event $r_p \geq r_{p,lim} = 2.8$ m and the influence of the tangential modulus E_t ranks second due to it being the main parameter for the plastic softening behaviour. The influence of residual cohesion c_r and Poisson's ratio ν are insignificant and they may therefore be treated as deterministic parameters in further analyses.

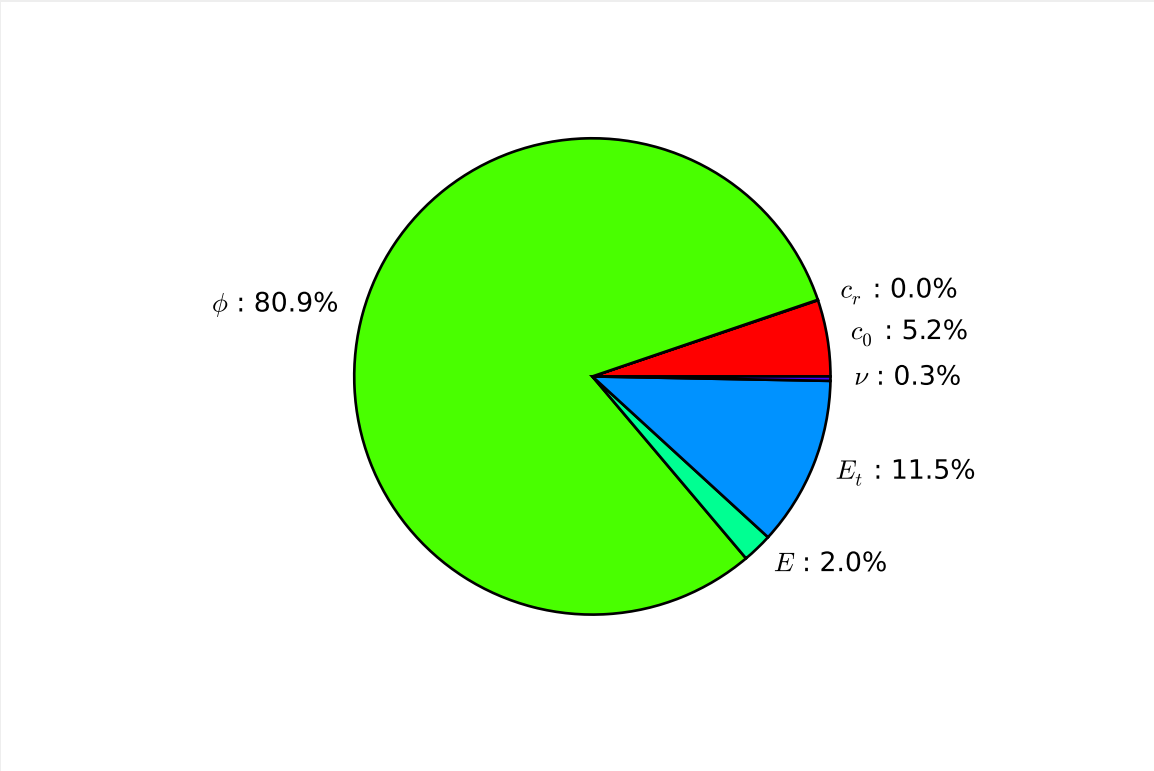

Figure 3.20: Pie chart of FORM importance factors (analytical softening model).

3.3.3.1 Concluding remarks

The preliminary assessment brackets favourably well the radial displacement measurements. The proposed probabilistic framework provides a way to assess the probability of unsatisfactory performance in terms of the exceedance of a certain plastic limit. The extent of the plastic zone indicates the possible range of the excavation damaged zone and the results lie within the range predicted by other models. However, the idealised isotropic model is not able to predict anisotropic convergence measurements.

3.3.4 Numerical model investigation

Deterministic analysis

The stability of the GCS drift is here numerically assessed using the PLAXIS FE software (version 2D AE) (Plaxis, 2014).

i. Model set-up

A 2D plane strain investigation has been performed, with Fig. 3.21 showing the basic set-up (including geometry dimensions, boundary conditions and mesh discretisation) of the tunnel model for a deterministic analysis at the main level (i.e. -490 m). The boundary conditions are: a fixed bottom, and left and right sides fixed in the horizontal direction and free in the vertical direction. The domain is discretised by 8043 elements with 65016 nodes, using 15-node triangular elements, and refined in the close vicinity of the tunnel opening. The calculation phases are: (1) Initial phase: the K0 procedure; (2) Phase 1: remove the upper part of the mesh from the initial domain (Fig. 3.21(a)), resulting in a 80 $\times$ 160 m model domain with a total vertical stress of $\sigma'_z = 5.8$ MPa applied along the top boundary (Fig. 3.21(b)); (3) Phase 2: remove soil from inside the tunnel; (4) Phase 3: simulate the convergence of the host rock by imposing a contraction on the tunnel lining.

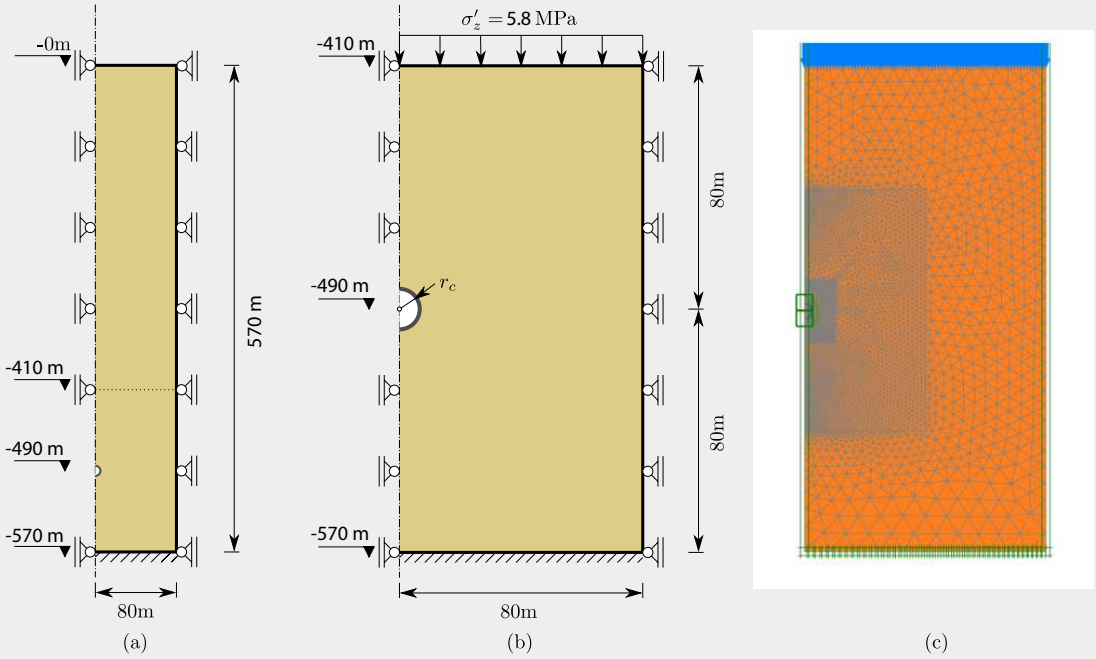

Figure 3.21: Problem geometry, boundary conditions and mesh discretisation for a plane strain analysis at -490 m depth: (a) Initial domain for K0 procedure; (b) Model domain; (c) Finite element mesh using 15-node triangles.

ii. Material parameters

The hardening soil (HS) model is used in this investigation, as also used in Arnold et al. (2015) for Boom Clay. The model material parameters used are listed in Table 3.4.

The cohesion and friction angle were set equal to the mean values shown in Table 3.2. The values of the secant modulus, E_{50}, was set equal to the Young's modulus, E (see Table 3.2). The

Table 3.4: Hardening soil model parameters for COx claystone.

Property	Symbol	Unit	Value
Cohesion	c	[MPa]	8.6
Friction angle	ϕ	[°]	20.7
Secant modulus	E_{50}^{ref}	[MPa]	4300
Unloading/reloading modulus	E_{ur}^{ref}	[MPa]	4300×3
Oedometer modulus	E_{oed}^{ref}	[MPa]	4300
Unloading/reloading Poisson's ratio	ν_{ur}	[-]	0.29
HS model exponent	m	[-]	0.5
Dilation angle	ψ	[°]	0.0
Earth pressure at rest	K_0	[-]	1.0
Over-consolidation ratio	OCR	[-]	2.2
Unit weight	γ	[kPa/m]	24.2
Void ratio	e	[-]	0.7
Reference stress	p^{ref}	[kPa]	100
Failure ratio	R_f	[-]	0.9
Earth pressure coefficient (at rest NC-state)	K_0^{NC}	[-]	1-sinϕ

unloading/reloading modulus, E_{ur}, was set to be three times the secant modulus based on Plaxis (2014c), i.e. $E_{ur} = 3E_{50}$. The oedometer modulus, E_{oed}, was set equal to the secant modulus. The reference values have been approximated for a minor principle effective stress of $\sigma_3' \approx$ -7 MPa, considering an isotropic stress state at -490 m depth, via the following equations:

$$E_{50} = E_{50}^{ref} \left(\frac{c\cos\phi - \sigma_3' \sin\phi}{c\cos\phi + p^{ref}\sin\phi} \right)^m \tag{3.9}$$

$$E_{ur} = E_{ur}^{ref} \left(\frac{c\cos\phi - \sigma_3' \sin\phi}{c\cos\phi + p^{ref}\sin\phi} \right)^m \tag{3.10}$$

$$E_{oed} = E_{oed}^{ref} \left(\frac{c\cos\phi - \frac{\sigma_3'}{K_0^{NC}} \sin\phi}{c\cos\phi + p^{ref}\sin\phi} \right)^m \tag{3.11}$$

Figs. 3.22 and 3.23 show the effective radial and tangential stress distributions in the horizontal direction from the centre of the tunnel opening to the far field on the right-hand side, and the total radial and tangential stress and pore water pressure distributions in the vertical direction from the centre of the tunnel opening to a depth of -460 m. Whereas the analytical model presented in Section 3.3.3 focuses on the post-peak (failure) response described by a softening plastic zone, the numerical HS model used in this section highlights the pre-peak hardening behaviour (i.e. damage initiation and growth up to peak strength). The hardening plastic zone indicates the extension of the micro-crack zone in the vicinity of the tunnel opening. Fig. 3.24 shows the extent of hardening zone (HZ) around the cavity (superscripts h and v in the figure indicate horizontal and vertical extent, respectively). A hardening radius of $r_{HZ} \approx 5$ m (i.e. $r_{HZ} - r = 0.92r$, see Fig. 3.19) was observed in this case. Moreover, the extent of the hardening zone in the horizontal direction is virtually identical to that in the vertical direction, due to an isotropic in-situ stress (i.e. the earth pressure coefficient

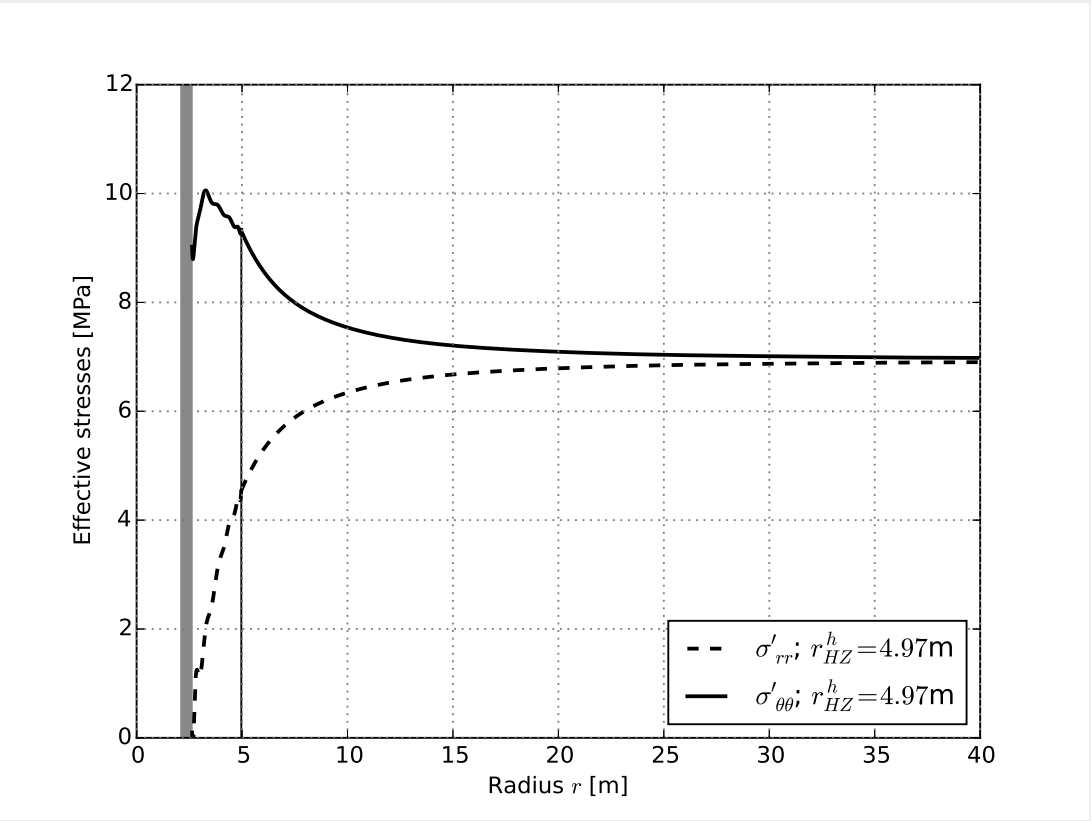

Figure 3.22: Effective radial and tangential stress distributions in the horizontal direction.

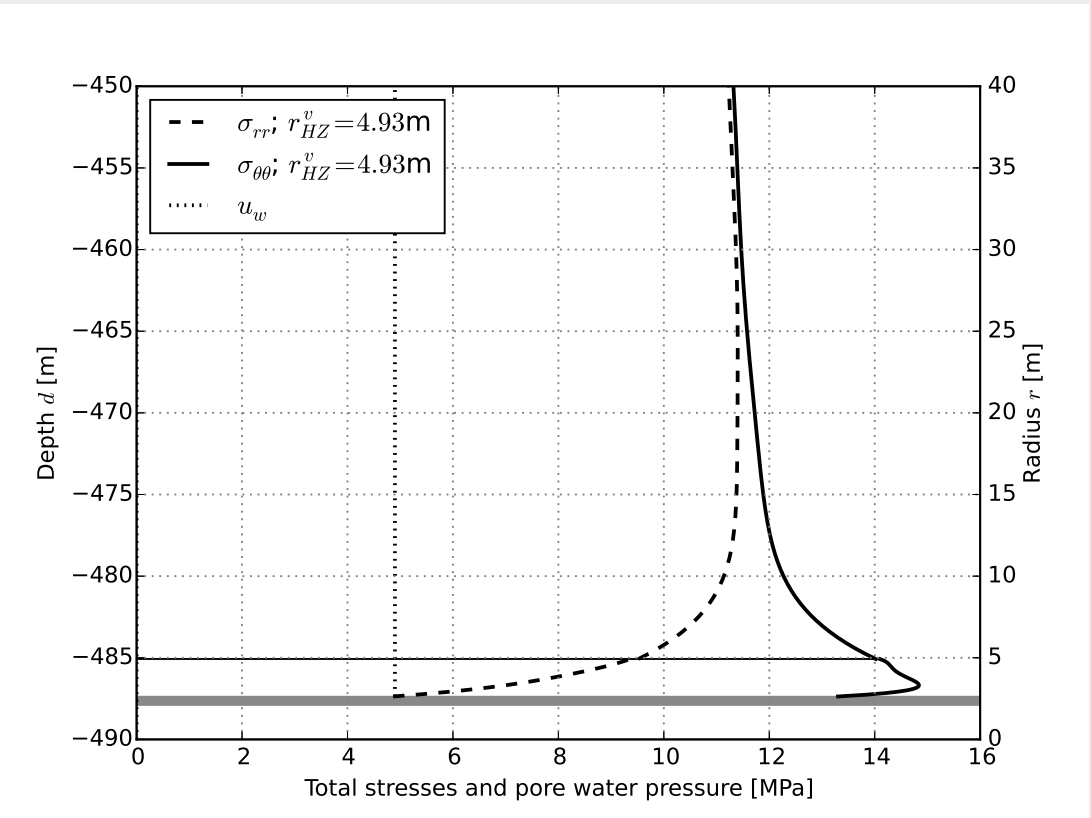

Figure 3.23: Total radial and tangential stress and pore water pressure distributions in the vertical direction.

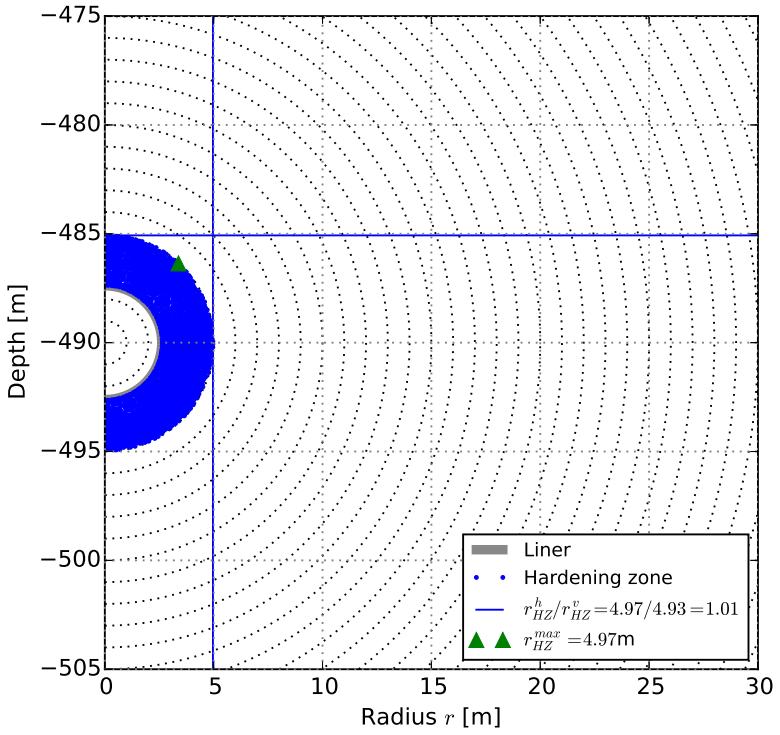

Figure 3.24: Gaussian integration points showing the extent of the Hardening Zone (HZ).

at rest being $K_0 = 1$).

Response Surface Method + FORM importance

In this section, FORM analysis combined with the deterministic response surface method has been carried out to investigate the importance factors for the Plaxis HS numerical model. The statistics and distribution types for the four HS soil model variables are listed in Table 3.5, with the remaining model parameters being deterministic and equal to their respective mean values as in Table 3.4. Fig. 3.25 shows the FORM importance factors in the form of a pie chart. It shows that the secant modulus is the most important variable in assessing the probability of exceedance of a plastic hardening zone limit; in contrast, the importance of other variables is negligible. This is different from the general findings reported in Chapter 7 of Arnold et al. (2015), where both secant modulus and friction angle

Table 3.5: Point statistics describing the properties of COx claystones at MHM URL for Hardening Soil model.

Variable X	Symbol	Unit	μ_X	$Cov(X) = \sigma_X/\mu_X$	Distribution type
Cohesion	c	MPa	8.6	0.21	Normal
Friction angle	ϕ	°	20.7	0.29	Normal
Secant modulus	E_{50}	MPa	4257	0.34	Normal
Un-/re-loading Poisson's ratio	ν_{ur}	-	0.29	0.28	Normal

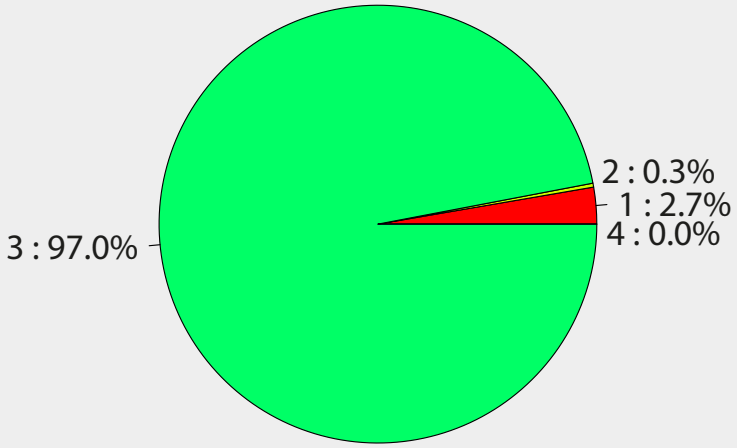

Figure 3.25: Pie chart of FORM importance factors for the numerical Hardening Soil model (1: cohesion c, 2: friction angle ϕ, 3: secant modulus E_{50}, 4: un-/re-loading Poisson's ratio ν_{ur}).

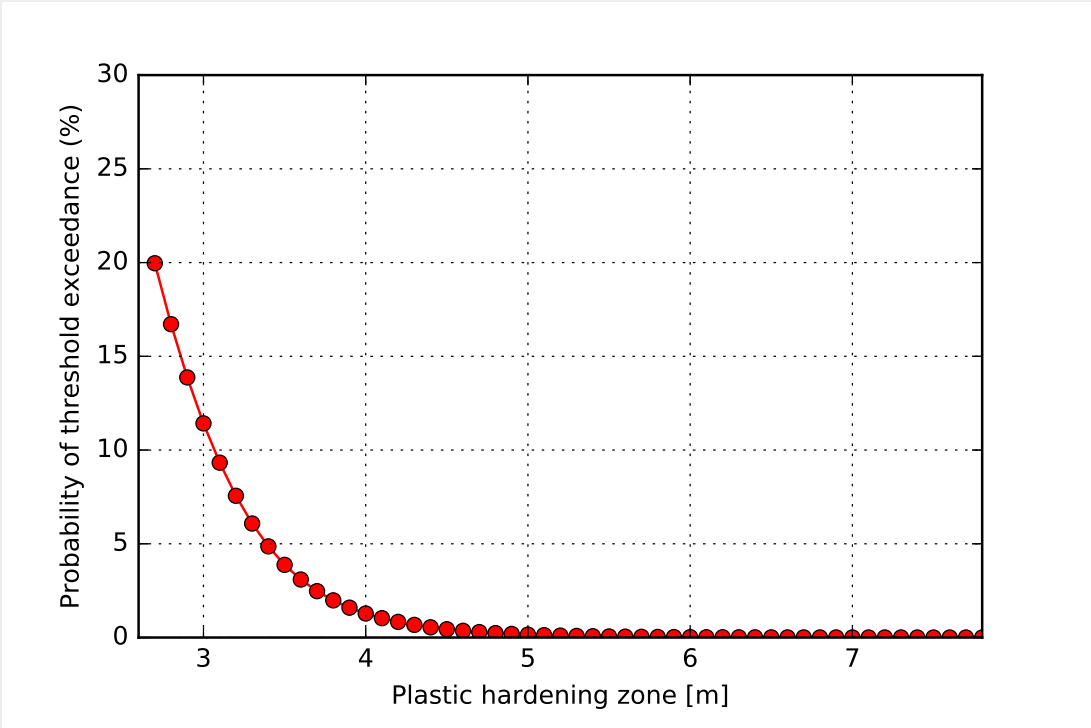

Figure 3.26: Probability of exceedance of a hardening zone limit ($r \leq r_{HZ,lim} \leq 3r$, $r = 2.6$ m).

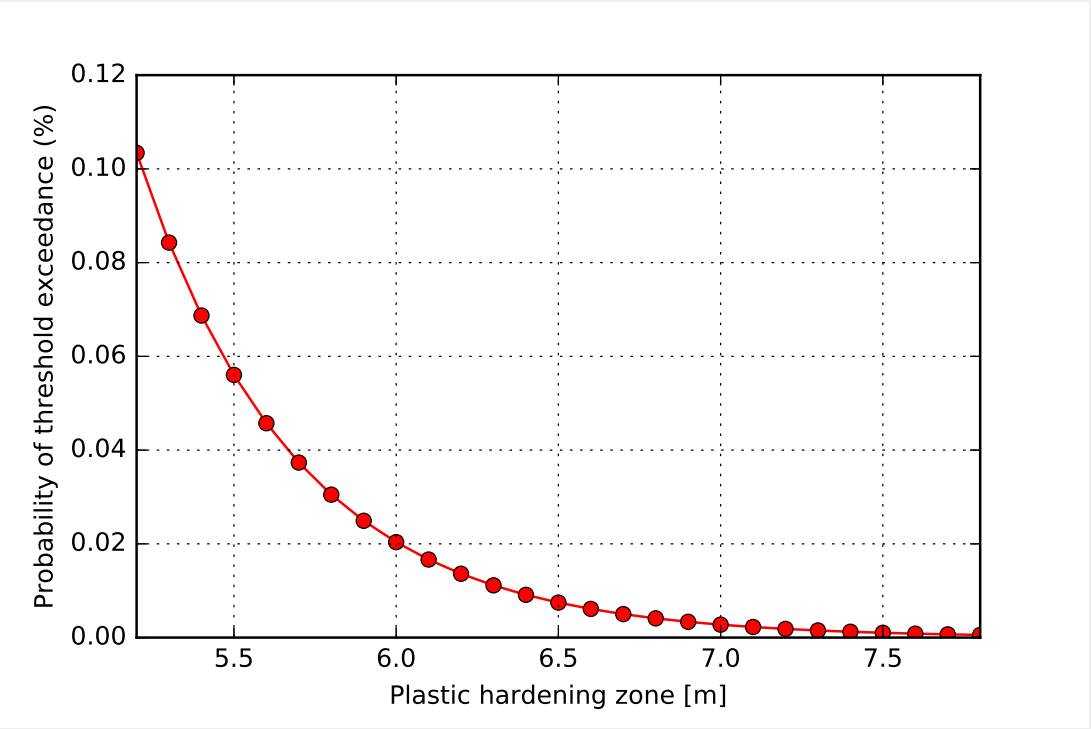

Figure 3.27: Probability of exceedance of a hardening zone limit ($2r \leq r_{HZ,lim} \leq 3r$, $r = 2.6$ m).

were shown to be important random variables. The reasons why E_{50} is more important than ϕ in this case are: (1) the mean of E_{50} for the French case is one magnitude higher than that for Boom Clay: as indicated in Fig. 7.21 of Arnold et al. (2015), the higher the mean of a random variable, the more influence of this variable and the less influence of the others, particularly, ϕ; (2) this investigation looks at the importance factors with respect to the extent of the hardening zone (where E_{50} is relevant) whereas Arnold et al. (2015) looked at the importance factors with respect to the extent of the plastic (failure) zones (where ϕ is relevant). The first reason also explains why c is more important in this case compared to Boom Clay, as c is also one magnitude higher than that of Boom Clay. In fact, when looking at the performance function related to the extent of the hardening zone, the HS model for the two materials (i.e. Boom Clay and French COx claystone) shows consistent results; that is, E_{50} and c are more important than ϕ (see Fig. 6.7 in Chapter 6 of Arnold et al. (2015) and comparing the relative influence of random variables on the hardening zone extent); (3) the coefficient of variation of E_{50} is higher than those of the other variables; therefore, the greater the influence of this random variable (see Fig. 7.22 in Arnold et al. (2015)).

Fig. 3.26 shows the probability of exceedance of a hardening zone limit as a function of hardening zone limit $r_{HZ,lim}$ ranging from r to $3r$. It is seen that the probability of threshold exceedance decreases as the threshold limit increases; that is, the chances of having a damaged zone become smaller for a larger limit value. Fig. 3.27 shows this trend in a focused zone for $2r \leq r_{HZ,lim} \leq 3r$. It is seen that the probability for $r_{HZ,lim} = 3r = 7.8$ is as small as 5.65×10^{-4}.

3.3.5 Concluding remarks

A hardening soil model within Plaxis has been used to investigate the performance of a drift in the COx claystone. In contrast to the softening soil model which has implications for macro-fractured zones with regards to softening plastic limit, the hardening soil model is used to investigate the extent of the hardening plastic zone which has implications for micro-fractured zones. The model results fit well within the range reported in literature. However, it is not able to predict the anisotropic

fracture behaviour observed in measurements due to the model not taking account of the bedding planes and anisotropic elasticity. Statistics of the COx properties derived from literature have been used to compute the probability of threshold exceedance as well as the FORM importance factors. The results are consistent with the results of the Boom Clay analysis, and differences are consistent with the different material properties values.

3.4 Investigation of tunnels in Opalinus Clay

3.4.1 Modelled experiment: ED-B tunnel

The ED-B mine-by experiment was conducted at Mont Terri in 1997–1998, and consisted of a 35 m long, 3.6 m diameter circular excavation at a depth of approximately 270m (Corkum and Martin, 2007a). This experiment has provided data from a number of instruments such as piezometers, inclinometers, extensometers and convergence arrays.

Following the installation of instrumentation, the ED-B tunnel was excavated full face using a roadheader from a northwest to a southeast direction. The tunnel was stable during excavation and 200 mm thick steel fibre reinforced shotcrete support was installed approximately 7 m behind the excavation face. The tunnel location is shown in Fig. 2.9(b) in plan view and in Fig. 3.28 in isometric view. The in-situ stress tensor direction is shown in Fig. 3.29 together with the tunnel excavation

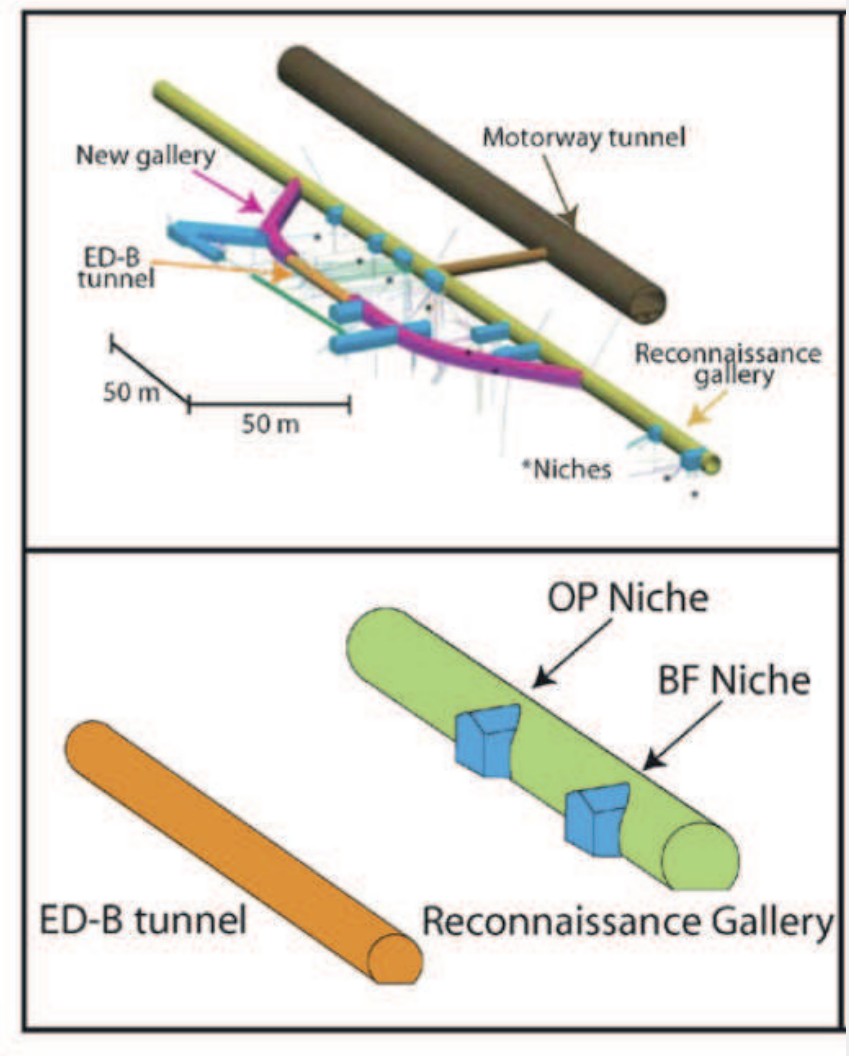

Figure 3.28: Relative location of the ED-B tunnel to the Motorway tunnel and Reconnaissance gallery (Corkum and Martin, 2007a).

direction, and the magnitude is shown in Table 3.6. Due to the anisotropic in-situ stress state, only the numerical model has been investigated in the following section, as the analytical model is only applicable for an isotropic in-situ stress state.

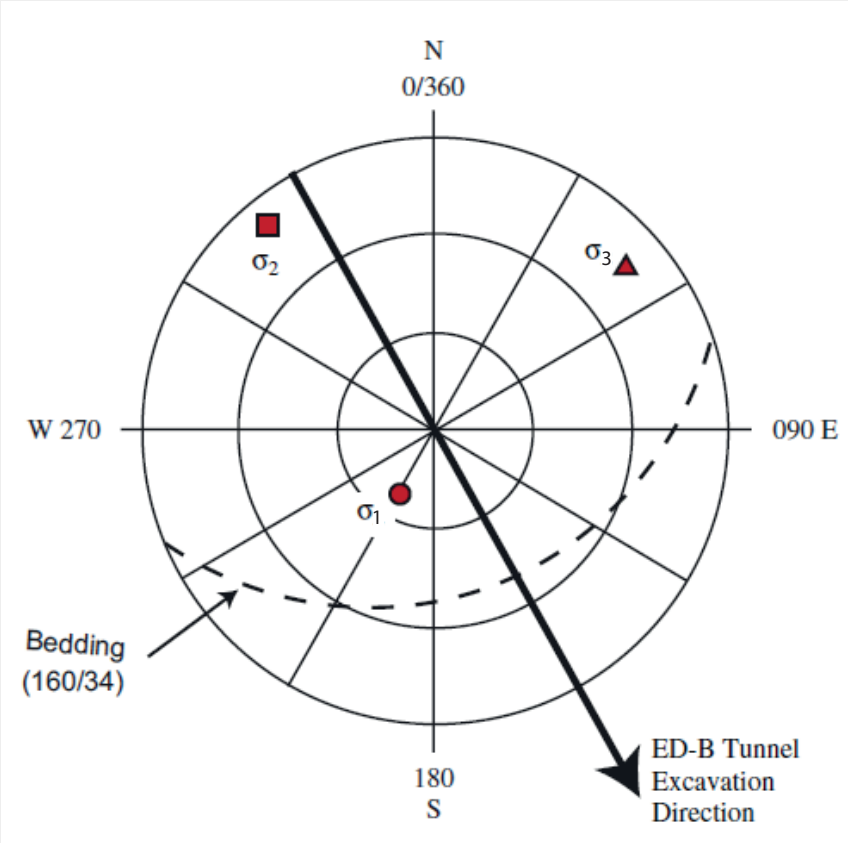

Figure 3.29: Orientation of the stress tensor for in-situ state and the ED-B tunnel excavation direction (Corkum and Martin, 2007a).

Table 3.6: Magnitude and orientation of in-situ stress, based on Corkum and Martin (2007a).

Principal stress	Magnitude (MPa)	Dip direction (°)	Dip (°)
σ_1	6–7	210	70
σ_2	4–5	52	18
σ_3	2–3	320	7

3.4.2 Numerical model investigation

The stability of the ED-B tunnel is here numerically assessed using the PLAXIS FE software (version 2D AE) (Plaxis, 2014).

i. Model set-up

A 2D plane strain analysis has been performed. Fig. 3.30 shows the basic set-up (including geometry dimensions, boundary conditions and mesh discretisation) of the tunnel model for a deterministic analysis at the main level (i.e. -270 m). The boundary conditions are: a fixed bottom, and left and right sides fixed in the horizontal direction and free in the vertical direction. The domain is discretised by 5188 elements with 41994 nodes using 15-node triangular elements and refined in the close vicinity of the tunnel opening. The calculation phases are: (1) Initial phase: the K0 procedure; (2) Phase 1: remove the upper part of the mesh from the initial domain (Fig. 3.30(a)), resulting in a 80 $\times$ 160 m model domain with a total vertical stress of $\sigma'_z = 2.75$ MPa applied along the top boundary (Fig. 3.30(b)); (3) Phase 2: remove soil from inside the tunnel; (4) Phase 3: simulate the convergence of the host rock by imposing a contraction on the tunnel lining.

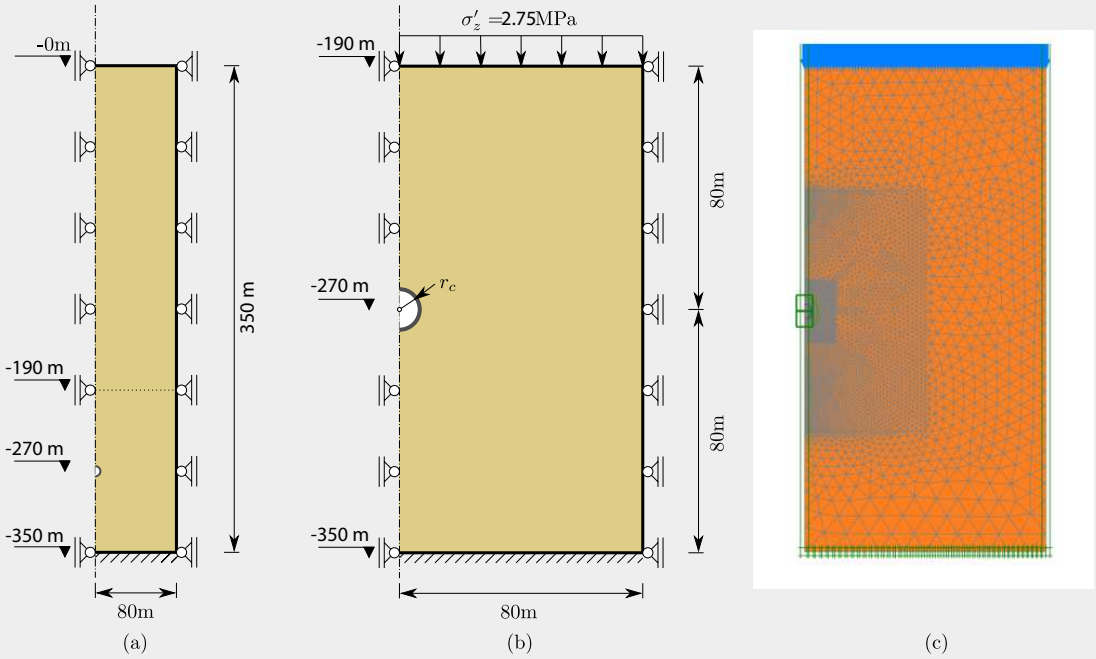

Figure 3.30: Problem geometry, boundary conditions and mesh discretisation for a plane strain analysis at -270 m depth: (a) Initial domain for K0 procedure; (b) Model domain; (c) Finite element mesh using 15-node triangles.

ii. Parameters

The hardening soil model is again used in this investigation. The model parameters used are listed in Table 3.7.

iii. Results

Figs. 3.31 and 3.32 show the effective radial and tangential stress distributions in the horizontal direction from the centre of the tunnel opening to the far field on the righ-hand side, and the total

Table 3.7: Hardening soil model parameters for OPA claystone (* indicates strength parameters for bedding planes, based on Corkum and Martin, 2007a).

Property	Symbol	Unit	Value
Cohesion	c	[MPa]	3.6 (1.0*)
Friction angle	ϕ	[°]	24.0 (23.0*)
Secant modulus	E_{50}^{ref}	[MPa]	4000
Unloading/reloading modulus	E_{ur}^{ref}	[MPa]	4000×3
Oedometer modulus	E_{oed}^{ref}	[MPa]	4000
Unloading/reloading Poisson's ratio	ν_{ur}	[-]	0.30
HS model exponent	m	[-]	0.5
Dilation angle	ψ	[°]	0.0
Earth pressure at rest	K_0	[-]	0.34
Over-consolidation ratio	OCR	[-]	2.2
Unit weight	γ	[kPa/m]	24.5
Void ratio	e	[-]	0.7
Reference stress	p^{ref}	[kPa]	100
Failure ratio	R_f	[-]	0.9
Earth pressure at rest NC-state	K_0^{NC}	[-]	1-sinϕ

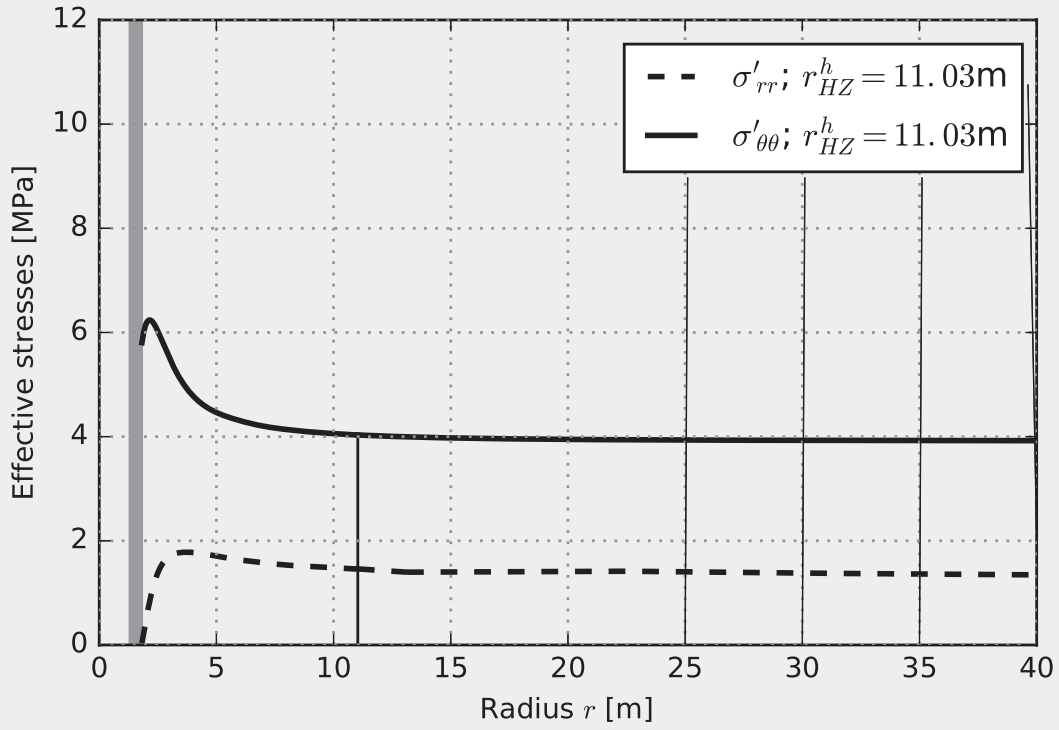

Figure 3.31: Effective radial and tangential stress distributions in the horizontal direction.

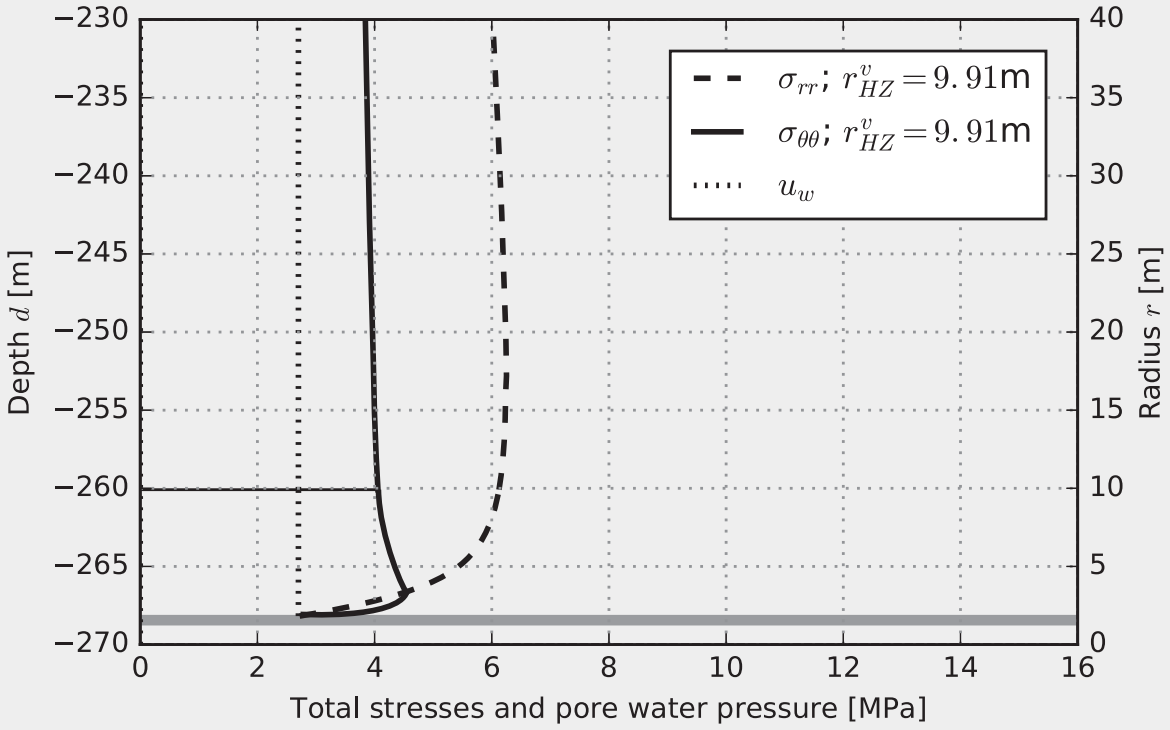

Figure 3.32: Total radial and tangential stress and pore water pressure distributions in the vertical direction.

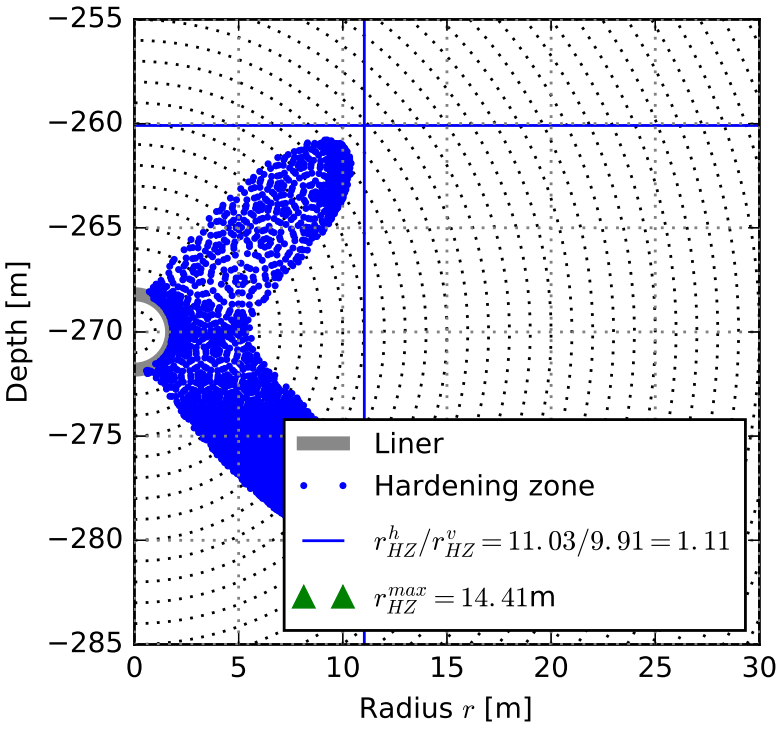

Figure 3.33: Gaussian integration points showing the extent of the Hardening zone (HZ) ($c = 3.6$ MPa, $\phi = 24.0°$).

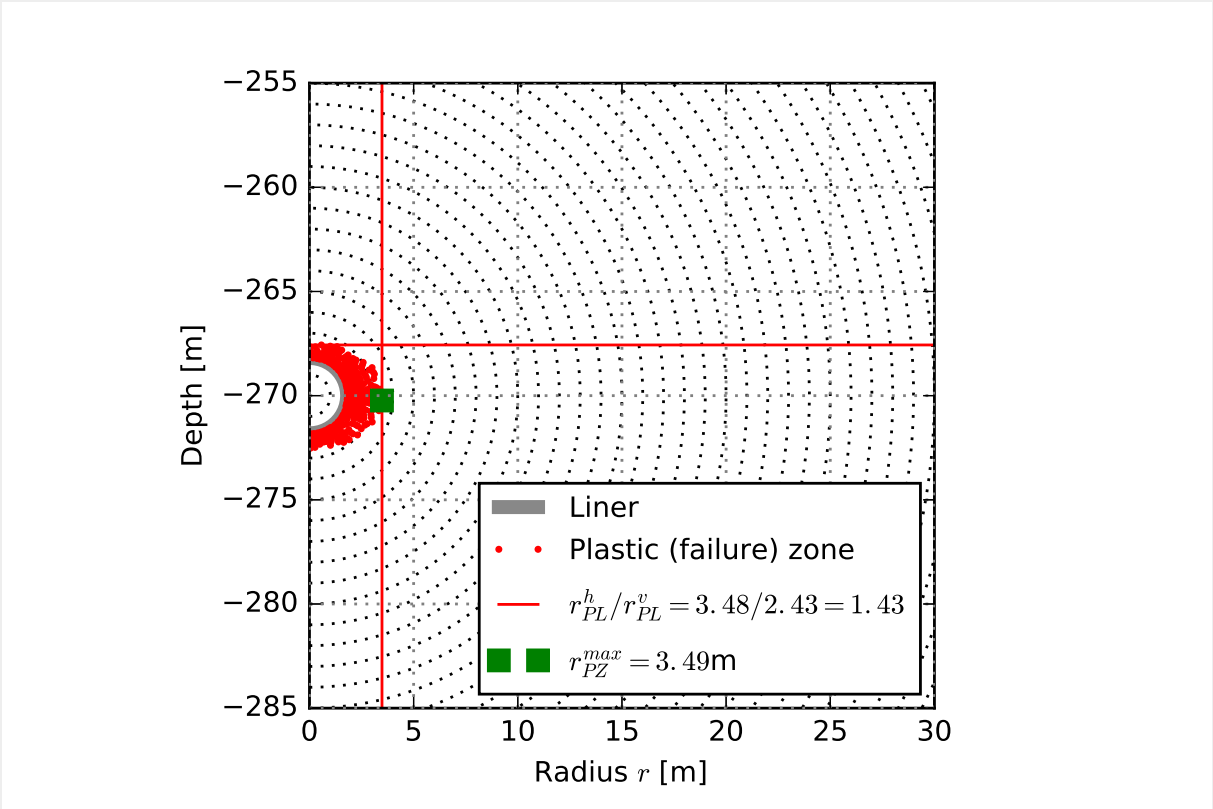

Figure 3.34: Gaussian integration points showing the extent of the plastic zone (PZ) ($c = 1.0$ MPa, $\phi = 23.0°$).

radial and tangential stress and pore water pressure distributions in the vertical direction from the centre of the tunnel opening to a depth of -230 m. Fig. 3.33 shows the extent of the hardening zone (HZ) around the cavity (superscripts h and v in the figure indicate horizontal and vertical extent, respectively), using 'best estimate' model parameters based on Table 2.2. The extent of the hardening zone in this case takes on an 'X' shape, due to the anisotropic in-situ stress (i.e. the earth pressure coefficient at rest being $K_0 = 0.34$). Fig. 3.34 shows the extent of Plastic (failure) zone (PZ) around the cavity (superscripts h and v in the figure indicate horizontal and vertical extent, respectively). A plastic failure zone of 0.6 m from the tunnel surface in the vertical direction and 1.7 m from the tunnel surface in the horizontal direction was observed. The strength parameters for joints have been used to allow a basic representation of the bedding planes and the resulting extent of failure zone represents an upper bound of the EDZ. This range lies within the reported value of 1–2 m (Bossart et al., 2004).

3.4.3 Concluding remarks

One of the so-called mine-by tests in the Mont Terri laboratory was investigated using the Plaxis numerical model. The results indicates favorable comparisons with observations. However, due to model limitations, the importance of bedding planes in controlling the failure mechanisms around the underground opening cannot be captured. Nevertheless, the model provides a comparable range of the EDZ observed in field and the importance of in-situ stress anisotropy is highlighted.

4 New Boom Clay simulations

During the OPERA project, additional experimental tests were undertaken on Boom Clay samples, which were sampled from the HADES underground research laboratory in Belgium at a depth of 223 m (Harrington et al., 2017). A suite of tests were carried out on the consolidation, hydraulic, swelling, fracture transport, gas migration and mechanical properties. The samples were tested at as close as possible to in-situ conditions, both for the HADES site and conditioned, i.e. consolidated, to conditions expected at 500 m depth in the Netherlands. This assumes that samples will be normally consolidated at this depth.

This chapter presents updated analytical models to compare the impact of new experimental data with the work of Arnold et al. (2015). An insufficient number of new tests were made to update the statistical models; therefore, only new deterministic models are presented.

4.1 Material properties

Three new triaxial tests and an unconfined compressive strength test were undertaken after conditioning at 500 m stress levels, leading to a new set of material parameters. The Young's modulus in these material properties are slightly different to those presented in Chapter 9 of Harrington et al. (2017) as, in this material model, the initial hardening phase is incorporated in the Young's modulus, as explained in detail in Arnold et al. (2015). The test data and material model are presented in Fig. 4.1. The Young's modulii here are $200, 120, 150, 150$ MPa for Test 1 (normally consolidated), Test 2 (OCR $= 1.5$), Test 3 (OCR $= 3$) and UCS tests. A mean value of 155 MPa has been used in the analysis.

The Mohr-Coulomb failure envelope has been analysed for both the peak and residual conditions. This has been plotted on an $s - t$ plane, where $s = (\sigma_1 + \sigma_3)/2$ and $t = (\sigma_1 - \sigma_3)/2$, shown in Fig. 4.2. It can be seen that there is little softening apparent; in particluar, for normally consolidated conditions.

The full set of material properties required is presented Table 4.1. These differ slightly from those presented by Harrington et al. (2017), due to the constraints and assumptions in the model; however, they are in close agreement. In partcular, the Young's modulii are slightly lower and the peak strengths are slightly higher due to the linearisation of the behaviour. The parameters chosen can be seen via Figs. 4.1 and 4.2 to closely reproduce the experimental results. The second hardening observed at high strain levels is not incorporated in the model, or the parameters, as this is assumed to be (i) an experimental artefact due to increases in area, and (ii) the material is unlikely to achieve such high strain levels.

In comparison with the material parameters used in Arnold et al. (2015), the Young's modulus is around 50% lower here than the mean case in Arnold et al. (2015) (300 MPa), the initial cohesion and friction angle are higher here than the mean case in Arnold et al. (2015) (0.5 MPa and 12.5°, respectively). The residual cohesion was also lower in Arnold et al. (2015) (0.25 MPa), and substantially smaller in proportion to the initial cohesion. The friction angle, being the most important parameter (Arnold et al., 2015), is seen to be around the high estimate used in that work, and the likely impact of reducing the plastic radius will be exacerbated by the lower Young's modulus.

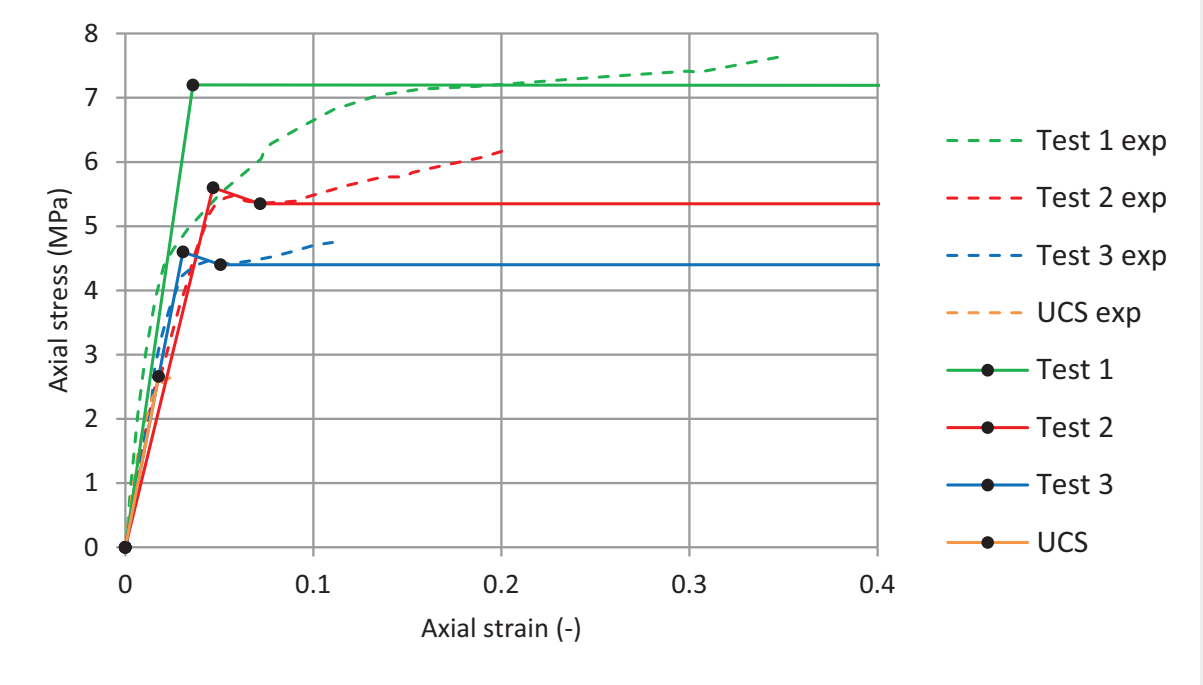

Figure 4.1: Material model interpretation for new experimental tests overlaying experimental data. Experimental data after Chapter 9 of Harrington et al. (2017).

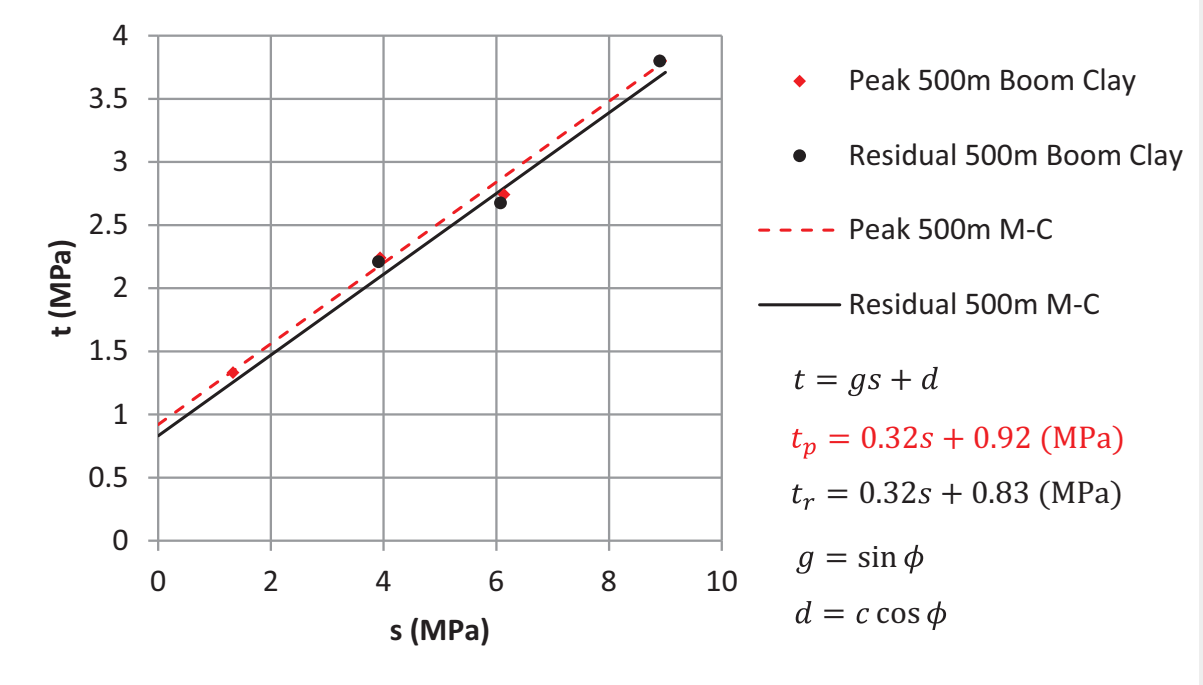

Figure 4.2: Mohr-Coloumb failure envelope interpretation for new experimental tests, in s-t plane.

Table 4.1: Material properties of Boom Clay interpreted from Chapter 9 of Harrington et al. (2017).

Property	Symbol	Unit	Value
Initial cohesion	c_0	MPa	0.97
Residual cohesion	c_r	MPa	0.88
Friction angle	ϕ	°	18.6
Young's modulus	E	MPa	155
Tangent modulus	E_t	MPa	10
Poisson's ratio	ν	-	0.10

4.2 Model

The model used is the same as that used in Arnold et al. (2015) (Section 4.7 and 7.3). In summary, the initial vertical and horizontal total stresses are set to $\sigma_{v,0} = \sigma_{v,0} = 10$ MPa, with the initial pore water pressure set to $u_{w,0} = 5$ MPa. Two galleries are shown here, a High Level Waste (HLW) disposal gallery ($r_c = 1.6$ m) and a Low and Intermediate Level Waste (LILW) disposal gallery ($r_c = 2.4$ m). A 75 mm overcut during tunnel construction is assumed. For the concrete properties, high strength concrete is used, but, as found in Arnold et al. (2015), this is unlikely to affect the plastic radius or pressure on the liner, given the similar elastic properties.

4.3 Results

The results are presented in Figs. 4.3 and 4.4. The stresses and the stress paths are shown, both for the analyses based on the material parameters presented here and the analyses presented in Arnold et al. (2015). In all cases, as expected, the plastic radius is reduced. As can be seen by comparing Figs 4.3(a) and 4.3(c), the plastic radius has reduced from 3.27 m to 2.12 m. This offers the chance to reduce spacing between the tunnels, where needed or beneficial, and decreases the zone where properties are significantly changed, e.g. has increased in permeability. Similar conclusions are seen for the LILW galleries in Fig. 4.4.

Additionally, the stresses on the liner (the radial stresses at the cavity) are also reduced, but by a limited amount, a maximum of 14%. This offers the opportunity to reduce the liner thickness, possibly substantially if high strength concrete is used.

The observed reduction in softening behaviour, indicates that a less brittle failure may occur and therefore less discrete fractures. This increases the likelihood that large discrete fractures, which enhance permeability substantially, will not occur. Additionally, self-healing or self-sealing behaviour may additionally reduce this effect. It is noted that in both the case modelled here, and originally in Arnold et al. (2015), the extent of the plastic zone as well as the consequences in terms of long term safety, would be quite limited.

The newly performed tests, where the Boom Clay has been mechanically conditioned to conditions equivalent of 500 m depth, provide new insight into the likely material properties. These tests are extremely valuable (and costly), but are limited in number and in the range of sampling locations. Therefore statistical interpretation is not possible, and uncertainties and confidence are not able to be systematically and quantitatively assessed. A possible approach is to utilise expert judgement to estimate the uncertainty and variability, and this could form the basis of further work.

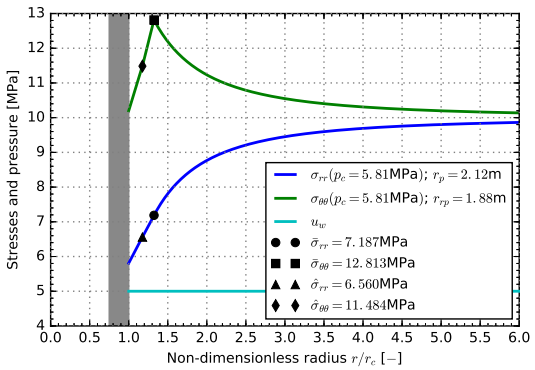

(a) Stress distributions, new parameters

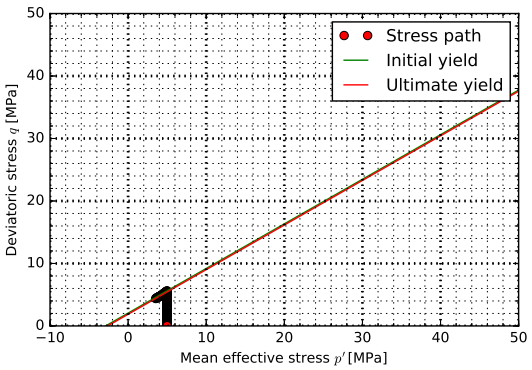

(b) Stress path, new parameters

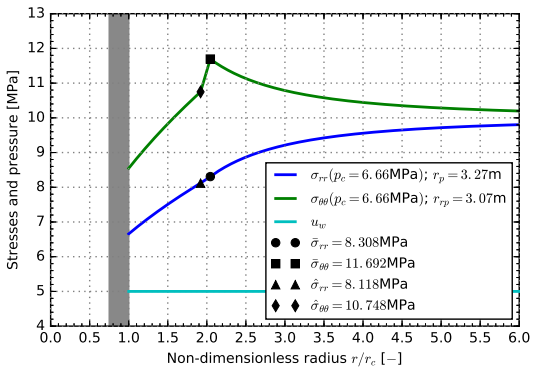

(c) Stress distributions, Arnold et al. (2015) parameters

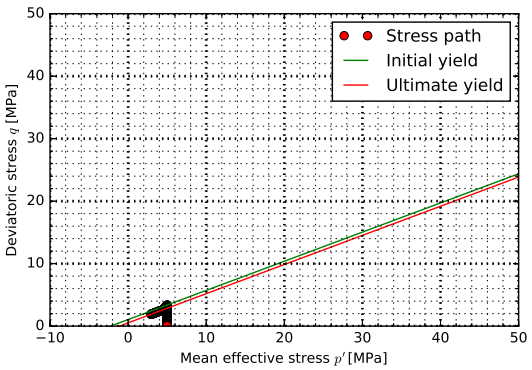

(d) Stress path, Arnold et al. (2015) parameters

Figure 4.3: The stress distributions and stress paths for the HLW disposal gallery $r_c = 1.6$ m.

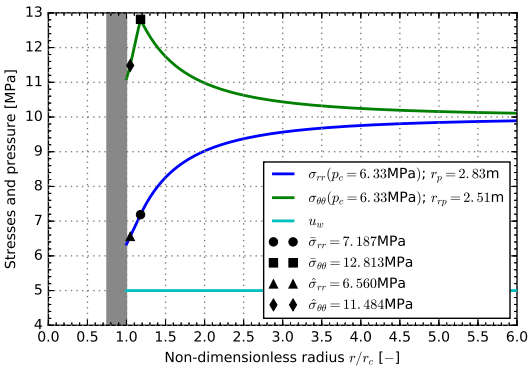

(a) Stress distributions, new parameters

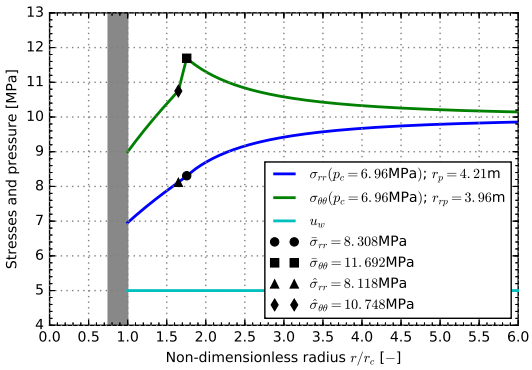

(b) Stress distributions, Arnold et al. (2015) parameters

Figure 4.4: The stress distributions and stress paths for the LILW disposal gallery $r_c = 2.4$ m.

5 Discussion

5.1 Introduction

The disposal of radioactive waste is an important societal and scientific topic. Within the OPERA research programme, research has been performed on the Dutch disposal concept in Boom Clay. One of the issues investigated is the principal technical feasibility of the OPERA reference design of a radioactive waste disposal facility in Boom Clay at a depth of about 500 m. This chapter highlights key findings of the work performed by this consortium (Arnold et al., 2015; Vardon et al., 2017; Yuan et al., 2017a,b; this report) in this context. Firstly, the methods used are summarised, with the efforts taken to validate these approaches. Following that, the key findings are summarised in terms of answering some of the key questions with regard to the design using these models. This chapter concludes with a discussion on how to move forward in further enhancing the OPERA Safety Case with respect to properties and mechanical behavior of Boom Clay.

5.2 Model development

The assessment of the technical feasibility of the OPERA reference design requires a quantitative understanding of the geotechnical behaviour of the disposal facility and the subsurface strata around it. A quantitative understanding involves the behaviour of the Boom Clay host rock during different phases of the facility operation, and it is essential to capture the features of the Boom Clay and processes that potentially may affect the isolating properties of the host rock and therefore the safety of the repository. As an example, it is recommendable to determine a probability of failure of the concrete gallery lining for different design options. This way, the design can be optimised and be made as robust as possible.

5.2.1 Analytical modelling (Chapter 4, Arnold et al., 2015)

By applying simplified, analytical formulations of physical problems fast evaluations of essentially complicated processes may be obtained. However, because of the simplifications, their applicability is usually limited. Still, they can be very useful: the tractability of the treatment encourages a physical understanding of relevant aspects and processes, and the speed with which analytical calculations can be performed facilitates a fast evaluation of important features of the system under consideration. This provides the modeller with tools for facilitating fast uncertainty and sensitivity evaluations and application in a probabilistic framework. InArnold et al. (2015) a closed-form analytical solution was formulated for the mechanical response of the subsurface upon excavation of a deep tunnel in an elasto-plastic soil, i.e. the clay host rock, with linear strain softening. Figure 3.1 schematically presents the zones of the qualitative response of the host rock as a function of distance from the liner of a waste disposal gallery, and the associated stresses. The solution was formulated for a single circular tunnel in plane strain conditions, with an elastic, impermeable liner. An important simplification was the assumption of an isotropic stress state and axisymmetric loading of the liner. The radius of the failing zones (the residual plastic zone and the softening plastic zone) was investigated as a function of host rock parameters, such as the cohesion, the friction angle and the elastic moduli. This sensitivity analysis revealed that the most influential parameter is the friction angle. Therefore, in practical applications this value needs to be determined as accurately

as possible for the in-situ conditions prevailing at the depth of the repository. At the same time, the limited extent of the plastic zone suggested that the spacing between the disposal galleries may be reduced. This, however, needs to be underpinned by numerical simulations accounting or mechanical interaction between neighbouring tunnels. In addition, the effects of anisotropy of the Boom Clay on the extent of the plastic zone around the disposal galleries need further consideration, although it is anticipated that this feature of the host rock may be difficult to capture by means of analytical models.

5.2.2 Numerical modelling approaches (Chapter 5, Arnold et al., 2015, Vardon et al., 2017)

Numerical approaches allow more elaborate constitutive models for analyzing (thermo-) mechanical features and processes of the host rock. Within the finite element software PLAXIS, a choice can be made for different models that incorporate non-linear and plastic soil behaviour. This enables the quantification of the effects of these models in relation to the behaviour of the host rock surrounding the galleries of the repository. Four of these models were tested:

(i) MC; the Linear Elastic-Perfectly Plastic Mohr Coulomb model. The response of this model is linearly elastic up to the point where the Mohr-Coulomb shear failure envelope is reached.

(ii) MCC; the Modified Cam-Clay model. This model is formulated in the framework of critical state soil mechanics. It employs an elliptical yield locus and thus also facilitates the simulation of compaction failure of the host rock.

(iii) SSC; the Soft Soil Creep model. This model is also formulated within the framework of critical state soil mechanics, but it employs a Mohr-Coulomb failure criterion and an expanding MCC cap due to creep.

(iv) HS; the Hardening Soil model. The model is based on a hyperbolic stress-strain relationship and consists of a shear hardening cone-type yield locus and a compression hardening cap-type yield locus. A specific feature of this model is an enhanced description of the stiffness of the clay as function of stress.

The models were tested against selected experimental data obtained by triaxial and oedometer tests (not performed as part of the OPERA programme). For example, the results of three consolidated-drained, strain-controlled triaxial tests performed on Boom Clay samples (from 220 m depth) were used. These tests began with isotropic loading. In the first test, the sample was then immediately sheared; in the second and third tests, first an isotropic unloading was performed. Given these data, each of the four models was fitted to the three tests simultaneously (see Figure 5.3 of Arnold et al. (2015)). Comparing the best fits of the four models to the data, the Hardening Soil model performed best. Therefore, this model was used for subsequent analysis.

The mechanical response can be used to assess the feasibility of facility construction and the mechanical stability during operations. However, an additional concern is the response of the plastic zone to heat production of the disposed radioactive waste. To model this, a coupling with hydraulic and thermal behaviour must be pursued in the numerical modelling. The authors utilised a newly developed feature in the utilised software, which enabled thermal (heat) transport and the coupling to hydraulics and mechanics. An important observation was the effect of the large difference between the thermal expansion coefficient of water and that of clay. In the typically low-permeability host rocks, this causes a significant pore pressure increase upon heating, an associated lower effective stress and consequently a larger plastic zone. This highlights the need for careful assessment of the heat production and for prolonged monitoring of the temperature in and around the disposal facility.

It is, however, noted that, given the surface storage period in the Netherlands (of at least 100 years), the heat emission from the HLW will be reduced compared to the disposal programmes in other countries.

5.2.3 Probabilistic modelling (Chapter 7, Arnold et al., 2015)

There are numerous sources of uncertainties which need to be accounted for in the engineering design of a deep geological radioactive waste disposal facility. By using Reliability Based Design (RBD) rather than design approaches based on deterministic analyses, these uncertainties can be accounted for in a rational and quantified manner.

The performance of a system is usually assessed deterministically as a first approximation. However, given the great variety of uncertainties a probabilistic assessment of relevant features and processes would be considered the next step of the integrated safety assessment. A probabilistic setting, however, requires a selection of parameter values representative of the anticipated conditions and their distributions includ any knowledge of the uncertainties of these values. In RBD, the probability of failure is then defined as the probability that the system performance is unsatisfactory for a given probability density distribution of the random variables. Different methods exist to approximate this number, because usually the full joint probability density function is not known and direct integration is not possible. The most comprehensive RBD method uses Monte Carlo modelling. In this method, a sequence of independent realisations is created, for which each uncertain variable is sampled from the joint probability density function for the random vector formed by all these variables. The drawback of Monte Carlo modelling is that usually large numbers of realizations are required. This is a particular drawback when probabilities of failure are small – indeed, a significant number of realizations must lead to failure in order to estimate the probability of failure probabilistically. To reduce the number of simulations required, approximate probabilistic methods can be employed. The First and Second Order Reliability Methods (FORM / SORM) are examples of these. In these methods, an assumption is made about the form of the limit state surface in a transformed variable vector space. Once the critical design point is found, the probability of failure is found from the fraction of the transformed variable vector space that is occupied at the failure side of the limit state surface.

This has allowed an analysis of the most important parameters, which are the friction angle and the stiffness of the Boom Clay, with the frictional behaviour being more important. Quantitiative assessment of the likelihood of plastic radii were undertaken, with the conclusion that it is likely that horizontal spacing between disposal galleries could be reduced. However, more data on material properties are needed.

5.3 Code validation (this report)

Building trust in geotechnical modelling requires code validation. Since there is not yet an operational facility available at depth in the Boom Clay, and little experimental testing has been done on samples from this depth, such a validation cannot be performed on an actual case, and alternative ways must be pursued. Such alternatives include testing against laboratory experiments, cross validation between different modelling approaches, or between the new approaches and literature results, and validation of the code applied to comparable facilities in comparable environments. The selection of the most suitable constitutive model discussed in the previous section can be viewed as testing against laboratory experiments. In this report, the methods have been applied to facilities in comparable environments. Two geological disposal programmes have been considered: the French disposal programme in Callo-Oxfordian (COx) Clay at a depth of 490 m, and the Swiss disposal programme with the Mont Terri URL in Opalinus Clay at a depth of 300 m. There was more information avaiable

publically on the results obtained for the French programme, and therefore this has made up the majority of this report.

In France, an underground research facility in Eastern France, on the boundary between the Meuse and Haute-Marne districts had been constructed in the Callovo-Oxfordian Clay. A host of measurements were available for the elastic moduli and the shear strength. These were used to obtain probability density functions for initial cohesion, residual cohesion, friction angle, Young's modulus, tangent modulus, and Poisson's ratio. Of particular interest are the correlations between these parameters; together with their variances they are represented in the covariance matrix. In a first deterministic analysis, displacements around the cavity upon its construction were calculated with the analytical approach. Results with two values of the Young's modulus were seen to bracket the experimental results (Fig. 3.10). Displacements further away match better the stiffer analysis; closer to the tunnel they match the less stiff analysis.

In a probabilistic analysis, the probability was assessed that the plastic radius would exceed a certain threshold. Such a threshold represents a limit that should not be exceeded, e.g. a plastic radius around parallel tunnels should not intersect. Here it became clear how important are the correlations within the probability density distribution: the calculated probability of exceedance of the plastic radius threshold when discarding the non-diagonal covariance numbers (i.e. assuming no correlation between the stochastic variables) was a far greater number than the number calculated with account of these numbers. In fact, as compared to the uncorrelated case, the probability of the rock having both a small coherence and a small friction angle is much smaller for the correlated case; a better and more substantiated prediction of these system parameters provide more confidence in the strength of the host rock and the associated probability of failure resulting from such combinations reduces. More comprehensive calculations were performed using the numerical Hardening Soil model to investigate the extent of the hardening plastic zones. The calculated results fitted well within the range reported in literature. However, the model cannot predict the anisotropic fracture behaviour observed in measurements, as it does not account for bedding planes and anisotropic elasticity. These topics woud need further analysis.

For the results of the Swiss disposal programme, due to the highly anisotropic stress regime, a numerical modelling approach was used. The results match well the limited data available.

The modelling approaches are able to simulate the effects of the different material properties. In Boom Clay the plastic behaviour yields a large hardening zone, but a more limited failure zone. The COx exhibits a more brittle behaviour, with a very limited disturbed zone surrounding the tunnel. The hardening zone is likely to have a significantly higher permeability than the Boom Clay due to the brittle behaviour, whereas the hardening zone in Boom Clay is likely to be larger. In the Opalinus Clay, the hardening zone exhibits a typical X-shape as a result of the stress anisotropy, and the failure zone is relatively limited.

5.4 Model application

The models formulated can be employed to investigate questions pertinent to the technical feasibility of a Dutch radioactive waste repository in Boom Clay. Four issues were addressed; these are highlighted in the following subsections.

5.4.1 Tunnel construction (Chapter 6, Arnold et al., 2015)

A deterministic calculation was performed to assess the feasibility of constructing a tunnel in Boom Clay using the 2D and the 3D numerical code with the Hardening Soil model. The extent of the hardening and the plastic zones were calculated, and assessed for their sensitivity to typical input variables for the in-situ stresses, the elastic moduli and the failure parameters. For example, Figure 6.5 of Arnold et al. (2015) shows results for varying levels of the cohesion and for the stress anisotropy.

5.4.2 Plugs and seals (Yuan et al., 2017a)

Effective plugging of the disposal galleries after emplacement of radioactive waste is of importance for the operational and long term safety. The plug must be both mechanically stable and hydraulically sealing. A coupled model was set up to facilitate calculations to assess these issues. Different types of conceptual plug designs were addressed in a study to determine the plug lengths required to achieve mechanical stability and hydraulic sealing. The analyses showed that, under the assumed conditions, a relatively small plug would satisfy the design requirements. Options were given as to whether to remove tunnel lining segments or not, and the consequences calculated in terms of the required plug length. A number of recommendations were provided requiring further analysis to finalise a design, including the hydraulic conductivty of all components, and the swelling pressure of the bentonite seal due to a variety of aspects, e.g. geochemical evolution, concrete shrinkage and material creep.

5.4.3 Tunnel crossings (Yuan et al., 2017b)

The repository layout that is foreseen in the OPERA programme encompasses an entrance shaft, a main gallery, secondary galleries and deposition tunnels. Different tunnel crossings will thus be present. It is important to assess the mechanical stability of such crossings. Calculations to that end were performed in a sequence of stages: after a calculation of the initial stresses, simulations were performed on the excavation and construction of a parent tunnel; then on the local removal of the tunnel lining; and finally on the excavation and construction of a child tunnel. In addition, a possibility was included to apply an additional support before local liner removal. The stages of the two construction methods are highlighted in Fig. 2.2 of Yuan et al. (2017b).

The simulations revealed that the tunnel lining was exposed to significantly increased forces due to the construction of a child tunnel and that extended plastic and hardening zones developed around the crossing. The lining would need to be reinforced in a limited zone around the child tunnel opening. However, the way the construction was implemented had only limited impact on these zones. The largest impact was found in the choice of the friction parameters and the stress anisotropy. The choice of stages in the construction method had a direct impact on the amount of reinforcement needed in the tunnels.

5.4.4 Effect of heating (Vardon et al., 2017)

A limited amount of radioactive waste considered for disposal in the Netherlands is heat producing. As a result, temperatures in the vicinity of the heat producing waste containers may rise, which may lead to a number of effects, including pore pressure increase and thermal expansion. The consequences of heat production on the structural integrity and the water tightness of a disposal facility were therefore investigated. This was done with a coupled thermo-hydro-mechanical model. An analysis similar as the tunnel construction analysis was extended with a heating stage (Chapter 4, Vardon et al., 2017), where a heat flux representing the flux from the emplaced waste was applied to the tunnel boundary. An analysis for typical input scenarios showed that the heat output can indeed be expected to cause significant coupled hydro-mechanical processes. In particular, excess pore pressures will be generated, which will not easily dissipate due to the low permeability of the Boom Clay. The increased pore pressures will reduce the effective stresses and increase the damaged zone around the repository tunnels. Two results of the changing stresses are that the forces applied to the tunnel lining will increase and that the Boom Clay may yield and be damaged. The latter could cause an increase in permeability and should thus be taken into account when assessing the repository performance. The temperature increase would be, however, moderate and temporary. Consequentially, the disturbed zone of the host may return to conditions close to its previous state several decades after the disposal. These temporary effects and its healing after mechanical disturbance would require additional analysis.

5.5 Newly collected data from Boom Clay experiments (this report)

Newly collected experimental data, conditioned to stresses equivalent to 500 m depth, have provided input for new deterministic analyses. The friction angle found was close to the largest value used in Arnold et al. (2015) and therefore the results give a reduced plastic zone, which could allow closer spacing of the disposal galleries compared to the previous analysis and the current proposed design. The forces exerted by the host rock on the liner are also reduced, which suggests a possible reduction in liner thickness. However, the new tests give a single new data point, which while extremely valuable, does not allow additional statistical interpretation, highlighting an example of the disadvantage of the statistical methods. A reasonable approach could be to estimate the uncertainty and variability, based on expert opinion. This could form the basis of further work.

5.6 Future

The construction of an underground repository for radioactive waste in Boom Clay is a complicated operation with many unknowns and a number of risks. Careful modelling is required to optimise the operations and to minimise the risks. The first requirement for careful modelling of the consequences of disturbing the Boom Clay host rock is the choice of a representative constitutive model. This requirement has been met with the selection of the Hardening Soil model, which provides the best results in terms of comparison with other analyses and experimental results on the mechanical behavior of various types of clay. As is any model, of course, this one also is an abstraction of the overall behaviour, and it may therefore not capture all the features observed in the behaviour of the subsurface. We believe that careful parameter determination, extensive modelling of the facility construction and operation, and a probabilistic approach will provide the best possible results given the prevailing uncertainties. The addition of a model that includes long term creep for modeling the healing properties of Boom Clay after its disturbance and its return to ambient conditions may be a valuable extension.

A start has been made, in the investigations reported here, into modelling the subsurface behaviour upon the construction and operation of the proposed underground disposal facility. Such modelling needs further enhancement and detailing once a particular site is chosen. In the first place, this requires extensive laboratory testing of sample material. An example of such testing is available from the French site discussed in Section 2.2.3. The elastic and plastic parameters of the local subsurface material can then be constrained better – and, even more importantly, their distribution and internal correlations can be assessed and mapped with a covariance matrix. An analytical model may suffice to estimate some of the immediate responses and correlations obtained from the testing campaign, but a numerical model is required to assess the complete and integrated behaviour. Only then can the peculiarities of the material constitutive behaviour can be captured, and only then the actual situation with 3D constructions, stress and permeability anisotropies and heterogeneities be accounted for.

A probabilistic approach is useful for a number of reasons. A probabilistic approach will provide a range of outcomes and thus bracket the real behaviour. In addition, a probabilistic approach recognises that the mechanical parameters of the soil model cannot be determined exactly. There will always be variations due to the anisotropic and heterogeneous properties of the Boom Clay, measurement inaccuracy, experimental variations, and inadequacy of the model used. A large collection of laboratory measurements, if possible accompanied by the results of in-situ tests, will cover these variations and partially conceal the effects of variations of host rock properties and model deficiencies. The last reason for probabilistic testing is the ability to determine limit state probabilities, which can quantitatively feed into performance assessment. Different approaches can be chosen here (Monte Carlo; FORM / SORM; others), but sensible failure probabilities cannot be achieved without an indication of the distribution of mechanical responses resulting from the distribution of mechanical

parameters.

Modelling of the facility construction and operation has been started in the work described here. Attention has been given to specific issues, like the behaviour of tunnel crossings and the selection of the length of the sealing plug in front of a deposition tunnel. The treatment, however, is not exhaustive. For instance, an issue that was not addressed here is the realisation of single-ended tunnels. It is likely that these tunnels would have to be built with demountable tunnel boring machines and this may pose a challenge for construction, as such machines are not commonly available. As the benefit in safety is thought to be only limited in comparison with tunnels which end at the adjacent gallery, due to the possible use of plugs and seals, this alternative might be considered.

Once an underground repository has been built, monitoring is key for its prolonged safe operation. Such monitoring must include temperatures and pressure in the repository and around it. This issue is being addressed in the EU project Modern2020.

6 Summary and conclusions

Following from Arnold et al. (2015), where little experimental data were available, the proposed geomechanical models have been validated against data from other geological disposal programmes, more specifically from France and Switzerland. The validations revealed that both the analytical and numerical models considered in this report were shown to perform well in terms of capturing the most relevant phenomena occurring in the host rock after disturbing it, i.e. during and after the excavation of disposal galleries.

In the case of the French geological disposal programme, material parameters were reinterpreted statistically from literature. Both the analytical (softening) and numerical (hardening) models have been used in the stability assessment of a tunnel drift in the French repository case, to demonstrate the functionality of the modelling framework. The extent of the plastic zone calculated in the present models matches within the range reported in the literature, as do the deformations. The probability of plastic limit threshold exceedance has been evaluated in the proposed probabilistic framework. In the case of the Swiss geological disposal programme, only deterministic parameter values were available, and the initial stress field was highly anisotropic. In this case, only the numerical model was appropriate. Again, the plastic radius predicted fits very well with the values reported in literature.

From properties derived from additional experimental data on Boom Clay, a single additional deterministic analysis has been undertaken. From this analysis, due mainly to the larger friction angle, reduced plastic and failure extents are exhibited and lower liner stresses are seen compared to previous work performed within OPERA Task 3.1. This indicates that, compared to the results reported earlier, the disposal gallery spacing and the liner thickness may be reduced and advective transport around the galleries may be reduced.

Additional confidence may be gained and uncertainties reduced by performing supplementary testing of the Boom Clay properties, preferably under in-situ conditions. This is expecially necessary when considering a region or a site for constructing a geological disposal facility.

References

ANDRA (2005a). *Dossier 2005 Argile, Synthesis, Evaluation of the feasibility of a geological repository in an argillaceous formation*. Andra, Chatenay-Malabry, France.

— (2005b). *Dossier 2005 Argile, Tome, Phenomenological evolution of a geological repository*. Andra, Chatenay-Malabry, France.

Armand, G., A. Noiret, J. Zghondi and D.M. Seyedi (2013). Short-and long-term behaviors of drifts in the Callovo-Oxfordian claystone at the Meuse/Haute-Marne Underground Research Laboratory. In: *Journal of Rock Mechanics and Geotechnical Engineering* 5 (3), 221–230.

Armand, G., F. Leveau, C. Nussbaum, R. de La Vaissiere, A. Noiret, D. Jaeggi, P. Landrein and C. Righini (2014). Geometry and properties of the excavation-induced fractures at the Meuse/Haute-Marne URL drifts. In: *Rock mechanics and rock engineering* 47 (1), 21–41.

Arnold P.and Hicks, M.A. (2011). A stochastic approach to rainfall-induced slope failure. In: *Proceedings of 3rd Int Symp Safety and Risk*.

Arnold, P., P.J. Vardon and M.A. Hicks (2014). Preliminary Assessment of Tunnel Stability for a Radioactive Waste Repository in Boom Clay. In: *Engineering Geology for Society and Territory* 6, 545–549.

Arnold, P., P.J. Vardon, M.A. Hicks, J. Fokkens and P.A. Fokker (2015). *A numerical and reliability-based investigation into the technical feasibility of a Dutch radioactive waste repository in Boom Clay*. OPERA-PU-TUD311. Centrale Organisatie Voor Radioactief Afval (COVRA N.V.) URL: https://covra.nl/downloads/opera/OPERA-PU-TUD311.pdf.

Bossart, P. and M. Thury (2008). *Characteristics of the Opalinus Clay at Mont Terri, Mont Terri Rock Laboratory, Project programme 1996 to 2007 and results.* 3. Swiss Geological Survey.

Bossart, P., P. M. Meier, A. Moeri, T. Trick and J.-C. Mayor (2002). Geological and hydraulic characterisation of the excavation disturbed zone in the Opalinus Clay of the Mont Terri Rock Laboratory. In: *Engineering Geology* 66 (1), 19–38.

Bossart, P., T. Trick, P. M. Meier and J.-C. Mayor (2004). Structural and hydrogeological characterisation of the excavation-disturbed zone in the Opalinus Clay (Mont Terri Project, Switzerland). In: *Applied clay science* 26 (1), 429–448.

Box, G.E.P. and K.B. Wilson (1951). On the experimental attainment of optimum conditions. In: *Journal of the Royal Statistical Society. Series B (Methodological)* 13 (1), 1–45.

Bucher, C.G. and U. Bourgund (1990). A fast and efficient response surface approach for structural reliability problems. In: *Structural safety* 7 (1), 57–66.

Corkum, A.G. and C.D. Martin (2007a). Modelling a mine-by test at the Mont Terri rock laboratory, Switzerland. In: *International Journal of Rock Mechanics and Mining Sciences* 44 (6), 846–859.

— (2007b). The mechanical behaviour of weak mudstone (Opalinus Clay) at low stresses. In: *International Journal of Rock Mechanics and Mining Sciences* 44 (2), 196 –209. ISSN: 1365-1609. DOI: https://doi.org/10.1016/j.ijrmms.2006.06.004. URL: http://www.sciencedirect.com/science/article/pii/S1365160906001122.

Freissmuth, H. (2002). L'influence de l'eau sur le comportement mécanique des roches argileuses. PhD thesis. Paris, ENMP.

Guayacán-Carrillo, L.-M., J. Sulem, D.M. Seyedi, S. Ghabezloo, A. Noiret and G. Armand (2016). Analysis of long-term anisotropic convergence in drifts excavated in Callovo-Oxfordian Claystone. In: *Rock Mechanics and Rock Engineering* 49 (1), 97–114.

Harrington, J. F., R. J. Cuss, A. C. Wiseall, K. A. Daniels, C. C. Graham and E. Tamayo-Mas (2017). *Scoping study examining the behaviour of Boom Clay at disposal depths investigated in OPERA*. OPERA-PU-BGS523&616. Centrale Organisatie Voor Radioactief Afval (COVRA N.V.) URL: https://covra.nl/downloads/opera/OPERA-PU-BGS523&616.pdf.

Hoteit, N., O. Ozanam and K. Su (2000). Geological radioactive waste disposal project in France: conceptual model of a deep geological formation and underground research laboratory in Meuse/Haute-

Marne Site. In: *4th North American Rock Mechanics Symposium*. American Rock Mechanics Association.

Lumb, P. (1970). Safety factors and the probability distribution of soil strength. In: *Canadian Geotechnical Journal* 7 (3), 225–242.

MartÃŋn, L.B., F. Hadj-Hassen, M. Tijani and G. Armand (2011). New numerical modelling of the mechanical long-term behaviour of the GMR gallery in ANDRAâĂŹs Underground Research Laboratory. In: *Physics and Chemistry of the Earth, Parts A/B/C* 36 (17), 1872–1877.

Miehe, B. (2004). Modélisation de la zone endommagée induite par le creusement du puits d'accés au laboratoire souterrain de Meuse/Haute-Marne (argilites de l'Est). PhD thesis. École Nationale Supérieure des Mines de Paris.

Nagra (2016). *Mont Terri, the rock laboratory*. http://www.mont-terri.ch/internet/mont-terri/en/home/rock_lab/map.html.

OpenTURNS (2016). *Reference Guide, OpenTURNS 1.7*. http://doc.openturns.org/__old/openturns-1.7/16.03/html/ReferenceGuide/.

Plaxis (2014). *PLAXIS 2D Anniversary Edition - Reference Manual*. Delft, The Netherlands: Plaxis bv.

Rackwitz, R. (2000). Reviewing probabilistic soils modelling. In: *Computers and Geotechnics* 26 (3), 199–223.

Seyedi, D., M. N. Vu, G. Armand and A. Noiret (2015). Numerical Modeling of Damage Patterns around Drifts in the Meuse/Haute-Marne Underground Research Laboratory. In: *13th ISRM International Congress of Rock Mechanics*. International Society for Rock Mechanics.

Tsang, C.-F., J. D. Barnichon, J. Birkholzer, X. L. Li, H. H. Liu and X. Sillen (2012). Coupled thermo-hydro-mechanical processes in the near field of a high-level radioactive waste repository in clay formations. In: *International Journal of Rock Mechanics and Mining Sciences* 49, 31–44.

Uzielli, M., S. Lacasse, F. Nadim and K. K. Phoon (2006). Soil variability analysis for geotechnical practice. In: *Characterization and engineering properties of natural soils* 3, 1653–1752.

Vardon, P.J., K. Liu and M.A. Hicks (2016). Reduction of slope stability uncertainty based on hydraulic measurement via inverse analysis. In: *Georisk: Assessment and Management of Risk for Engineered Systems and Geohazards* 10 (3), 223–240.

Vardon, P.J., P. Buragohain, M.A. Hicks, J. Hart, P.A. Fokker and C.C. Graham (2017). *Technical feasibility of a Dutch radioactive waste repository in Boom Clay: Thermo-hydro-mechanical behaviour*. OPERA-PU-TUD321c. Centrale Organisatie Voor Radioactief Afval (COVRA N.V.) URL: https://covra.nl/downloads/opera/OPERA-PU-TUD321c.pdf.

Verhoef, E., E. Neeft, J. Grupa and A. Poley (June 2014). *Outline of a disposal concept in clay, OPERA-PG-COV008, First update*. Centrale Organisatie Voor Radioactief Afval (COVRA N.V.) URL: https://covra.nl/downloads/opera/OPERA-PG-COV008_rev1.pdf.

Wileveau, Y. and F. Bernier (2008). Similarities in the hydromechanical response of Callovo-Oxfordian clay and Boom clay during gallery excavation. In: *Physics and Chemistry of the Earth, Parts A/B/C* 33, S343–S349.

Wong, F.S. (1985). Slope reliability and response surface method. In: *Journal of Geotechnical Engineering* 111 (1), 32–53.

Xu, B. and B.K. Low (2006). Probabilistic stability analyses of embankments based on finite-element method. In: *Journal of Geotechnical and Geoenvironmental Engineering* 132 (11), 1444–1454.

Yuan, J., P.J. Vardon, M.A. Hicks, J. Hart and P.A. Fokker (2017a). *Technical feasibility of a Dutch radioactive waste repository in Boom Clay: Plugs and seals*. Centrale Organisatie Voor Radioactief Afval (COVRA N.V.)

— (2017b). *Technical feasibility of a Dutch radioactive waste repository in Boom Clay: Tunnel crossings*. OPERA-PU-TUD321b. Centrale Organisatie Voor Radioactief Afval (COVRA N.V.) URL: https://covra.nl/downloads/opera/OPERA-PU-TUD321b.pdf.

Zhang, C. and T. Rothfuchs (2004). Experimental study of the hydro-mechanical behaviour of the Callovo-Oxfordian argillite. In: *Applied Clay Science* 26 (1), 325–336.

OPERA

Meer informatie:

Postadres
Postbus 202
4380 AE Vlissingen

T 0113-616 666
F 0113-616 650
E info@covra.nl

www.covra.nl